UNIVERSITÀ DEGLI STUDI DI SALERNO

UNIVERSITÀ DEGLI STUDI DI SALERNO
Dipartimento di Farmacia

PhD Program
in **Drug Discovery and Development**
XXXII Cycle — Academic Year 2019/2020

Abstract of PhD Project

Development and Evaluation of Innovative Stationary Phases for Separation of Pharmaceuticals, Metabolites and Biocompounds

Candidate

Giuliana Grasso

Supervisor(s)

Prof. *Carlo Crescenzi*
Prof.ssa *Nunziatina De Tommasi*

PhD Program Coordinator: Prof. Dr. *Gianluca Sbardella*

To my Dad, my Mom,
and the Snowy Mountains
that are guiding me.

List of Publications and Communications at International and National Conferences related to the scientific activity performed during the three years PhD course in "Drug Discovery & Development":

Papers:

1. Li, Q.; Shinde, S., **Grasso, G.**, Caroli, A., Abouhany, R., Lanzillotta, M., Pan, G., Wan, W., Rurack, K., Sellergren, B., Fluorescent Sensory Core-shell Particles for Selective Detection of Sphingosine1-Phosphate. *Submitted*.

2. **Grasso, G.**, Abouhany, R., Sommella, E., Merciai, F., Campiglia, P., Crescenzi, C, Sellergren, B., Synthesis and Evaluation of Molecularly Designed Materials as Selective Capture Phase for Improvement of Phospho-monoester Lipids Detection. *Manuscript in preparation*.

3. **Grasso, G.**, Cárdenas, M., Marìc, S.; Crescenzi, C; Sellergren, B., "PC-MIP: Targeting Phosphatidylcholine by Molecularly Imprinted Polymers". *Manuscript in preparation*.

4. Iadaresta, F., **Grasso, G.**, Viola, A., Cascone C., Holmbäck J., Crescenzi C., "Separation of phospholipids by high temperature liquid chromatography using porous graphitic carbon as stationary phase. *Manuscript in preparation*.

List of Communications to Conferences:

Oral communications:

1. **Grasso, G.**, Li, Q., Shinde, S., Crescenzi, C., Sellergren, B., Fluorescent Sensory Core-shell Particles for Selective Detection of Sphingosine 1-Phosphate and Phosphatidic Acid, *XVVIII Congresso della Divisione di Chimica Analitica (SCI)*, September 22-26, 2019, Bari (IT).

2. **Grasso, G.**, Crescenzi, C., Sellergren, B., Synthesis and Evaluation of Molecularly Designed Materials as Selective Capture Phase for Improvement of Phospho-monoester Lipids Detection, *48th International Symposium on High-Performance Liquid Phase Separation and Related Techniques (HPLC2019)*, June 16-20, 2019, Milan (IT).

3. **Grasso, G.**, Shinde, S., Crescenzi, C., Sellergren, B., Improving LC-MS Detection of Phospholipids by Molecularly Designed Class Selective SPE Sorbents, *XXVII Congresso della Divisione di Chimica Analitica (SCI)*, September 16-20, 2018, Bologna (IT).

Posters:

1. **Grasso, G.**, Colin, C., Cárdenas, M., Marìc, S., Crescenzi, C, Sellergren, B., PC-MIP: Targeting Phosphatidylcholine by Molecularly Imprinted Polymers, *Materials and Formulations at Biointerfaces Forum 2019*, October 23-25, 2019, Malmö (SE).

2. **Grasso, G.**, Li, Q., Shinde, S., Wan, W., Rurack, K., Sellergren, B., Fluorescent Sensory Core-shell Particles for Selective Detection of Sphingosine 1-Phosphate and

Phosphatidic Acid, *8th Graduate Student Symposium on Molecular Imprinting (GSS MIP 2019)*, August 28-30, 2019, Berlin (DE).

3. **Grasso, G.**, Li, Q., Shinde, S., Abouhany, R., Crescenzi, C., Sellergren, B., Affinity Solid Phase Extraction and Optical Sensing for Highly Sensitive Detection of Signalling Lipids, *Affinity 2019*, June 26-28, 2019, Stockholm (SE).

4. **Grasso, G.**, Crescenzi, C., Sellergren, B., Improvement of Phospho-monoester Lipids LC-MS Detection by Selective Capture using Molecularly Designed Materials, *Annual Meeting of American Society of Mass Spectrometry (ASMS 2019)*, June 2-6, 2019, Atlanta (USA).

5. Incel, A., **Grasso, G.**, Sellergren, B., Molecularly Designed Materials for Capturing and Enrichment of Phosphopeptides and Phospholipids, *Biofilms Forum 2018*, October 26-28, 2018, Malmö (SE).

6. **Grasso, G.**, Shinde, S., Crescenzi, C., Sellergren, B., Study and Comparison of Affinity Capture of Molecularly Designed Sorbents Towards Sphingosine 1-Phosphate and Fingolimod Phosphate to Improve LC-MS Detection, *1st National Meeting of the Swedish Chemical Society (SCS)*, June 17-20, 2018, Lund (SE).

7. Li, Q., Caroli, A., **Grasso, G.**, Shinde, S., Crescenzi, C., Malitesta, C., Sellergren, B., Fluorescent Core-shell Molecular Imprinted Nanoparticles for Detection of Sphingosine 1-Phosphate, *XXVI Congresso Nazionale della Società Chimica Italiana (SCI)*, September 10-14, 2017, Paestum (IT).

TABLE OF CONTENTS

ABSTRACT

Biofluids are typical complex matrices representing a source of potential biomarkers, but often require high demands in sample preparation prior to analysis. With this purpose, several techniques have been developed including solid phase extraction and methods based on the molecular recognition, such as immuno-affinity sorbents and molecularly imprinted polymers. Lipidomics is a research field in which it is needed to develop efficient techniques for sample pre-treatment in order to obtain reliable and reproducible results. Lipids are involved in many processes, as cellular structures, signaling, within the cell and between cells, and energy storage. Because of the role of lipids and all their functions, the field of Lipidomics is emerging with the focus on identifying alterations in lipids metabolism and lipid-mediated signalling processes that regulate cellular homeostasis and trying to understand the relationship between these processes in health and disease (Han & Gross, 2003). Following from that, when there is a disruption of lipid metabolism there is connection with the onset and progression of various metabolically linked diseases, including cancer (Santos & Schulze, 2012). The complexity of Lipidomics, expressed in lipids classes and subclasses present in human plasma, brings to highlight that the concentration range is quite wide, going from few pmol/L to mmol/L (Burla *et al*., 2018). Among other phospholipids, in this project we focused on Sphingosine 1-Phosphate (S1P), whose levels in circulatory stream have been recently determined below the nmol (Yatomi *et al*., 1997). S1P is a bioactive sphingolipid with broad range of activities coupled to its role in G-protein coupled receptor signalling. It is also an emerging biomarker for a variety of conditions comprising cancer, multiple sclerosis, rheumatoid arthritis and sepsis (Maceyka *et al*, 2012). In view of the dynamic nature of cell signaling, the time- and space-resolved quantification of S1P is crucial for both fundamental understanding and for developing

improved diagnostic tests. Robust means of real-time lipid quantification *in-situ* are still to be realized. This requires the development of affinity techniques or probes (e.g. immunosensors) capable of continuously reporting the lipid levels in biofluids. Such methods would be particularly beneficial for monitoring S1P in blood or in living cells, but of equal urgency are sensors for Fingolimod (FTY720, Gilenya™, Novartis), a sphingosine analogue and S1P-receptor antagonist, approved by Food and Drug Administration (FDA) for the treatment of relapsing-remitting multiple sclerosis (Aktas *et al.,* 2010).

We here report on three approaches to achieve these purposes. The *first* is based on LC-MS analysis to deep profiling selected classes of lipids in biofluids. It combines the use of solid phospholipid capture phases, specific for phosphomonoesters, with MS/MS, and allows extremely sensitive detection of phosphosphingolipids. The *second* approach concerns the use of fluorescent sensory core-shell molecularly imprinted polymer (MIP) particles responsive to near physiologically relevant levels of S1P and the S1P-receptor antagonist Fingolimod Phosphate (FP) in spiked human serum samples. Imprinting was achieved using FP-TBA salt or 1,2-dipalmitoyl-*sn*-glycero-3-phosphate sodium salt (DPPA(Na)) as templates, in combination with a polymerizable nitrobenzoxadiazole (NBD)-urea monomer with the dual role of capturing the phosphorus-anion and signaling its presence. In order to extend the capacity and ability of stationary phases to retain phosphorus-molecules, such as phospholipids, target molecules of our studies, the *third* approach developed was focused on the synthesis of materials created by the combination of two functional monomers (FM), 1,3-diarylurea based FM (neutral) and bis-imidazolium FM (cationic), using two different templates, phenyl phosphonic acid (PPA) and DPPA(Na), both mimicking the common phosphorus-moiety of phospholipids and probing the affinity towards the phosphate group.

Finally, we demonstrated the potential use of the above techniques for monitoring S1P and FTY720 P in human plasma and human serum.

Nevertheless, we considered this work as a first step towards a general sensory platform for phospholipids detection.

PART 1

INTRODUCTION

This section was created to give the readers an overview of the PhD thesis, and it is divided into the following parts:

1. background
2. target molecules
3. analytical methods
4. aim of the project
5. general conclusions

1. Background

The production of artificial molecular recognition media, using biological functionalities of enzymes and antibodies, has been the first approach for using molecular recognition in analytical and separation sciences. Unfortunately, conventional affinity gels based on biomolecules suffer of poor stability and high costs of production. The synthesis of intelligent materials with molecular recognition abilities can be easily obtained by engaging the molecular imprinting approach. This novel technique finds its roots in the scientific research community since 1894 by Emil Fisher, Paul Ehrlich (1900), Linus Pauling and Frank Dickey's (1940s) theories, respectively the *key-lock model*, an early way to explain the specificity in the interaction between enzyme and substrate, the *side-chain theory*, practically the explanation of the interaction between antigens in the blood and antibodies, and their production, and the discovery of *α-helix and β-sheet structures* with practical and chemical implications of the nature of the chemical bonds, especially with respect to protein structure and functions

(Sellergren, 2001). The concept of molecular recognition has been then further developed in the last two decades, finding many applications in different fields, such as in catalysis, sensors, separations, and biotechnologies, and it is bringing a relevant impact in the tool market with several commercially available Molecularly Imprinted Polymers (MIPs), demonstrating their industrial and commercial potentiality, since they are usually low cost, easy to realize, stable and robust materials, resistant to a wide range of pH, extreme temperature and presence of organic solvents.

2. Target Molecules

Lipids are a large group of naturally occurring molecules that play fundamental biological roles. The definition of lipids relies on their solubility. In fact, lipids are all compounds soluble in organic solvent and insoluble in water. The International Lipid Classification and Nomenclature Committee (ILCNC) describes lipids as *"hydrophobic or amphipathic small molecules that may originate entirely or in part by carbanion based condensation of thioester (fatty acyls, glycerolipids, glycerophospholipids, sphingolipids, saccharolipids, and polyketides) and/or by carbocation-based condensations of isoprene units (prenol lipids and sterol lipids)"* (Brügger, 2014). They are involved in energy storing, signalling, and structural components of cell membranes. The Sphingolipid class, core of this project, includes a backbone termed sphingoid base, also termed long chain base (LCB) or sphingosine, that is an unsaturated long chain amino alcohol (Pruett *et al.*, 2008). Sphingolipids, in particular glycosphingolipids, are common constituents of plasma membranes, especially embedded in neural cells (Aureli *et al.*, 2015). In fact, they represent an important class of lipids, considered as units in membranes building blocks and components of myelin, fundamental substance that covers nervous fibers and allows neurons connection. The simple physiological metabolite of the sphingosine pathway,

Sphingosine 1-Phosphate (S1P), performs a plethora of functions, and has been recognized as a relevant biomarker for neurodegenerative diseases. S1P is formed intracellularly by the phosphorylation of sphingosine (which is derived from the deacylation of ceramide), a process that is catalysed by two sphingosine kinases: SPHK1 and SPHK2. S1P is then exported out of cells where it can act on five specific G protein-coupled receptors (S1P receptor 1 (S1PR1) to S1PR5) and can also act on some direct intracellular targets before being broken down by S1P lyase.

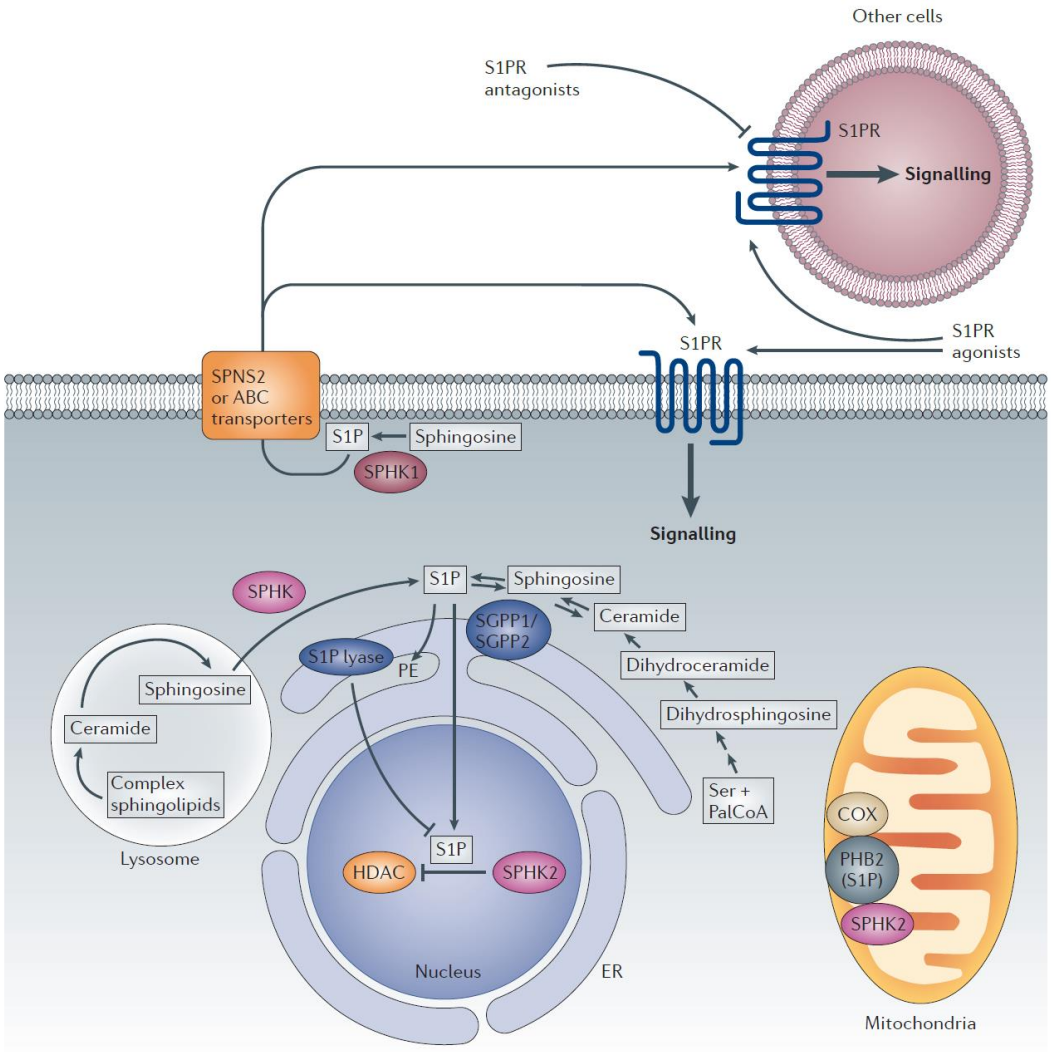

Figure 1: *S1P biosynthesis, degradation, export and signalling* (Kunkel *et al*, 2013).

Sphingosine, the substrate of sphingosine kinases (SPHKs), is not generated *de novo* but through the degradation of complex sphingolipids and ceramide, which can occur in the lysosome as well as on the endoplasmic reticulum (ER) and other membranes. SPHK1 is mainly located in the cytosol and is translocated to the plasma membrane upon activation. This leads to the formation of S1P, which can be exported out of the cell by specific transporters. Binding to S1P receptors (S1PRs) initiates downstream signalling pathways. SPHK2 is localized to the ER, mitochondria and nucleus. At the ER, S1P is irreversibly degraded by S1P lyase or dephosphorylated by S1P phosphatases to sphingosine, which is reused for the synthesis of ceramide. S1P produced in the mitochondria and nucleus by SPHK2 also has direct intracellular targets. These include prohibitin 2 (PHB2), which stabilizes cytochrome *c* oxidase (COX), and histone deacetylases (HDACs), which remove acetyl groups from histones.

Cellular levels of S1P are controlled by its synthesis and degradation. S1P is irreversibly degraded by S1P lyase, an enzyme that is localized in the endoplasmic reticulum and cleaves the sphingoid base into ethanolamine phosphate and hexadecenal. S1P can also be dephosphorylated by two phosphatases localized in the endoplasmic reticulum: S1P phosphatase 1 (SGPP1) and SGPP2, which are members of the lipid phosphate phosphohydrolase (LPP) family. It is possible that other phosphatases are also able to dephosphorylate S1P. The resultant sphingosine can be reused for the synthesis of ceramide and complex sphingolipids (**Figure 1**). Signaling of S1P through its cell surface S1PRs is further controlled through localization: S1P formed inside the cell must be secreted or flopped out of the cytoplasm to bind to and activate these receptors in paracrine or autocrine manners. Although it has been shown that several ABC transporters, including ABCA1, ABCC1 and ABCG2 (Kim *et al.*, 2009) transport S1P, the identity of the transporter in red blood cells or platelets remains unclear. Interestingly, recent studies have demonstrated that the SPNS2 protein, which belongs to the large major facilitator superfamily of transporters, regulates S1P

release from endothelial and lymph-endothelial cells, and controls S1P levels in plasma and lymph (Kawahara *et al*., 2009; Nagahashi *et al.*, 2013; Hisano *et al.*, 2012; Fukuhara *et al.*, 2012; Mendoza *et al.*, 2012). Because lymphocyte egress is suppressed in *Spns2*-deficient mice, targeting SPNS2 could be a new therapeutic avenue for autoimmune diseases (Kawahara *et al.*, 2009).

The S1P axis refers to the signalling molecule S1P, its receptors and intracellular targets, as well as the proteins that synthesize, transport and degrade S1P. Many stimuli have been shown to activate S1P synthesis inside cells, which can then either act on intracellular targets or be secreted to act on cell surface receptors. The latter process is termed 'inside-out' signalling and occurs when S1P acts in an autocrine and/or paracrine fashion. An S1P gradient also exists, with high S1P levels in the circulation and low S1P levels in tissues. This gradient is maintained by a balance between the synthesis of S1P - which probably occurs in red blood cells, platelets and endothelial cells - and the degradation of S1P in tissues. The S1P gradient promotes the trafficking of haematopoietic cells from lymphoid tissues into the blood and is dependent on the expression of S1P receptors. Each of these steps, that makes up the so-called S1P axis, could be therapeutically targeted (Kunkel *et al.*, 2013) (**Table 1**).

Experimental evidence suggests that the S1P axis is controlled by synthesis, secretion and degradation. The activation of SPHKs and subsequent S1P-dependent activation of S1PRs is required for the full effects of many signalling molecules such as growth factors and cytokines (Pyne & Pyne, 2010; Spiegel & Milstien, 2011); this is referred to as 'inside-out' signalling. In addition, the S1P gradient between the blood and lymphoid organs is required for S1PR1-mediated egress of lymphocytes, and either disruption of this gradient or S1PR1 inhibition (using Fingolimod) induces lymphopenia and immunosuppression in mice (Cyster & Schwab, 2012). Moreover, recent studies have demonstrated that the secretion of S1P by SPNS2 expressed on endothelial cells regulates T and B lymphocyte egress from their respective

primary lymphoid organs (Nagahashi *et al*, 2013; Hisano *et al.*, 2012; Mendoza *et al.*, 2012). It has also been suggested that LPP3 promotes efficient export of mature T cells from the thymus into the circulation by destroying thymic S1P (Breart *et al*., 2011). Together, these studies, which were carried out in mice, demonstrate that the generation, destruction and secretion of S1P is tightly regulated and that the S1P gradient is crucial for lymphocyte trafficking.

First- and second-generation agonists and antagonists that are specific for one or a subset of S1PRs have been developed (**Table 1**). ***Fingolimod*** has been clinically approved for the treatment of relapsing and remitting multiple sclerosis in the United States and Europe (Brinkmann *et al.*, 2010), and several other compounds are in clinical trials (**Table 2**). Fingolimod is a sphingosine analogue that is phosphorylated primarily by SPHK2 to form ***phosphorylated Fingolimod***, which is an agonist at all of the S1PRs except for S1PR2 (Mandala *et al.*, 2002; Brinkmann *et al.*, 2002). However, persistent activation of S1PR1 by phosphorylated fingolimod causes S1PR1 internalization and degradation, and so fingolimod acts as a functional antagonist at this receptor (Brinkmann *et al.*, 2010; Graler & Goetzl, 2004). Drug-induced downregulation of the expression of cell surface S1PRs on lymphocytes prevents their egress from lymphoid organs and induces lymphopenia and immunosuppression (Brinkmann *et al.*, 2010; Gonzalez-Cabrera *et al.*, 2012). These effects are advantageous for the treatment of autoimmune diseases such as multiple sclerosis (Kunkel *et al*, 2013).

Table 1: *Compounds that target the S1P axis* (Kunkel *et al*, 2013).

Compounds (alternative names)	Targets	Mechanism of action	Preclinical effects in animal models of disease
SKI-I	SPHK1	SPHK1-specific inhibitor (K_i = 10 μM)	Decreases cancer progression, angiogenesis, lymphangiogenesis and airway hyperresponsiveness
Safingol	SPHK1, SPHK2	SPHK1 (K_i = 5 μM) and PKC inhibitor	Decreases cancer progression
SKi (2-(*p*-hydroxyanilino)-4-(*p*-chlorophenyl)thiazole or SKI-II)	SPHK1, SPHK2	SPHK inhibitor (IC_{50} = 16 μM for SPHK1; IC_{50} = 8 μM for SPHK2)	Decreases cancer progression
PF-543	SPHK1	SPHK1-specific inhibitor (K_i = 3.6 nM)	No effect observed on cell growth
ABC294640	SPHK2	SPHK2-specific inhibitor (K_i = 9.8 μM), partial oestrogen receptor antagonist	Decreases cancer progression, liver transplant graft injury and rheumatoid arthritis
LX3305 and LX2931	S1P lyase	Both compounds inhibit S1P lyase activity	Reduces rheumatoid arthritis and cerebral malaria
THI (2-acetyl-4-tetra-hydroxybutylimidazole)	S1P lyase	Inhibits S1P lyase activity	Reduces muscular dystrophy
Fingolimod and phosphorylated fingolimod	S1PR1, S1PR3, S1PR4, S1PR5	S1PR1 agonist and functional antagonist (IC_{50} = 0.2–6 nM for S1PR1, S1PR3, S1PR4 and S1PR5)	Suppresses EAE, inhibits lymphocyte trafficking, prevents transplant rejection and decreases colitis and cancer progression
KRP-203 and phosphorylated KRP-203	S1PR1, S1PR4	S1PR1 agonist and functional antagonist (ED_{50} = 0.84 nM)	Decreases rejection of heart allografts, colitis, atherosclerosis and renal injury
AUY954	S1PR1	Agonist (EC_{50} = 1.2 nM)	Decreases experimental autoimmune neuritis, heart transplant rejection and EAE
SEW2871	S1PR1	Agonist (EC_{50} = 14–140 nM)	Decreases ischaemic renal failure and blocks diabetic nephropathy
CS-0777 and phosphorylated CS-0777	S1PR1	S1PR1 agonist and functional antagonist (EC_{50} = 1.1 nM)	Decreases EAE
AAL(R) and phosphorylated AAL(R)	S1PR1, S1PR3, S1PR4, S1PR5	Agonist (EC_{50} = 1 nM)	Inhibits cytokine storm
TASP0277308	S1PR1	Antagonist (IC_{50} 2 nM)	Ameliorates collagen-induced arthritis
CYM-5442	S1PR1	Agonist (EC_{50} = 1.35 nM)	Inhibits cytokine storm resulting from viral infection and decreases EAE
VPC23019	S1PR1, S1PR3	Antagonist (pK_i = 7.9 for S1PR1; pK_i = 5.9 for S1PR3)	Used for receptor function testing in cells and *ex vivo* tissue preparations
W146	S1PR1	Antagonist (K_i = 10–20 nM)	Induces lymphopenia and inhibits hyperalgesia
VPC44116	S1PR1	Antagonist (K_i = 30 nM)	Decreases Hodgkin's lymphoma
JTE-013	S1PR2	Antagonist (K_i = 17 nM)	Decreases osteoporosis and atherosclerosis
Ponesimod (ACT-128800)	S1PR1	S1PR1-specific agonist (EC_{50} = 5–9.1 nM)	Decreases delayed-type hypersensitivity and arthritis
ASONEP and iSONEP	S1P	S1P-blocking antibody (K_d = 100 pM)	Decreases cancer progression, angiogenesis and choroidal neovascularization
Siponimod (BAF312)	S1PR1, S1PR5	Agonist (EC_{50} = 0.4 nM for S1PR1)	Decreases EAE
ONO-4641	S1PR1, S1PR5	Agonist (EC_{50} = 0.03 nM S1PR1)	Decreases EAE and colitis
VPC23153	S1PR4	Agonist (K_d = 38 nM)	Induces vasoconstriction
W-061	S1PR1, S1PR4, S1PR5	Agonist (K_i = 4 μM for S1PR1; 65 μM for S1PR4; 10 μM for S1PR5)	Decreases colitis and graft-versus-host disease
NIBR-0213	S1PR1	Antagonist (IC_{50} = 2 nM)	Decreases EAE

Table 2: *Drugs in clinical trials targeting S1P axis* (Kunkel *et al*, 2013).

Drug	Mechanism of action	Indications	ClinicalTrials.gov identifier	Phase
Fingolimod (Gilenya; Novartis)	S1PR modulator, S1PR1 functional antagonist	Relapsing–remitting multiple sclerosis	-	Approved
		Acute, non-infectious intermediate, posterior and pan-uveitis	NCT01791192	II
		Amyotrophic lateral sclerosis	NCT01786174	II
		Schizophrenia	NCT01779700	I
		Acute demyelinating optic neuritis	NCT01757691	II
		Relapsing–remitting multiple sclerosis with depression, in combination with antidepressants	NCT01436643	IV
		Chronic inflammatory demyelinating polyradiculoneuropathy	NCT01625182	III
		Kidney transplant	NCT00099801	III
Safingol	Sphingosine derivative, PKC inhibitor	Solid tumours, combined with fenretinide	NCT01553071	I
		Solid tumours, combined with cisplatin	NCT00084812	I (completed)
Sonepcizumab	S1P-specific monoclonal antibody	Exudative age-related macular degeneration	NCT01414153	II
		Pigment epithelial detachment	NCT01334255	I (terminated)
		Neovascular age-related macular degeneration	NCT00767949	I
		Solid tumours	NCT00661414	I (completed)
		Unresectable and refractory renal cell carcinoma	NCT01762033	II
ABC294640	SPHK2 inhibitor	Pancreatic cancer	NCT01488513	I
KRP203	S1PR1 agonist	Sub-acute cutaneous lupus erythematosus	NCT01294774	II (terminated)
		Ulcerative colitis	NCT01375179	II (terminated)
		Haematological malignancies	NCT01830010	I
Siponimod (BAF312)	S1PR1 and S1PR5 modulator	Hepatic impairments	NCT01565902	I
		Relapsing–remitting multiple sclerosis	NCT00879658	II
		Relapsing–remitting multiple sclerosis	NCT01185821	II
		Secondary progressive multiple sclerosis	NCT01665144	III
		Polymyositis, dermatomyositis	NCT01148810	II (terminated)
RPC1063	S1PR1 modulator	Relapsing–remitting multiple sclerosis	NCT01628393	II
		Ulcerative colitis	NCT01647516	II
ONO-4641	S1PR1 and S1PR5 agonist	Multiple sclerosis	NCT01226745	II
LX3305	S1P lyase inhibitor	Rheumatoid arthritis	NCT00847886	I (completed)
		Rheumatoid arthritis	NCT00903383	II (completed)
GSK2018682	S1PR1 agonist	Relapsing–remitting multiple sclerosis	NCT01466322	I (completed)
		Relapsing–remitting multiple sclerosis	NCT01431937	I (completed)
Ponesimod ACT-128800	S1PR1 agonist	Plaque psoriasis	NCT00852670	II (completed)
		Relapsing–remitting multiple sclerosis	NCT01093326	II
		Psoriasis	NCT01208090	II (completed)
		Relapsing–remitting multiple sclerosis	NCT01006265	II (completed)

In multiple sclerosis (MS), pathogenic central memory T (T_{CM}) cell clones committed to T helper 1 (T_H1) and T_H17 lineages are expanded following low-intensity cross-reaction on self-antigens in lymph nodes that drain the antigen from the central nervous system (CNS). T_{CM} cells egress from lymph nodes and recirculate to blood in a sphingosine 1-phosphate receptor 1 (S1PR1)-dependent manner (Matloubian *et al.*, 2004), and they invade the CNS following restimulation by self-antigen presented on leptomeningeal phagocytes (Bartholomäus, *et al.*, 2009). In the CNS, T_{CM} cells are reactivated by self-antigen presented on microglia and/or dendritic cells and this causes proliferation and local differentiation of effector T cells (T_E) and, perhaps, effector memory T cells (T_{EM}) (Kivisakk *et al.*, 2004). T_E cells activate astrocytes through interleukin-17 (IL-17) (Kang *et al.*, 2010), directly kill neural cells (Kebir *et al.*, 2007) and secrete inflammatory cytokines that activate sphingosine kinases (SPHKs) in many cell types (Chalfant & Spiegel, 2005). This increases the production of S1P, which may signal S1P receptors on many cell types to enhance neuroinflammation and gliosis (Sorensen *et al.* 2003; Chalfant & Spiegel, 2005; Nayak *et al.*, 2010; Rouach *et al.*, 2006). Down-modulation of lymphocytic $S1P_1$ receptors by fingolimod leads to retention of self-reactive T_{CM} cells in the lymph nodes and prevents their invasion into the CNS and their local clonal expansion and differentiation into T_E and T_{EM} cells (Matloubian, *et al.*; 2004; Pham *et al.*, 2008; Fujino *et al.*, 2003). It seems likely that fingolimod may retain all T_{CM} cell subsets in the lymph nodes, irrespective of T_H1, T_H2, T_H17 or cytolytic commitment, but it may spare all these subsets at the T_{EM} stage; this would not affect the therapeutic activity of fingolimod as terminal differentiation of T_{CM} cells into MS-pathogenic T_{EM} cells occurs at CNS sites rather than at peripheral lymphoid tissues (Kivisakk *et al.*, 2004; Bartholomäus, *et al.*, 2009; Chang *et al.*, 2003). In the CNS, down-modulation of S1P receptors on neural cells may reduce hyperactivation, particularly of astrocytes, by excess S1P (Kulakowska *et al.*, 2010; Choi *et al.*, 2009; Rouach *et al.*, 2006),

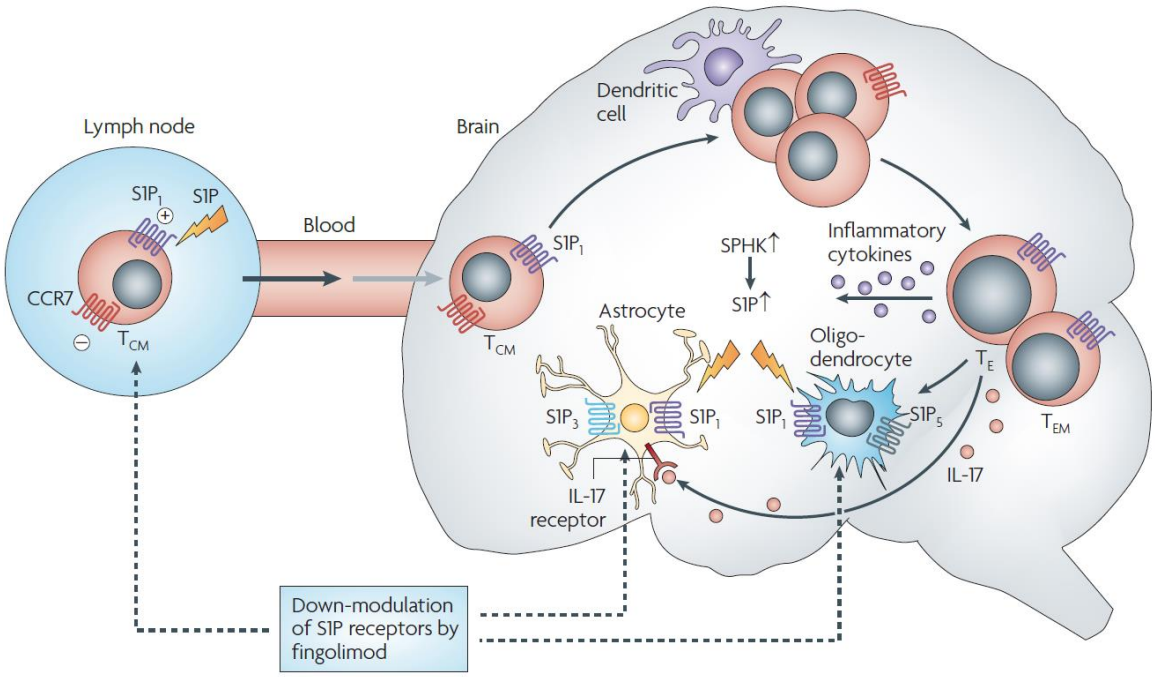

Figure 3: *Proposed model of the mode of action of Fingolimod in multiple sclerosis*

(Kunkel *et al*, 2013).

3. Analytical Methods

In contrast to other biological molecules, such as proteins, lipids constitute a highly diverse group whose physic-chemical nature can vary tremendously. Analytical methods based on identification, purification, separation and quantification of biomarkers constitute a challenge in the contemporary analysis. Human blood is a self-regenerating lipid-rich biological fluid that is routinely collected in hospital settings. The inventory of lipid molecules found in blood plasma (plasma lipidome) offers insights into individual metabolism and physiology in health and disease. Disturbances in the plasma Lipidome also occur in conditions that are not directly linked to lipid metabolism; therefore, plasma Lipidomics based on MS is an emerging tool in an array of clinical diagnostics and disease management. However, challenges exist in the

translation of such lipidomic data to clinical applications. These relate to the reproducibility, accuracy, and precision of lipid quantitation, study design, sample handling, and data sharing (Burla *et al*., 2018). However, the phenomenon of matrix effect is of primary concern in bioanalysis, when ESI LC-MS detection is used for quantitative purpose. The presence of co-eluted compounds affecting pH, ionic strength, surface tension or competing for the ionization process may strongly affect the ionization yield of target analytes compounds. Because the relevance of this problem FDA explicitly recommends investigating the occurrence of such effects when developing analytical methods (FDA. Bioanalytical Method Validation: Guidance for Industry, updated in May 2018). The most common techniques applied for the analysis of lipids are gas-chromatography (GC) and high-performance liquid chromatography (HPLC). Selective extraction of target analytes might reduce the matrix effects resulting in more accurate quantitative determination. On this edge, the so-called "*Molecularly Designed Materials Science*", defined as *the construction of ligand selective recognition sites in synthetic polymers where a template (atom, ion, molecule, complex or a molecular ionic or macromolecular assembly, including micro-organism)* could be an helpful technique to apply in the analytical field (Whitcombe *et al*., 2014). In fact, is employed in order to facilitate recognition site formation during the covalent assembly of the bulk phase by a polymerization or polycondensation process, with subsequent removal of some or all of the template being necessary for recognition to occur in the spaces vacated by the templating species. So, the Molecularly Imprinting Technology (**Figure 4**) constitute a method of making lock to match a molecular key, and it is a technique for the creation of molecular imprinting polymers (Chen *et al.*, 2016).

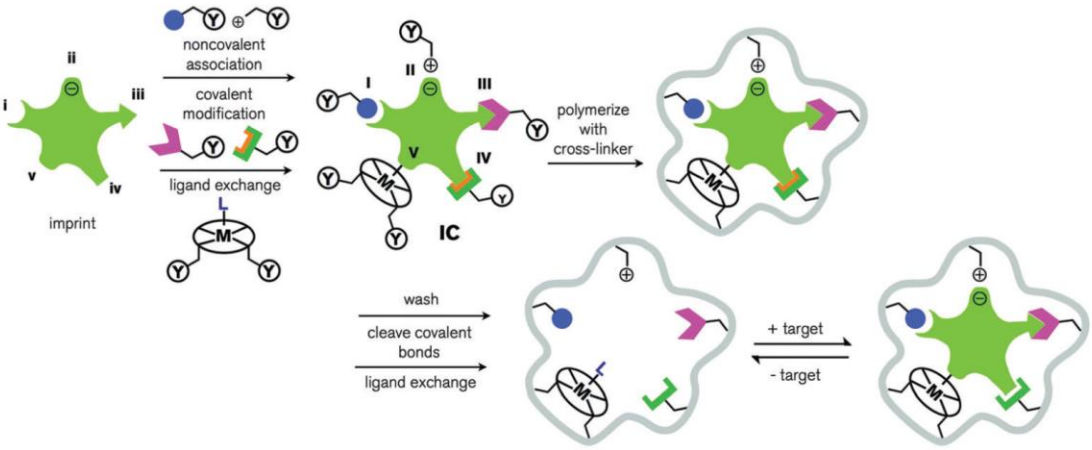

Figure 4: *Schematic representation of MIT*.

In the last years, attractive and competitive MIPs have found a wide range of applications, as diagrammatically shown in **Figure 5**. As seen, MIPs are widely used in sample pre-treatment and chromatographic separation (SPE, monolithic column chromatography, etc.) and sensing (electrochemical sensing, fluorescence sensing, etc.) of active molecules, pharmaceuticals, environmental pollutants and so on (Chen *et al.*, 2016).

So, in this contest, we designed our project.

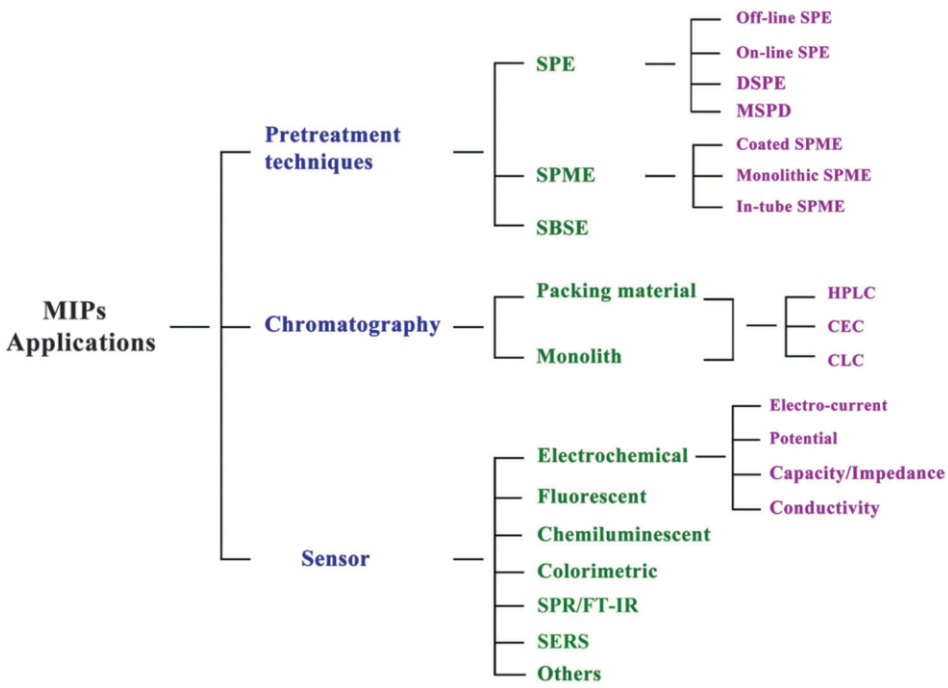

Figure 5: *Structural diagram of the applications of MIPs in pre-treatment techniques, chromatography and sensors* (Chen *et al.*, 2016).

4. Aim of the Project

The major aim of this project was the *development of advanced molecularly designed materials*, using the combination of the imprinting approach and supramolecular recognition properties (Lehn, 1995) of the macromolecules and of the solid substrate obtained, and their *evaluation* as media for selective pre-concentration and/or samples clean-up of pharmaceuticals, metabolites and biocompounds, assisting the research of biomarkers and drug discovery. In particular, we focused on the following points:

- the **synthesis of innovative stationary phases** selective for our target molecules. Due to elective steric interactions, realized using specific functional monomers, the materials behaviour could emulate the interactions established by natural receptors when retaining a selective target molecule. Moreover, because of their porous structure, these polymers usually had high adsorption capacity, and found an excellent application as stationary phases in the Solid Phase Extraction (SPE) technique.
- in parallel, the **validation of analytical methods** for easy, accurate, and fast detection of the targets. The analytical techniques employed in this project were liquid chromatography methods (UHPLC) coupled to UV-Vis spectroscopy and mass spectrometry (tandem mass, MS/MS). On the other end, fluorimetric methodologies represented another innovative way of quali-quantification of the biomarkers.
- the **application and assessment of useful platforms** in the clinical field. Since complex matrices, such as biofluids, consist of biomarkers treasure, it resulted of relevant importance to develop new diagnostic tools and improve the existing ones, in order to reduce the difficulty in obtaining reliable quantitative real-time results.

5. General Conclusions

At the end of the three years PhD activities, it was possible to selectively target biomarker molecules. We synthesized four different ***selective capture phases***: a *bulk resin*, a *composite sorbent* and an *etched material* were obtained combining the cationic bis-imidazolium functional monomer with divinylbenzene (DVB) crosslinker; fluorescent core-shell nanoparticles were obtained by RAFT polymerization of NBD-urea fluorescent monomer. All these synthesized stationary phases were designed ***to selectively target*** the signaling lipid ***S1P and the S1P-receptor antagonist FP***. Experiments on real samples (human plasma and human serum) were performed to study the matrix effect before and after samples pre-treatment. Recently, a ***new batches of selective capture phospholipids phases*** has been synthesized, by combination of phosphorous-recognition moieties of cationic bis-imidazolium and/or 1,3-diarylurea functional monomers and have been preliminarily tested.

In view of the methods optimization and applicability, and trying to obtain a LoD in the physio- (70-500 nM) and pathologically (higher than 10 µM) relevant concentrations of S1P, further work is required to ***translate these concepts into practically useful diagnostic systems***.

Bibliography

Aktas, O., Küry, P., Kieseier, B., Hartung, H. P., (2010), Fingolimod is a potential novel therapy for multiple sclerosis, *Nature Reviews. Neurology*, 6 (7), 373–82.

Aureli, M., Grassi, S., Prioni, S., Sonnino, S., Prinetti, A., (2015), Lipid membrane domains in the brain, *Biochimica et Biophysica Acta (BBA) – Molecular and Cell Biology of Lipids*, 1851 (8), 1006–16.

Bartholomäus, I., Kawakami, N., Odoardi, F., Schläger, C., Miljkovic, D., Ellwart, J.W., Klinkert, W.E., Flügel-Koch, C., Issekutz, T.B., Wekerle, H., Flügel, A., (2009), Effector T-cell interactions with meningeal vascular structures in nascent autoimmune CNS lesions, *Nature*, 462 (7269), 94–8.

Bioanalytical Method Validation, Guidance for Industry, U.S. Department of Health and Human Services, Food and Drug Administration, Center for Drug Evaluation and Research (CDER), May 2018, Biopharmaceutics, available at the following website link: http://www.fda.gov/Drugs/GuidanceComplianceRegulatoryInformation/Guidances/default.htm.

Breart, B., Ramos-Perez, W. D., Mendoza, A., Salous, A. K., Gobert, M., Huang, Y., Adams, R. H., Lafaille, J. J., Escalante-Alcalde, D., Morris, A.J., Schwab, S. R., (2011), Lipid phosphate phosphatase 3 enables efficient thymic egress, *Journal of Experimental Medicine*, 208 (6), 1267–78.

Brinkmann, V., (a) Davis, M.D., Heise, C.E., Albert, R., Cottens, S., Hof, R., Bruns, C., Prieschl, E., Baumruker, T., Hiestand, P., Foster, C.A., Zollinger, M., Lynch, K.R., (2002), The immune modulator, FTY720, targets sphingosine 1-phosphate receptors, *The Journal of Biological Chemistry*, 277 (24), 21453–57.

Brinkmann, V., (b) Billich, A., Baumruker, T., Heining, P., Schmouder, R., Francis, G., Aradhye, S., Burtin, P., (2010), Fingolimod (FTY720): discovery and development of an oral drug to treat multiple sclerosis, *Nature Reviews. Drug Discovery*, 9 (11), 883–97.

Brügger, B., (2014), Lipidomics: analysis of the lipid composition of cells and subcellular organelles by electrospray ionization mass spectrometry, *Annual Review of Biochemistry*, 83, 79–98.

Burla, B., Arita, M., Bendt, A.K., Cazenave-Gassiot, A., Dennis, E. A., Ekroos, K., Han, X., Ikeda, K., Liebisch, G., Lin, M. K., Loh, T. P., Meikle, P. J., Orešič, M., Quehenberger, O., Shevchenko, A., Torta, F., Wakelam, M. J. O., Wheelock, C. E., Wenk, M.R., (2018), MS-

based lipidomics of human blood plasma: a community-initiated position paper to develop accepted guidelines, *Journal of Lipid Research*, 59 (10), 2001-17.

Chalfant, C. E., and Spiegel, S., (2005), Sphingosine 1-phosphate and ceramide 1-phosphate: expanding roles in cell signalling, *Journal of Cell Science*, 118 (Pt. 20), 4605–12.

Chang, T. T., Sobel, R.A, Wei, T., Ransohoff, R.M., Kuchroo, V.K., Sharpe, A.H., (2003), Recovery from EAE is associated with decreased survival of encephalitogenic T-cells in the CNS of B7–1/B7-2-deficient mice, *European Journal of Immunology*, 33 (7), 2022–32.

Chen, L.; Wang, X.; Lu, W.; Wu, X.; Li, J., (2016), Molecular imprinting: perspectives and applications. *Chemical Society Reviews*, 45, 2137-2211.

Choi, J. W., Herr, D., Kennedy, G. and Chun, J., (2009), Astrocytic sphingosine 1-phosphate (S1P) receptor subtype 1 signalling influences levels of S1P and cytokines during experimental autoimmune encephalomyelitis and fingolimod (FTY720) intervention, *Multiple Sclerosis*, 15, S58.

Cyster, J. G., and Schwab, S. R., (2012), Sphingosine-1-phosphate and lymphocyte egress from lymphoid organs, *Annual Review of Immunology*, 30, 69–94.

Fujino, M., Funeshima, N., Kitazawa, Y., Kimura, H., Amemiya, H., Suzuki, S., Li, X.K., (2003), Amelioration of experimental autoimmune encephalomyelitis in Lewis rats by FTY720 treatment, *The Journal of Pharmacology and Experimental Therapeutics*, 305 (1), 70–7.

Fukuhara, S., Simmons, S., Kawamura, S., Inoue, A., Orba, Y., Tokudome, T., Sunden, Y., Arai, Y., Moriwaki, K., Ishida, J., Uemura, A., Kiyonari, H., Abe, T., Fukamizu, A., Hirashima, M., Sawa, H., Aoki, J., Ishii, M., Mochizuki, N., (2012), The sphingosine-1-phosphate transporter Spns2 expressed on endothelial cells regulates lymphocyte trafficking in mice, *Journal of Clinical Investigation*, 122 (4), 1416–26.

Gonzalez-Cabrera, P. J., Cahalan, S.M., Nguyen, N., Sarkisyan, G., Leaf, B.N., Cameron, M.D., Kago, T., and Rosen, H., (2012), $S1P_1$ receptor modulation with cyclical recovery from lymphopenia ameliorates mouse model of multiple sclerosis, *Molecular Pharmacology*, 81 (2), 166–174.

Graler, M. H., and Goetzl, E. J., (2004), The immunosuppressant FTY720 down-regulates sphingosine 1-phosphate G protein-coupled receptors, *The FASEB Journal*, 18 (3), 551–3.

Han, X., and Gross, R. W., (2003), Global analyses of cellular lipidomes directly from crude extracts of biological samples by ESI mass spectrometry, *Journal of Lipid Research*, 44 (6), 1071.

Hisano, Y., Kobayashi, N., Yamaguchi, A., Nishi, T., (2012), Mouse SPNS2 functions as a sphingosine 1-phosphate transporter in vascular endothelial cells, *PLoS ONE*, 7 (6), e38941.

Kang, Z., Altuntas, C.Z., Gulen, M.F., Liu, C., Giltiay, N., Qin, H., Liu, L., Qian, W., Ransohoff, R.M., Bergmann, C., Stohlman, S., Tuohy, V.K., Li, X., (2010), Astrocyte-restricted ablation of interleukin-17-induced Act1-mediated signalling ameliorates autoimmune encephalomyelitis, *Immunity*, 32 (3), 414–425.

Kawahara, A., Nishi, T., Hisano, Y., Fukui, H., Yamaguchi, A., Mochizuki, N., (2009), The sphingolipid transporter spns2 functions in migration of zebrafish myocardial precursors, *Science*, 323 (5913), 524–527.

Kebir, H., Kreymborg, K., Ifergan, I., Dodelet-Devillers, A., Cayrol, R., Bernard, M., Giuliani, F., Arbour, N., Becher, B., Prat, A., (2007), Human TH17 lymphocytes promote blood–brain barrier disruption and central nervous system inflammation, *Nature Medicine*, 13 (10), 1173–1175.

Kim, R. H., Takabe, K., Milstien, S., Spiegel, S., (2009), Export and functions of sphingosine-1-phosphate, *Biochimica and Biophysica Acta*, 1791 (7), 692–696.

Kivisakk, P., Mahad, D.J., Callahan, M.K., Sikora, K., Trebst, C., Tucky, B., Wujek, J., Ravid, R., Staugaitis, S.M., Lassmann, H., Ransohoff, R.M., (2004), Expression of CCR7 in multiple sclerosis: implications for CNS immunity, *Annuals of Neurology*, 55 (5), 627–638.

Kulakowska, A. Zendzian-Piotrowska, M., Baranowski, M., Konończuk, T., Drozdowski, W., Górski, J., Bucki, R., (2010), Intrathecal increase of sphingosine 1-phosphate at early stage multiple sclerosis, *Neuroscience Letters*, 477 (3), 149–152.

Kunkel, G. T., Maceyka, M., Milstien, S. and Spiegel, S., (2013), Targeting the sphingosine-1-phosphate axis in cancer, inflammation and beyond, *Nature Review. Drug Discovery*, 12 (9), 688-702.

Lehn, J. M., (1995), *Supramolecular Chemistry*, Wiley-VCH Verlag GmbH & Co. KGaA.

Maceyka, M., Harikumar, K. B., Milstien, S., Spiegel, S., (2012), Sphingosine 1-Phosphate signaling and its role in disease, *Trends in Cell Biology*, 22 (1), 50-60.

Mandala, S., Hajdu, R., Bergstrom, J., Quackenbush, E., Xie, J., Milligan, J., Thornton, R., Shei, G. J., Card, D., Keohane, C., Rosenbach, M., Hale, J., Lynch, C. L., Rupprecht, K., Parsons, W., Rosen, H., (2002), Alteration of lymphocyte trafficking by sphingosine-1-phosphate receptor agonists, *Science*, 296 (5566), 346–9.

Matloubian, M., Lo, C. G., Cinamon, G., Lesneski, M. J., Xu, Y., Brinkmann, V., Allende, M. L., Proia, R. L., Cyster, J. G., (2004), Lymphocyte egress from thymus and peripheral lymphoid organs is dependent on S1P receptor 1, *Nature*, 427 (6972), 355–60.

Mendoza, A., Bréart, B., Ramos-Perez, W. D., Pitt, L. A., Gobert, M., Sunkara, M., Lafaille, J. J., Morris, A. J., Schwab, S. R., (2012), The transporter Spns2 is required for secretion of lymph but not plasma sphingosine- 1-phosphate, *Cell Reports*, 2 (5), 1104–10.

Nagahashi, M., Kim, E.Y., Yamada, A., Ramachandran, S., Allegood, J. C., Hait, N. C., Maceyka, M., Milstien, S., Takabe, K., Spiegel, S., (2013), Spns2, a transporter of phosphorylated sphingoid bases, regulates their blood and lymph levels, and the lymphatic network, *The FASEB Journal*, 27 (3), 1001–11.

Nayak, D., Huo, Y., Kwang, W. X., Pushparaj, P. N., Kumar, S. D., Ling, E. A., Dheen, S. T., (2010), Sphingosine kinase 1 regulates the expression of proinflammatory cytokines and nitric oxide in activated microglia, *Neuroscience*, 166 (1), 132–44.

Pham, T. H., Okada, T., Matloubian, M., Lo, C. G. & Cyster, J. G., (2008), S1P1 receptor signaling overrides retention mediated by $G_{\alpha i}$-coupled receptors to promote T-cell egress, *Immunity*, 28 (1), 122–33.

Pruett, S. T., Bushnev, A., Hagedorn, K., Adiga, M., Haynes, C. A., Sullards, M. C., Liotta, D. C., Merrill, A. H., (2008), *Thematic Review Series*: Sphingolipids. Biodiversity of sphingoid bases ("sphingosines") and related amino alcohols, *Journal of Lipid Research*, 49 (8), 1621–39.

Pyne, N. J., and Pyne, S., (2010), Sphingosine 1-phosphate and cancer, *Nature Reviews. Cancer*, 10 (7), 489–503.

Rouach, N., Pébay, A., Même, W., Cordier, J., Ezan, P., Etienne, E., Giaume, C., Tencé, M., (2006), S1P inhibits gap junctions in astrocytes: involvement of G and Rho GTPase/ROCK, *European Journal of Neuroscience*, 23 (6), 1453–64.

Santos, C. R., and Schulze, A., (2012), Lipid metabolism in cancer, *FEBS Journal*, 279 (15), 2610–23.

Sellergren, B., (2001), *Molecularly Imprinted Polymers. Man-Made mimics of antibodies and their application in analytical chemistry*, Elsevier (Amsterdam).

Sorensen, S. D., Nicole, O., Peavy, R. D., Montoya, L. M., Lee, C. J., Murphy, T. J., Traynelis, S. F., Hepler, J. R., (2003), Common signaling pathways link activation of murine PAR-1, LPA, and S1P receptors to proliferation of astrocytes, *Molecular Pharmacology*, 64 (5), 1199–209.

Spiegel, S., and Milstien, S., (2011), The outs and the ins of sphingosine-1-phosphate in immunity, *Nature Reviews: Immunology*, 11 (6), 403–15.

Whitcombe, M. J., Kirsch, N., Nicholls, I. A., (2014), Molecular imprinting science and technology: a survey of the literature for the years 2004-2011, *Journal of Molecular Recognition*, 27, 297-401.

Yatomi, Y., Igarashi, Y., Yang, L., Hisano, N., Qi, R., Asazuma, N., Satoh, K., Ozaki, Y., Kume, S., (1997), Sphingosine 1-phosphate, a bioactive sphingolipid abundantly stored in platelets, is a normal constituent of human plasma and serum, *Journal of Biochemistry*, 121 (5), 969-73.

PART 2

Part 2

CHAPTER I

Synthesis and Evaluation of Molecularly Designed Materials as Selective Capture Phase for Improvement of Phosphor-Monoester Lipids Detection

1.1 Introduction

Sphingolipids represent an important class of lipids considered as units in membranes building blocks and components of myelin, fundamental substance that covers nervous fibers and allows neurons connection. Among them, Sphingosine 1-Phosphate (S1P) (Kunkel *et al.,* 2013; Yatomi *et al.,* 1997), a physiological metabolite of sphingosine pathway, has been recognized as a relevant biomarker for neurodegenerative diseases, and its analogue FTY720 (F, Fingolimod, commercially known as Gilenya™, Novartis) has been approved by FDA for the treatment of relapsing-remitting multiple sclerosis (Brinckmann *et al.*, 2010). Focusing on these targets, we here report about new selective sorbents to detect the natural biomarker S1P and its analogue drug FTY720-P (FTY720-P, FP). The bulk resin, the composite sorbent and the etched material microparticles were synthesized through a radical co-polymerization between the bis-imidazolium FM and the crosslinker divinylbenzene (DVB) in a porogen media, in presence of the thermal initiator ABDV. Early batch binding tests and the successively application, such as SPEs, using a mixture of standard lipids in pure solvent and then spiked real samples (human plasma and human serum) demonstrated the affinity of the synthesized stationary phases towards S1P and FTY720-P. This evidence proved that lipids containing phosphorus-diester moiety in their structures did not constitute obstacles for the interaction of phosphorus-monoester lipids when loaded into an SPE cartridge.

1.2 Results and Discussion

Nowadays, there is a constant need of adequate tools for studying important biomarkers, being obstacles for the development of effective diagnostic tools and treatment. Methods based on the molecular recognition, such as solid phase extraction (SPE), immuno-affinity extraction (IAE), and molecularly imprinted polymers (MIPs) have been developed and could be considered promising approach to identify and quantify specific biomarkers.

The phenomenon of matrix effect is of primary concern in bioanalysis when ESI LC-MS detection is used for quantitative purpose. The presence of co-eluted compounds, affecting pH, ionic strength, and surface tension or competing for the ionization process, may strongly affect the ionization yield of target analytic compounds. Because of the relevance of this problem, US-FDA explicitly recommend to investigate the occurrence of such effects when developing analytical methods (Bioanalytical Methods Validation, updated in May 2018). Selective extraction of target analytes might reduce the matrix effects resulting in more accurate quantitative determination. In this study new stationary phases were evaluated for the selective extraction of S1P and its analogue FP, arising from the administration of F.

With this aim, we here present molecularly designed materials able to capture phospholipids in a highly specific manner in complex bio-media, such as human plasma and human serum, greatly simplifying LC-MS/MS detection and quantification of the phosphometabolite S1P (**Figure 1.1**), its analogue FP (**Figure 1.2**), and the pro-drug F (**Figure 1.3**), whose structures are reported in the following page.

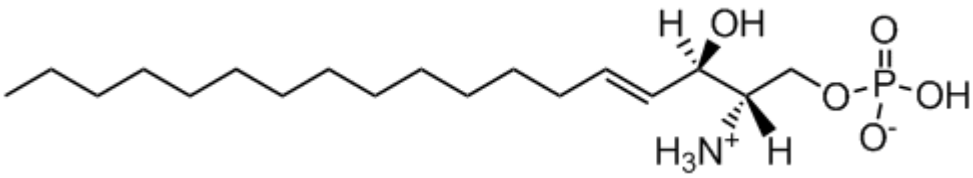

Figure 1.1: *Structure of Sphingosine 1-Phosphate (S1P).*

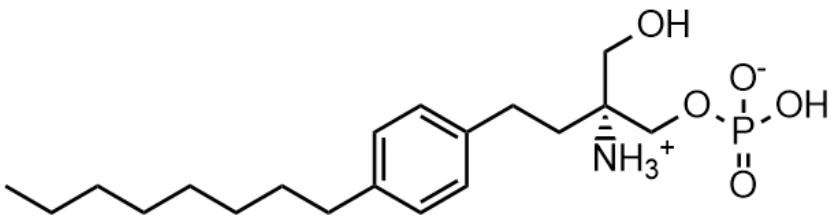

Figure 1.2: *Structure of S1P analogue Fingolimod Phosphate (FP).*

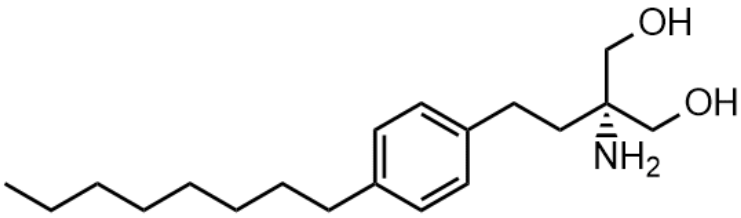

Figure 1.3: *Structure of the pro-drug Fingolimod.*

Based on previous studies carried out in our lab (Narayanaswamy *et al.*, 2014), the aim of this work was to investigate the ability of bis-imidazolium based FM to coordinate the phosphate group of target molecules S1P and FP in a hydrophobic network created by the crosslinker DVB, in the shape of a bulk material, and on the surface of amino-modified silica microparticles (D ≈ 25-40 µm), resulting in a composite sorbent and an etched material.

From a host-guest chemistry point of view, by molecular recognition it is possible to generate selective interactions. The design of monomers with specific functionalities bears to the creation of artificial receptors able to trap class-selective compounds. This kind of receptors can be divided into *charged hosts*, which recognition is driven by ion pairing (e.g. Brönsted acid-base interactions) (Beach & Shea, 1994; Wulff *et al*., 1997; Cutivet *et al*., 2009), and *neutral hosts* binding the anions primarily by hydrogen bonding (Hall *et al.*, 2005; Emgenbroich *et al.*, 2008). These categories of hosts typically display different solvent dependencies, for example, the ionic interactions which operate over a longer range are less susceptible to the presence of water than hydrogen bonding receptors where water can dramatically alter or even suppress binding (Langton *et al*., 2016; Wierzbicka (a) *et al*., 2017).

Since the majority of biofluids consists of high percentage of water, a polar solvent that is able to form hydrogen bonds, we choose as host monomer for this study the bis-imidazolium based FM, a charged receptor that can take advantage of the electrostatic effect, and thus compete more effectively with polar protic solvents. In fact, imidazolium-based receptors can interact with anions through $(C\text{-}H)^{+}$---X^{-} type of ionic hydrogen bond, as shown in **Figure 1.4** (Wierzbicka (b), 2017).

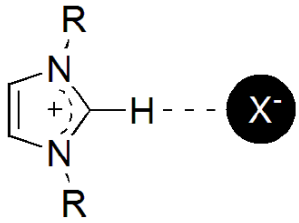

Figure 1.4: *Schematic representation of the ionic hydrogen bond interaction between imidazolium receptor and anion X⁻* (Wierzbicka (b), 2017).

In detail, imidazolium cycles (host) have been recognized as chemical moieties able to co-ordinate phosphate ions (guest) through strong hydrogen bonds between the carbon atoms (-C-H) of imidazolium and the oxygen atoms (O=P- and OH-P-) of $H_2PO_4^-$ (Kim *et al.*, (a) 2003). An additional hydrogen bond has been derived from the pyridinium heterocycle used as spacer (Q) between the imidazolium moieties and gave a further stabilization in the binding between host and guest (**Figure 1.5**). In this way, it has been possible to design class-selective materials in which bis-imidazolium functional monomer (Sulc *et al.*, 2017) has acted as receptor of phosphate anions in a co-operative manner (**Figure 1.6**).

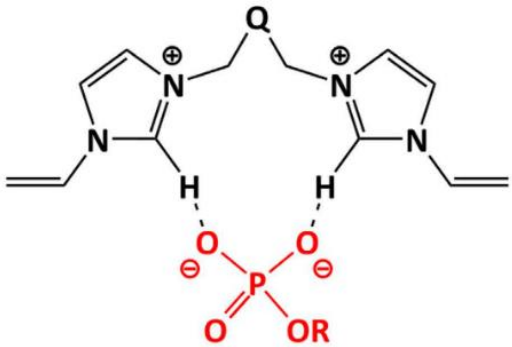

Figure 1.5: *Model of imidazolium moiety and its interaction with the phosphate targets. Q is a spacer specie.*

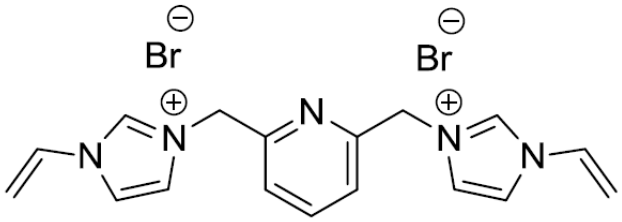

Figure 1.6: *Structure of bis-imidazolium based FM synthesized for in this study.*

The interaction between the bis-imidazolium based FM and anionic targets was accurately studied in the work of Sulc *et al*., 2017, using NMR titration. As they reported, bis-imidazolium hosts typically show preference for binding dianions and multiply charged species (Kim *et al*., (b) 2008). For this reason, they tested the ability of bis-imidazolium, having two cationic sites and so two hydrogen bond donor sites, to complex PPA-2TBA (**Figure 1.7**). The divalent anion interacted strongly with the monomer, when titration was performed in CD_3OD, confirming the strong electrostatic contribution to the binding (Wierzbicka (a) *et al*., 2017). In **Table 1.1** are reported experimental data obtained from the titration and the association constant K_a, resulted from curve fitting using Hill equation, was 1680 M^{-1}(Sulc *et al*., 2017; Wierzbicka (a) *et al*., 2017).

Table 1.1: *Association constant, stoichiometry and complexation induced shifts for complexes formed between bis-imidazolium host monomer and PPA-2TBA guest in methanol-d_4.*

[a] Complexation induced shifts (CIS) and Hill slope based on the shift value of the resonance signals indicated (Sulc *et al*., 2017; Wierzbicka (a) *et al*., 2017).

Host monomer	Guest	Proton	K_a (M^{-1})	Cplx (H:G)	CIS[a] (ppm)	h[a]
Bis-imidazolium	PPA-2TBA	CH (D, D)	1680±121	1:2	0.15	1.9

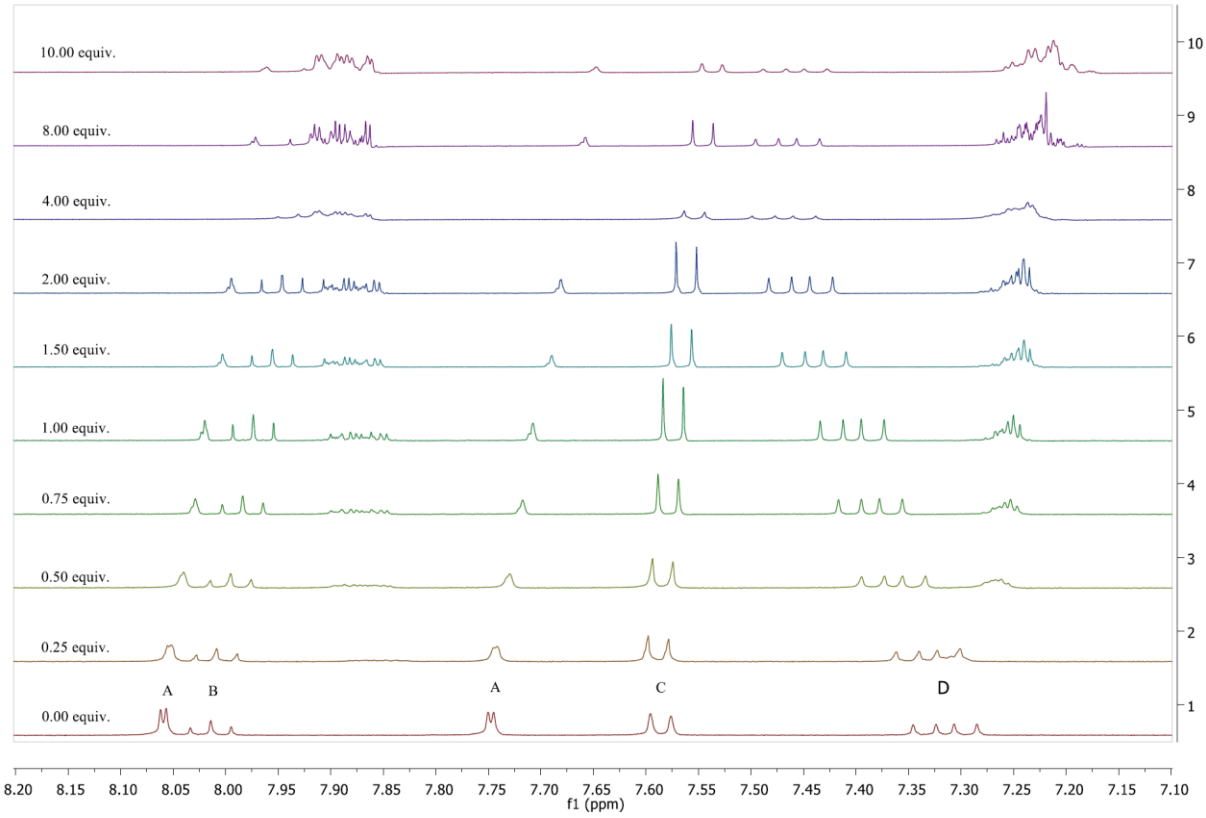

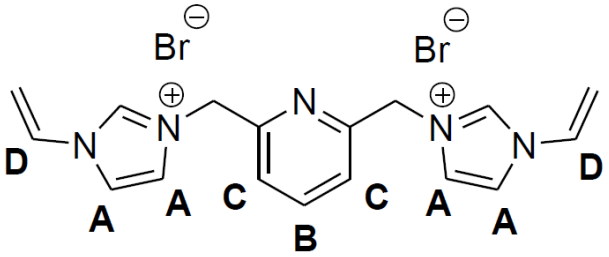

Figure 1.7: *^{1}H-NMR spectra of bis-imidazolium based FM upon increasing additions of up to 10 equivalents of PPA-2TBA in CD_3OD* (Sulc *et al*., 2017).

Based on these knowledges, a batch of molecularly designed materials was synthesized, and their formulation is reported in **Table 1.2**.

The monolith phase was prepared by co-polymerization using bis-imidazolium based FM and DVB or EGDMA as crosslinker. The FM-CL complex was dissolved in a porogen anhydrous MeOH:Toluene (1:1, v/v) solution, in 1:40 stoichiometric ratio. After polymerization, the synthesized bulk polymer was crushed and sieved to obtain particles in the size range 50-25 μm, then washed, and the solvent was extracted by Soxhlet apparatus. The final microparticles were dried in oven at 60°C overnight.

To obtain the composite polymer, amino-functionalized silica (NH_2@SiMPs) was modified to yield *N*-acetylated silica microparticles (AcNH@SiMPs). This process allowed protection and end-capping of silica particles. Deaerated and purged AcNH@Si could soak the pre-polymerization mixture, prepared with the same protocol used for the bulk material, until particles were freely flowing, indicating that all the pores were filled. At the end of the polymerization reaction, the sorbent was washed, and the solvent was extracted in a Soxhlet apparatus. The resulting composite beads were then dried under vacuum overnight. Part of the composite sorbent was processed with an etching solution (NH_4HF), in order to further improve the surface area binding sites. After treatment, the etched particles were washed, and the solvent extracted in a Soxhlet apparatus.

Table 1.2: *Composition of molecularly designed materials.*

POLYMERs	***FM***	***CL***	***Molar ratio FM/CL***	***Porogen***
Bulk resin DVB	Bis-IMI	DVB	1:40	MeOH/Tol
Bulk resin EGDMA	Bis-IMI	EGDMA	1:40	MeOH/Tol
Composite sorbent DVB	Bis-IMI	DVB	1:40	MeOH/Tol
Composite sorbent EGDMA	Bis-IMI	EGDMA	1:40	MeOH/Tol
Etched material DVB	Bis-IMI	DVB	1:40	MeOH/Tol
Etched material EGDMA	Bis-IMI	EGDMA	1:40	MeOH/Tol

In order to study the affinity and the maximum capacity of the materials to retain phosphorous-containing molecules S1P and FP, a basic and simple batch binding test was performed by RP HPLC-UV analysis, using as target PPA in a methanolic concentration range between 0.025-1 mM. After calibration curve plot, the peak areas obtained from the batch binding injections were used quantify the amount of analyte per unit mass of the polymer (B, in µmol g^{-1}) using the following equation:

$$B=(C_0-C_f)\cdot V/m$$

where C_0 was the initial standard concentration, C_f was the free target concentration detected in the supernatant solution, V was the total volume of the sample, and m was the mg of polymer used for the test.

Results reported in **Figure 1.8**, **Figure 1.9** and **Table 1.3** lighted up a better binding capacity for the bulk resin, the composite sorbent and the etched material prepared using DVB as CL, in comparison to the same EGDMA crosslinked materials.

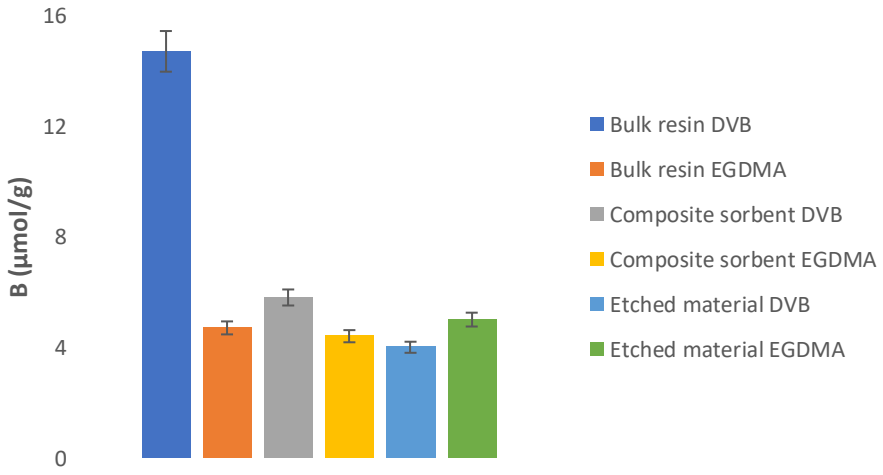

Figure 1.8: *Results of the batch binding test of PPA for resins, composite sorbents and etched materials. The bars show the average of three replicas and the error bars represent SD.*

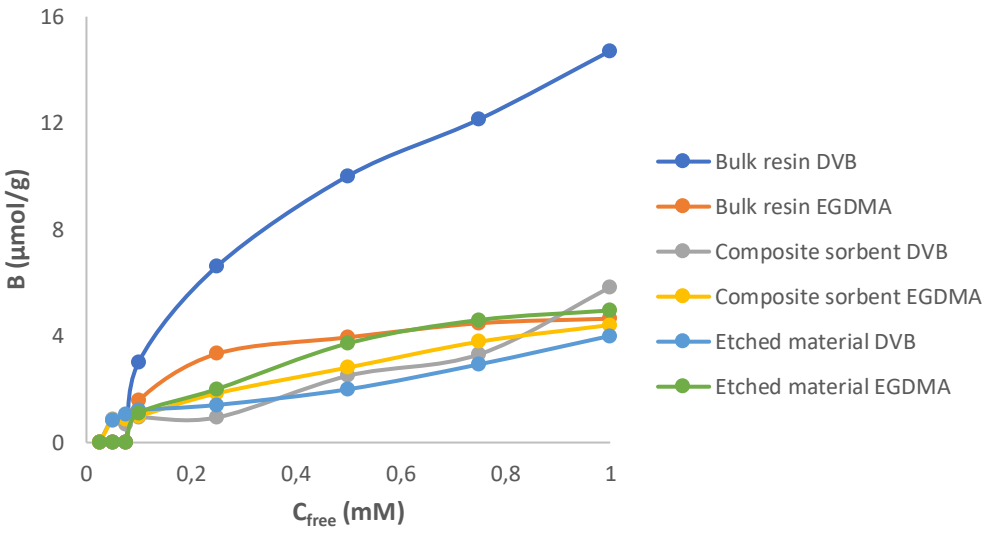

Figure 1.9: *Binding isotherm*. The data points were recorded for 0.025-1.0 mM concentration of the analyte PPA.

Table 1.3: *Binding capacity (B_{max}) towards PPA of synthesized materials*.

Polymers	**B_{max} (µmol/g)**
Bulk resin DVB	14,7
Bulk resin EGDMA	4,7
Composite sorbent DVB	5,8
Composite sorbent EGDMA	4,4
Etched material DVB	4
Etched material EGDMA	5

In order to compare and deeply investigate the cross-selectivity of the DVB crosslinked sorbent materials, SPE experiments were performed using our previous reported protocols (Narayanaswamy *et al.*, 2014; Shinde *et al.*, 2018). Standard mixture of monoester- and diester-phospholipids (**Table 1.4**) were loaded on each material after packing into SPE cartridges using on the top and at the bottom filters with 10 µm pore size (Mobicol Classic, MoBiTec).

For the bulk resin (particles size range 50-25 µm), the cartridge was equilibrated with 3 x 1 mL IPA. The loading fraction was passed through the cartridge twice. The washing steps were

executed with 1 mL 2-propanol and 1 mL MeOH:IPA (1/1, v/v). The elution fractions were collected with 2 x 0.8 mL MeOH:$CHCl_3$ (1/1, v/v) plus 1%TFA. For the composite sorbent and etched material, the cartridges were preliminary washed with H_2O and MeOH, suddenly were conditioned using 3 x 1 mL regeneration buffer MeOH/Acetic Acid/H_2O (6/3/1, v/v/v), 3 x 1 mL 2-propanol, 3 x 1 mL ACN. Next, the loading fraction was passed through the cartridge twice. The washing steps were performed with 1 mL ACN, 2 x 1 mL IPA. The elution fractions were collected three times by adding 0.8 mL MeOH plus 0.1% TFA.

All fractions were then dried under vacuum and reconstituted in 100 µL MeOH, sonicated for 10 minutes and transferred into insert vial for MALDI-TOF and LC-MS analysis. All the cartridges prepared have been reused after regeneration step (3 x 1 mL MeOH/Acetic Acid/H_2O (6/3/1, v/v/v%)) and equilibration to obtain experiments in triplicate.

The workflow of the experiment is schematically represented in **Figure 1.10**.

Table 1.4: *List of phospholipids used in SPE experiments*.

	Lipids	Abbr.	M. W. (g/mol)
Phosphorus-monoester lipids	Sphingosine 1-Phosphate	S1P	379.472
	Fingolimod Phosphate (FTY720-P)	FP	387.457
No Phosphorus-lipid	Fingolimod (FTY720)	F	307.471
Phosphorus-diester lipids	1,2-Dimyristoyl-sn-glycero-3-phosphorylglycerol (sodium salt)	DMPG	688.843
	1,2-Dimyristoyl-sn-glycero-3-phosphocholine	DMPC	677.933
	1,2-Dimyristoyl-sn-glycero-3-phosphoethanolamine	DMPE	635.853
	1,2-Dimyristoyl-sn-glycero-3-phosphoserine (sodium salt)	DMPS	701.844
	1,1',2,2'-tetramyristoyl cardiolipin (sodium salt)	CL	1285.597

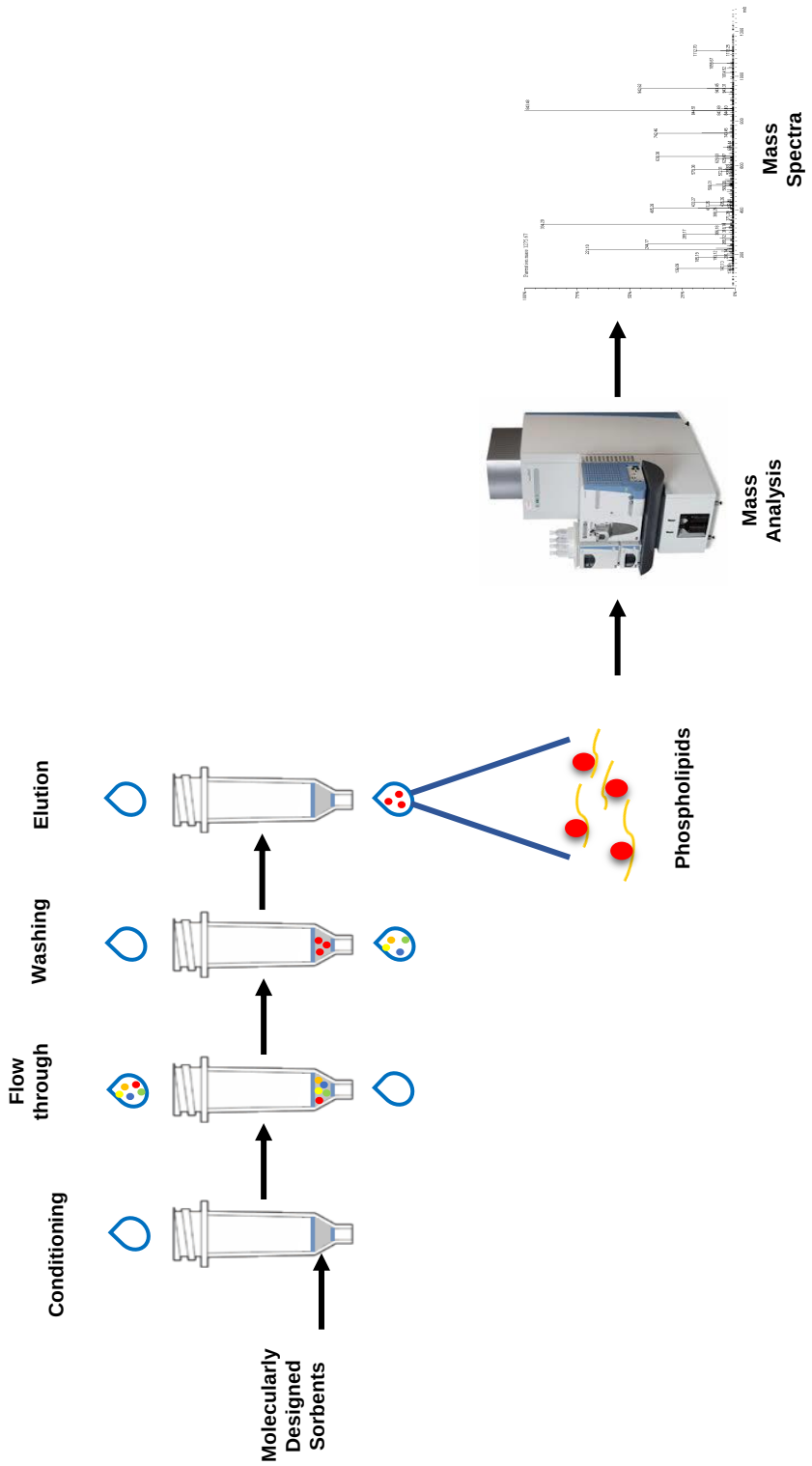

Figure 1.10: *Workflow of phospholipids enrichment and MS analysis.*

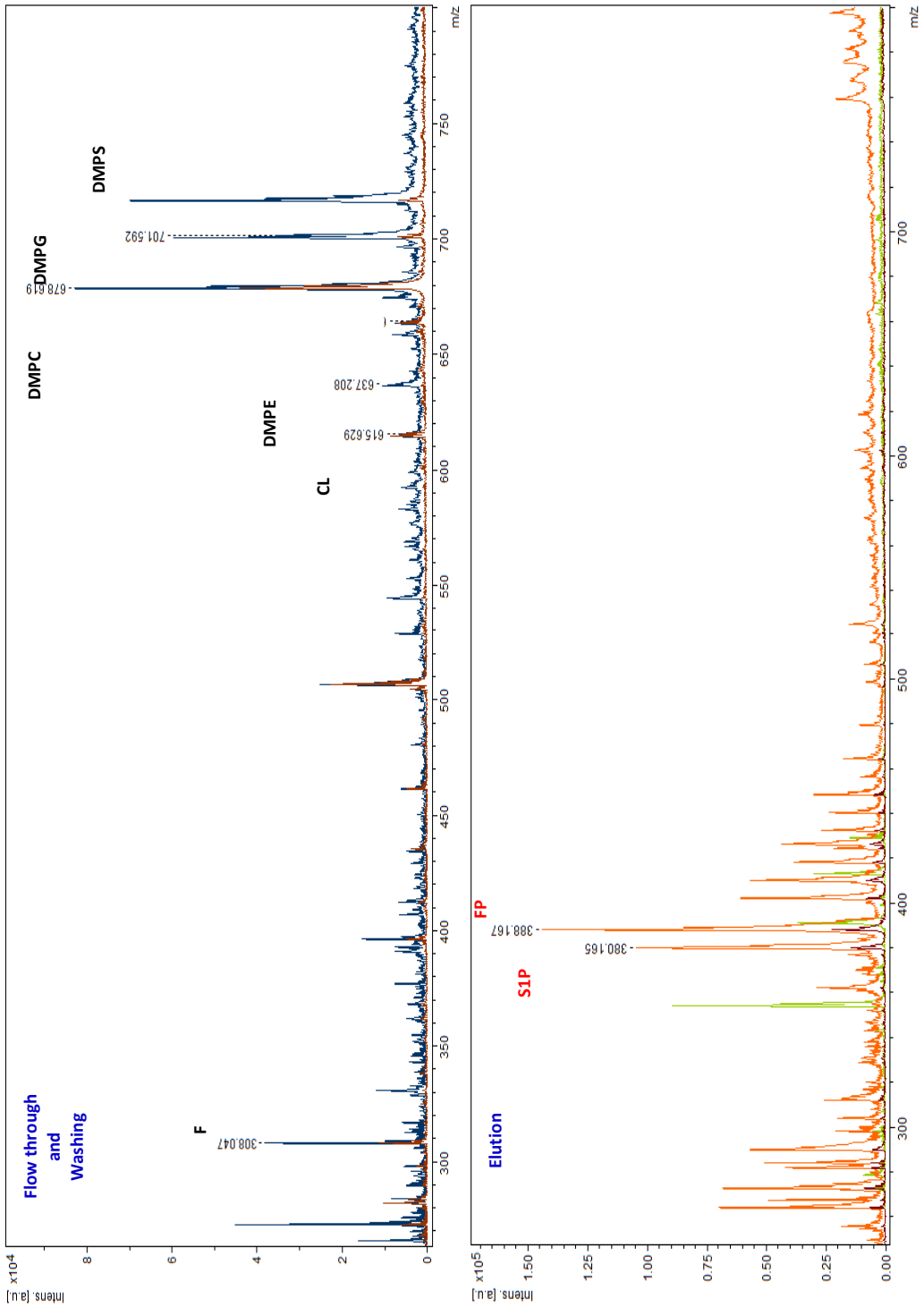

Figure 1.11: *MALDI MS recorded for phospholipids standards mixture of FT and W, and E SPE fractions after reconstitution in 100 µL of MeOH.* Marked in red letters are target molecules of interest, in black letters other lipids and phospholipids.

For a fast screening and low-cost check up of the SPE fractions, MALDI-TOF analysis, set up in linear mode, was performed. As it is possible to note from **Figure 1.11**, all lipids with no phosphate groups or with phosphorus-diester moiety in their structures were recovered in the loading and washing fractions, retaining and eluting only target molecules S1P and FP.

After optimization of LC-MS/MS method, using MRM mode, the effectiveness of DVB crosslinked materials was investigated for their use in SPE sample pre-treatment of real samples, such as human plasma and human serum samples. For the purpose, the effectiveness of the sample extraction/desorption procedure was preventively evaluated. Results of the elution curve of the composite sorbent, reported in **Figure 1.12,** demonstrated that analytes are efficiently retained by the SPE cartridge during the loading and the washing steps.

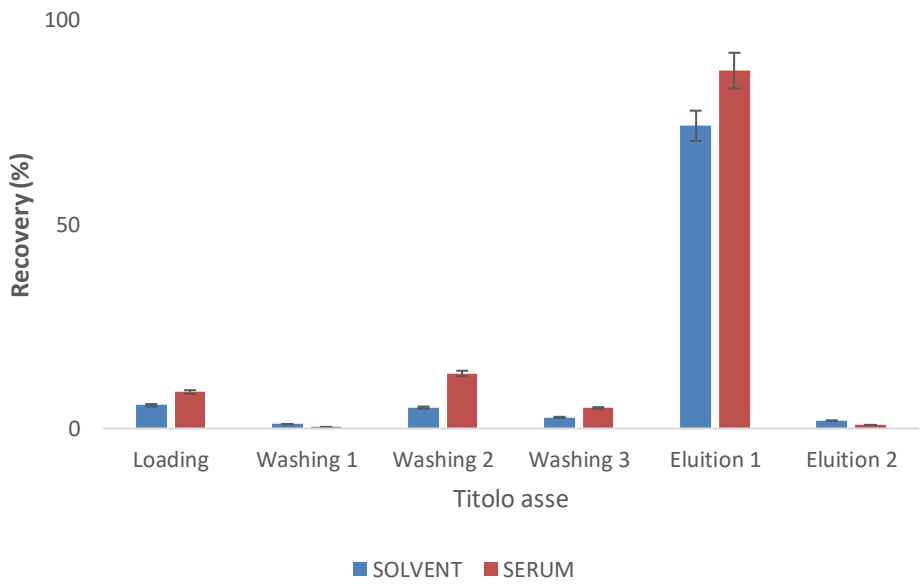

Figure 1.12: *Elution/desorption curve of S1P for selective SPE composite cartridges.*

Furthermore, the analytes are quantitatively desorbed using 1 ml of eluting solvent (**Figure 1.13**).

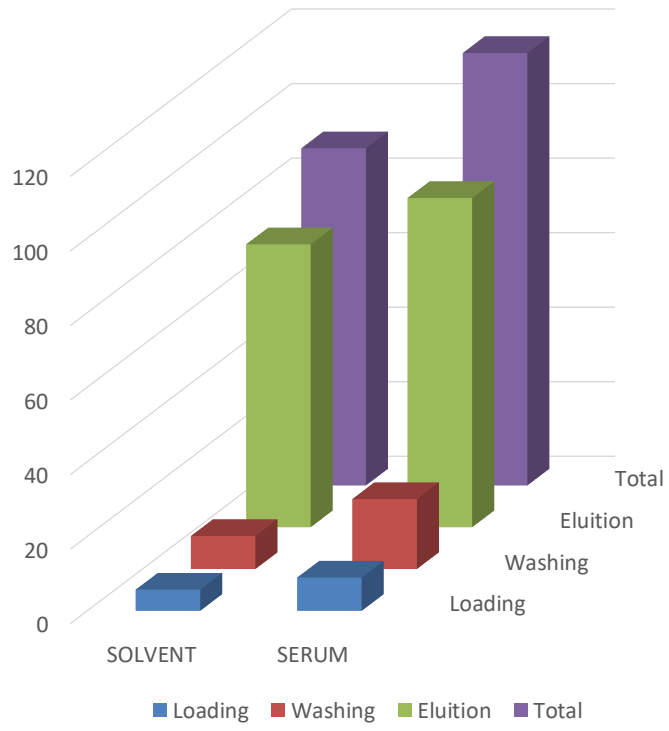

Figure 1.13: *The slight differences in recovery results calculated using the different calibration methods demonstrate the effective reduction of the matrix effect.*

Subsequently recovery experiments were performed from simulated (solvent) samples and real human samples. Recovery were calculated using external standards in both pure spiked solvent and spiked SPE pre-treated matrix samples. The results are reported in the following pages (**Table 1.5**, **Table 1.6**, **Table 1.7** and **Figure 1.14**).

So, the enrichment step represented a benefit for LC-MS detection of the target molecules that could be observed in a preference manner after sample pre-treatment using the composite sorbent.

Table 1.5: *Recovery studies of flow FT+W and E fractions of bulk resin in spiked H. plasma and serum*. Data reported are the results of averages of triplicate experiments.

***BULK RESIN in* H. Plasma**

H. plasma	Replicate 1	Replicate 2	Replicate 3	
	FT+W	**FT+W**	**FT+W**	**Mean**
S1P	15,1	10,4	12,8	12,8
FP	5,4	13,5	7,8	8,9
F	98	87,6	90,5	92
	E	**E**	**E**	**Mean**
S1P	80,2	62,5	59,6	67,4
FP	88,3	73,6	70,2	77,4
F	0,5	5,3	4,6	3,5

***BULK RESIN in* H. Serum**

H. serum	Replicate 1	Replicate 2	Replicate 3	
	FT+W	**FT+W**	**FT+W**	**Mean**
S1P	ND	7,0	50,3	16,5
FP	ND	10,4	5,4	5,3
F	84,5	91,7	58,7	7,.3
	E	**E**	**E**	**Mean**
S1P	99,4	90	47,3	77,6
FP	83,3	88,8	65,8	79,3
F	3,1	4,6	4,8	4,2

Table 1.6: *Recovery studies of flow FT+W and E fractions of composite sorbent in spiked H. plasma and serum*. Data reported are the results of averages of triplicate experiments.

***COMPOSITE SORBENT in* H. Plasma**				
H. plasma	**Replicate 1**	**Replicate 2**	**Replicate 3**	
	FT+W	**FT+W**	**FT+W**	**Mean**
S1P	0,7	0,6	0,9	0,7
FP	ND	ND	ND	0
F	131,0	119,4	127,9	126,1
	E	**E**	**E**	**Mean**
S1P	34,2	45,9	54,5	44,.8
FP	ND	ND	154,1	51,4
F	ND	ND	ND	0
***COMPOSITE SORBENT in* H. Serum**				
H. serum	**Replicate 1**	**Replicate 2**	**Replicate 3**	
	FT+W	**FT+W**	**FT+W**	**Mean**
S1P	60,0	45,0	45,0	16,7
FP	27,0	20,0	21,0	22,7
F	151,0	288,0	201,0	71,1
	E	**E**	**E**	**Mean**
S1P	101,5	105,2	100,1	102,2
FP	110,3	105,3	120,4	111,9
F	15	9	11,3	11,7

Table 1.7: *Recovery studies of FT+W and E fractions of etched material in spiked H. plasma and serum*. Data reported are the results of averages of triplicate experiments.

***ETCHED MATERIAL in* H. Plasma**				
H. plasma	**Replicate 1**	**Replicate 2**	**Replicate 3**	
	FT+W	**FT+W**	**FT+W**	**Mean**
S1P	0,2	0,2	0,5	0,3
FP	ND	ND	ND	0
F	132,6	118,6	102,3	117,8
	E	**E**	**E**	**Mean**
S1P	29,4	28,8	32,5	30,2
FP	91,9	91,9	83,1	89,0
F	ND	ND	ND	0
***ETCHED MATERIAL in* H. Serum**				
H. serum	**Replicate 1**	**Replicate 2**	**Replicate 3**	
	FT+W	**FT+W**	**FT+W**	**Mean**
S1P	0.6	0,5	0,3	0,5
FP	ND	ND	ND	0
F	100,7	116,4	108,9	108,7
	E	**E**	**E**	**Mean**
S1P	14,5	25,1	38,3	26,0
FP	44,7	114,0	78,3	79,0
F	ND	ND	ND	0

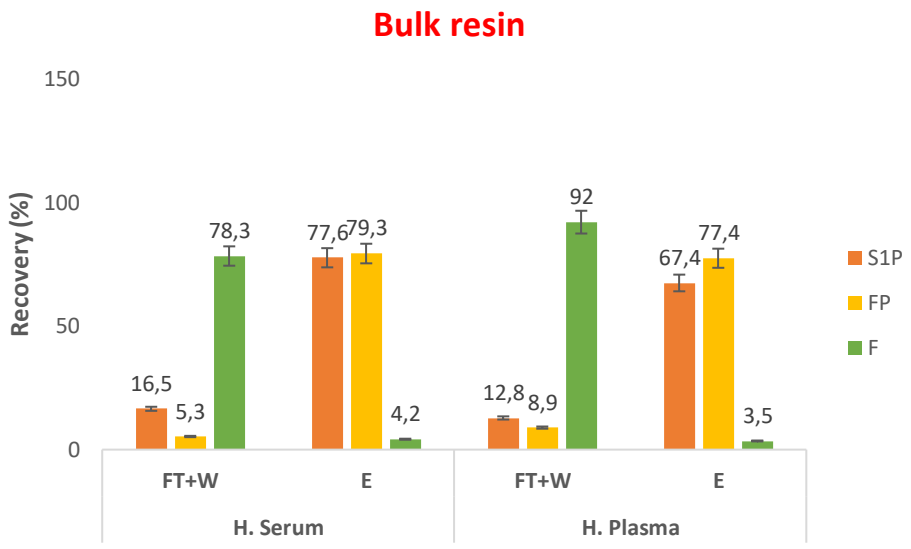
Bulk resin
150
100
50
0
Recovery (%)
16,5
5,3
78,3
77,6
79,3
4,2
12,8
8,9
92
67,4
77,4
3,5
FT+W
E
FT+W
E
H. Serum
H. Plasma
S1P
FP
F

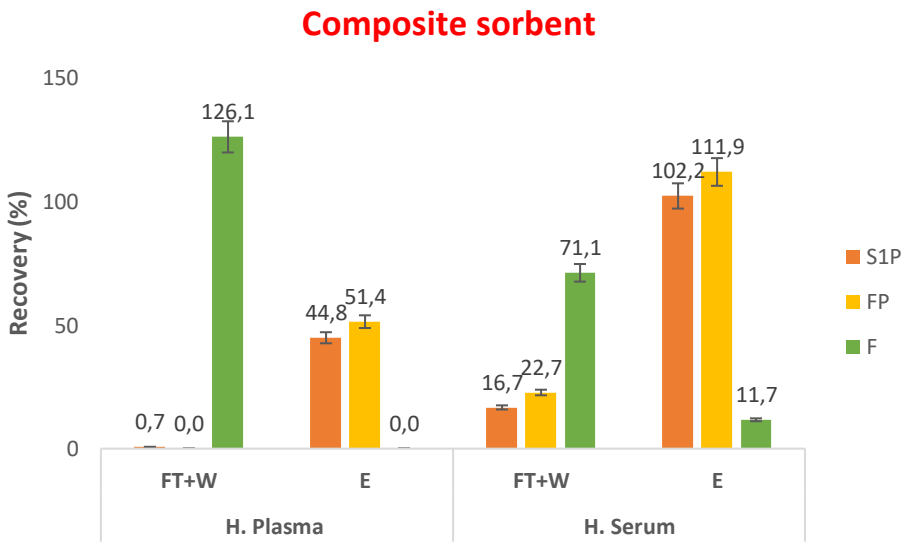
Composite sorbent
150
100
50
0
Recovery (%)
0,7
0,0
126,1
44,8
51,4
0,0
16,7
22,7
71,1
102,2
111,9
11,7
FT+W
E
FT+W
E
H. Plasma
H. Serum
S1P
FP
F

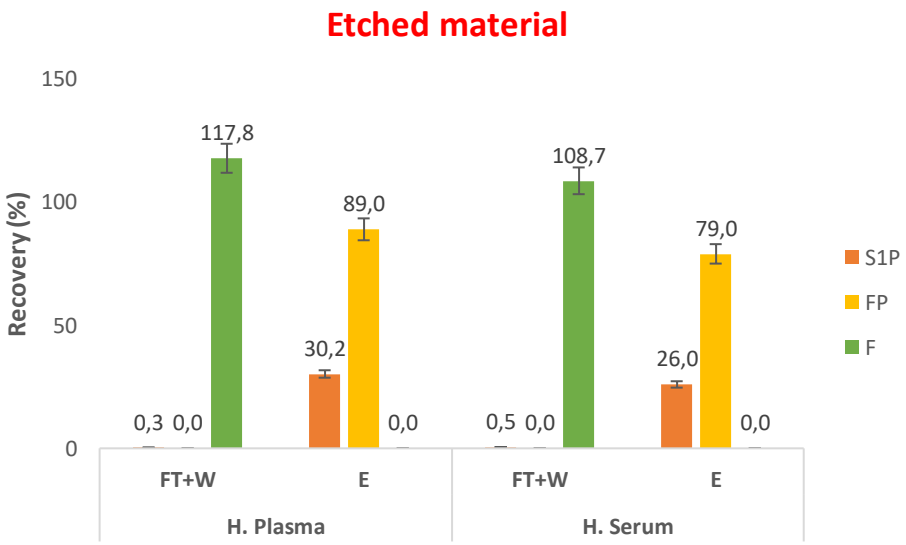

Figure 1.14: *Recovery % bar graphs for DVB materials.*

1.3 Conclusions

Concluding, three different materials, a ***bulk resin***, a ***composite sorbent*** and an ***etched material***, were synthesized to selectively target S1P and its active analogue FP. They were designed as a ***bis-imidazolium phosphor-monoester capture receptor*** prepared using DVB as matrix monomer, displaying enhanced affinity and selectivity for the targets in equilibrium batch binding tests and SPE experiments, carried out both in pure solvent and in real samples. These data allowed the study of the matrix effect before and after sample treatment.

1.4 Experimental

1.4.1 Chemicals and Materials

2,6-bis-(bromomethyl) pyridine, *N*-vinylimidazole, sulphur, acetonitrile anhydrous (99,8%), acetic acid (Ac. A), trifluoroacetic acid (TFA), phosphoric acid (PA), 2,5-dihydroxybenzoic acid (DHB), and ammonium formate for mass spectrometry (≥99.0%) were purchased from Sigma-Aldrich (Steinheim, Germany). Divinylbenzene (DVB) was purchased from Sigma-Aldrich (Steinheim, Germany) and was purified and activated prior to use. Ninhydrin were from Sigma-Aldrich (Milwaukee, USA). Dry dimethylformamide (dry DMF) was from Acros Organics. Acetic anhydride (Ac_2O) and formic acid (FA) were from Fluka (Deisenhofer, Germany). N,N'-azo-bis-(2,4-dimethyl)valeronitrile (ABDV) was purchased from Wako Chemicals GmbH (Neuss, Germany). Methanol anhydrous 99.9% (dry MeOH), acetonitrile (CAN) ≥99.8% HiPerSolv CHROMANORM® Reag. Ph. Eur., gradient grade for HPLC, methanol (MeOH) ≥99.8% HiPerSolv CHROMANORM® Reag. Ph. Eur., gradient grade for HPLC, 2-propanol ≥99.8% HiPerSolv CHROMANORM® Reag. Ph. Eur., gradient grade for HPLC, dimethyl sulphoxide-d6 (DMSO-d6) were from VWR chemicals (Radnor, PA, USA).

All additives and mobile phases were LC-MS grade and purchased from Sigma Aldrich (Milan, Italy). Amino-functionalized silica microparticles (NH_2@SiMPs), with an average particle size of 20-45 µm, were purchased from Fuji Silysia Chemical Ltd. (Kozoji-cho, Kasugai Aichi, Japan).

1.4.2 Lipid standards and real samples

Lipids used for recovery experiments were: Sphingosine 1-phosphate (d18:1) (S1P), 1,2-Dimyristoyl-*sn*-glycero-3-phospho-(1'-rac-glycerol) sodium salt (DMPG), 1,2-Dimyristoyl-*sn*-glicero-3-phosphatidylcoline (DMPC), 1,1',2,2'-Tetramyristoyl cardiolipin sodium salt (CL), 1,2-Dimyristoyl-*sn*-glycero-3-phospho-L-serine sodium salt **(**DMPS), 1,2-dimyristoyl-sn-glycero-3-phosphoethanolamine (DMPE) were purchased from Avanti Polar Lipid Inc. (Alabaster, Alabama, USA). 1,2-Dipalmitoyl-*sn*-glycero-3-phosphatidic acid sodium salt (DPPA) was purchased from Corden Pharma (Liestal, Switzerland). 1,2-Dipalmitoyl-*sn*-glycero-3-phosphatidylcholine-D62 was purchased by Larodan (Solna, Sweden). Fingolimod (FTY720) and Fingolimod Phosphate (FTY720-P, FP) were purchased from Novartis Institutes for BioMedical Research (Basel, Switzerland).

Human plasma was collected healthy pediatric volunteers in Ospedale Pediatrico 'Giovanni XXIII' (Bari, Italy). Commercial human serum from human male AB plasma, USA origin, sterile-filtered, was purchased from Sigma-Aldrich (Steinheim, Germany).

1.4.3 Apparatus

- **NMR spectroscopy.** Proton and carbon spectra were acquired with a Bruker 400 (400 MHz) instrument. The instrument was calibrated using as internal standards the deuterated solvents peaks.

- **High performance liquid chromatography coupled to UV-Vis detector (HPLC-UV-Vis).** Batch binding tests were performed using HPLC analysis by Alliance 2795 instrument (Waters, Milford, MA, USA) equipped with 2996 PDA detector (Waters, Milford, MA, USA). The stationary phase was a RP Luna C18 column, 100 Å, 250 x 4.6 mm, 5 µ particle size (Phenomenex, California, US), and the mobile phase prepared was H_2O/MeOH (68:32)

plus 1% TFA. The method run for 15 minutes, at a flow rate of 0.600 mL/min. The injection volume was 20 µL and the UV detector was set up at 225 nm.

- **MALDI-TOF-MS.** All mass spectra were obtained using a MALDI reflector time of flight mass spectrometer (Ultra-fleXtreme MALDI TOF/TOF MS/MS; Bruker Daltonics, Bremen, Germany) controlled by flexControl software (version 2.4, Bruker Daltonics, Bremen, Germany). The system was set up in positive ion linear mode in the m/z range of 200–1400. The matrix used in the experiment was a solution of 2,5-Dihydroxybenzoic acid (DHB, 20 mg/mL) in 50% acetonitrile (ACN), 0.1% trifluoroacetic acid (TFA), and 1% phosphoric acid (PA). Relative laser power was set at 60%. Signals came from an average of 1000 laser shots (5 x 200 shots). Samples were spotted on MTP 384 target plate polished steel BC (# 8280781). Mass spectrometric data analysis was performed using FlexAnalysis 3.4 software (Bruker Daltonik GmbH, Bremen, Germany).

- **Ultra High Performance Liquid Chromatography (UHPLC) coupled to tandem mass spectrometry (MS/MS).** UHPLC-MS/MS analysis was carried out with a Shimadzu Nexera (Shmiadzu, Milan, Italy) UHPLC consisting of two LC 30 AD pumps, a SIL 30AC autosampler, a CTO 20AC column oven, a CBM 20 A controller, and the system was coupled online to a triple quadrupole LCMS 8050 (Shimadzu, Kyoto, Japan) by a ESI source.

The separation was performed on a Kinetex EVO C18, 100Å, 150 x 2.1 mm, 2.6 µicron at a flow rate of 0.5 mL/min, employing as mobile phase A) ACN/Water: 60/40 (v/v %), 10mM $HCOONH_4$ plus 0.1% HCOOH (v/v %) and B) Isopropanol/ACN 90/10 (v/v %) plus 0.1% HCOOH (v/v %), with the following gradient: 0.0-2.0 min, isocratic at 0% B, 2.01-4.50 min, 0-50 % B, 4.51-8.00 min 50-80 % B, 8.01-9.00 min, 80-99 % B, isocratic for 1.50 min. Returning to 0% in 4.50 min. 2 µL were injected.

MS/MS analysis of lipids were conducted in Multiple Reaction Monitoring (MRM). The ESI was operated both in negative and positive ionization. The MS/MS analysis were performed setting the following parameters: Interface temperature 300°C, desolvation line temperature 250°C, Heat Block temperature 400°C; nebulizing gas, drying gas, and heating gas were set to 3,10,10 L/min.

For quantifying *Fingolimod Phosphate (FP)* was employed the following transition, the ESI was operated in positive ionization: 388.10>255.00, Q1 pre bias -21.0 V, collision energy (CE) -20.0, Q3 pre bias -26.0 V. Dwell time 50 msec. For quantifying *Fingolimod (F)* was employed the following transition, the ESI was operated in positive ionization: 308.20>255.50, Q1 pre bias -16.0 V, collision energy (CE) -15.0, Q3 pre bias -16.0 V. Dwell time 20 msec. For quantifying *Sphingosine 1-Phosphate (S1P)* was employed the following transition, the ESI was operated in positive ionization: 380.20>264.30, Q1 pre bias -12.0 V, collision energy (CE) -18.0, Q3 pre bias -30.0 V. Dwell time 100 msec. For quantifying *1,2-Dimyristoyl-sn-glycero-3-phosphoethanolamine (DMPE)* was employed the following transition, the ESI was operated in positive ionization: 637.30>496.30, Q1 pre bias -20.0 V, collision energy (CE) -23.0, Q3 pre bias -26.0 V. Dwell time 20 msec. For quantifying *1,2-Dimyristoyl-sn-glycero-3-phosphoserine sodium salt (DMPS)* was employed the following transition, the ESI was operated in negative ionization: 678.50>227.15, Q1 pre bias 20.0 V, collision energy (CE) 41.0, Q3 pre bias 24.0 V. Dwell time 50 msec (quantifier ion); 678.50>591.45, Q1 pre bias 26.0 V, collision energy (CE) 24.0, Q3 pre bias 28.0 V. Dwell time 50 msec (qualifier ion). For quantifying *1,2-Dimyristoyl-sn-glycero-3-phosphorylglycerol sodium salt (DMPG)* was employed the following transition, the ESI was operated in negative ionization: 665.50>227.30, Q1 pre bias 20.0 V, collision energy (CE) 38.0, Q3 pre bias 22.0 V. Dwell time 10 msec. For quantifying *1,2-Dimyristoyl-sn-glycero-3-phosphocholine (DMPC)* was employed the following transition, the ESI was operated in

positive ionization: 678.50>184.10, Q1 pre bias -20.0 V, collision energy (CE) -28.0, Q3 pre bias -29.0 V. Dwell time 10 msec (quantifier ion); 678.50>86.05, Q1 pre bias -20.0 V, collision energy (CE) -55.0, Q3 pre bias -15.0 V. Dwell time 10 msec (qualifier ion). For quantifying *1,2-Dipalmitoylphosphatidic acid (DPPA)* was employed the following transition, the ESI was operated in negative ionization: 647.60>255.30, Q1 pre bias 20.0 V, collision energy (CE) 35.0, Q3 pre bias 28.0 V. Dwell time 150 msec (quantifier ion); 647.60>152.95, Q1 pre bias 20.0 V, collision energy (CE) 42.0, Q3 pre bias 28.0 V. Dwell time 150 msec (qualifier ion). For quantifying *1,2-dipalmitoyl-d62-sn-glycero-3-phosphocholine (DPPC-d62)* was employed the following transition, the ESI was operated in positive ionization: 794.90>184.10, Q1 pre bias -24.0 V, collision energy (CE) -34.0, Q3 pre bias -11.0 V. Dwell time 50 msec. For quantifying *1,2-dipalmitoyl-sn-glycero-3-phosphocholine (DPPC)* was employed the following transition, the ESI was operated in positive ionization: 734.60>184.10, Q1 pre bias -22.0 V, collision energy (CE) -28.0, Q3 pre bias -3.0 V. Dwell time 20 msec (quantifier ion); 734.60>86.10, Q1 pre bias -22.0 V, collision energy (CE) -55.0, Q3 pre bias -15.0 V. Dwell time 20 msec (qualifier ion). For quantifying *1,1',2,2'-Tetramyristoyl cardiolipin sodium salt (CL)* was employed the following transition, the ESI was operated both in positive and negative ionization: 1263.90>495.40 (positive ionization), Q1 pre bias -38.0 V, collision energy (CE) -50.0, Q3 pre bias -23.0 V. Dwell time 100 msec (quantifier ion); 1263.90>274.95 (positive ionization), Q1 pre bias -38.0 V, collision energy (CE) -53.0, Q3 pre bias -22.0 V. Dwell time 100 msec (qualifier ion); 1263.90>769.30 (positive ionization), Q1 pre bias -38.0 V, collision energy (CE) -30.0, Q3 pre bias -38.0 V. Dwell time 100 msec (qualifier ion); 619.50>227.00 (negative ionization), Q1 pre bias 24.0 V, collision energy (CE) 32.0, Q3 pre bias 14.0 V. Dwell time 100 msec.

The instrumental calibration was performed through the external standard method, and a calibration line for each bio-compound was generated. For each lipid the stock solution was

prepared in MeOH solution at a concentration of 1000 µg mL^{-1}. Subsequently a mix lipid standard *solution* was realized in pure solvent.

In this way, for *FP* the calibration curve was obtained in a concentration range between 5 – 0.001 µg mL^{-1}, with six concentration levels and duplicate injection of each level were run. The linear regression was used to generate the calibration line with values of $R^2 \geq 0.99996$ ((y = 61715x + 5.92E+04).

For *F* the calibration curve was obtained in a concentration range between 1 – 0.001 µg mL^{-1}, with six concentration levels and duplicate injection of each level were run. The linear regression was used to generate the calibration line with values of $R^2 \geq 0.99997$ (y = 4E+06x + 1E+06).

For *S1P* the calibration curve was obtained in a concentration range between 5 – 0.001 µg mL^{-1}, with six concentration levels and duplicate injection of each level were run. The linear regression was used to generate the calibration line with values of $R^2 \geq 0.9998$ (y = 8E+06x - -8.82E+05).

For *DMPE* the calibration curve was obtained in a concentration range between 1 – 0.01 µg mL^{-1}, with five concentration levels and duplicate injection of each level were run. The linear regression was used to generate the calibration line with values of $R^2 \geq 0.9993$ (y = 2E+06x + 2.23E+05).

For *DMPS* the calibration curve was obtained in a concentration range between 5 – 0.001 µg mL^{-1}, with six concentration levels and duplicate injection of each level were run. The linear regression was used to generate the calibration line with values of $R^2 \geq 0.99963$(y= 7.24E+05x + 8.98E+04).

For *DMPG* the calibration curve was obtained in a concentration range between 5 – 0.001 µg mL^{-1}, with six concentration levels and duplicate injection of each level were run. The linear

regression was used to generate the calibration line with values of $R^2 \geq 0.9995$ (y = 1E+06x + 2.82E+04).

For *DMPC* the calibration curve was obtained in a concentration range between 1 – 0.001 µg mL^{-1}, with five concentration levels and duplicate injection of each level were run. The linear regression was used to generate the calibration line with values of $R^2 \geq 0.9996$ (y = 2E+07x + 4.82E+05).

For *DPPA* the calibration curve was obtained in a concentration range between 5 – 0.001 µg mL^{-1}, with six concentration levels and duplicate injection of each level were run. The linear regression was used to generate the calibration line with values of $R^2 \geq 0.9992$ (y = 1.18E+05x + 3.01E+05).

For *CL* the calibration curve was obtained in a concentration range between 5 – 0.01 µg mL^{-1}, with five concentration levels and duplicate injection of each level were run. The linear regression was used to generate the calibration line with values of $R^2 \geq 0.9993$ (y = 6.21E+04x+ 3.05E+04).

Subsequently calibration curves were obtained injecting SPE pretreated *human serum* spiked with the same standard solutions.

1.4.4 Methods

1.4.4.1 Synthesis of bis-imidazolium based functional monomer

1-Vinyl-3-{3-[(1-vinyl-1H-imidazol-3-ium-3-yl)methyl]benzyl}-1H-imidazol-3-ium dibromide (**Figure 1.15**) was prepared as reported in previous protocol used in our lab (Sulc *et al.*, 2017). A solution of 2,6-bis-(bromomethyl) pyridine (4 g, 15.09 mmol), *N*-vinylimidazole (2.755 mL, 30.42 mmol) in dry ACN (200 mL) was refluxed overnight, at 100°C, with a spatula tip of sulphur to avoid polymerization. After cooling down at room temperature, the reaction mixture was dried under vacuum and the final product was obtained through solubilization in ethanol and precipitation in diethyl ether. Yield: 83%.

^{1}H NMR (Bruker 400 MHz, in DMSO-d6): δ 5.43-5.44-5.45-5.46 (m, 2H), 5.61 (s, 4H), 5.96-5.97-6.00-6.01 (m, 2H), 7.32-7.34-7.36-7.38 (m, 2H), 7.53-7.55 (m, 2H), 7.84 (s, 2H), 7.96-7.98-8.00 (t, 1H), 8.20-8.21 (t, 2H), 9.60 (s, 2H) (**Figure 1.16**).

^{13}C NMR (Bruker 400 MHz, in DMSO-d6): δ 53.23, 109.41, 119.18, 122.70, 124.57, 129.21, 136.61, 139.29, 153.60 (**Figure 1.17**).

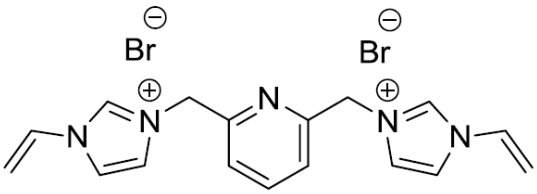

Figure 1.15: *Structure of bis-imidazolium based FM*.

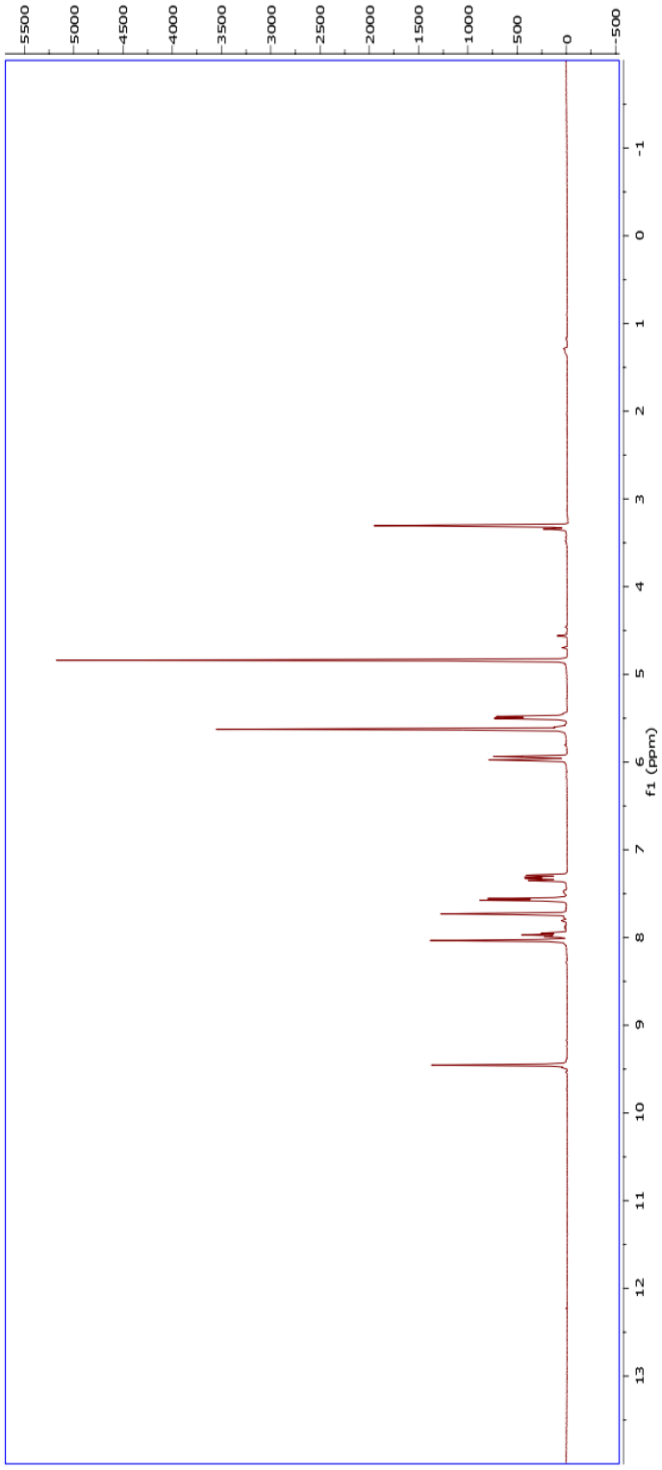

Figure 1.16: *^{1}H NMR spectrum of bis-imidazolium based FM.*

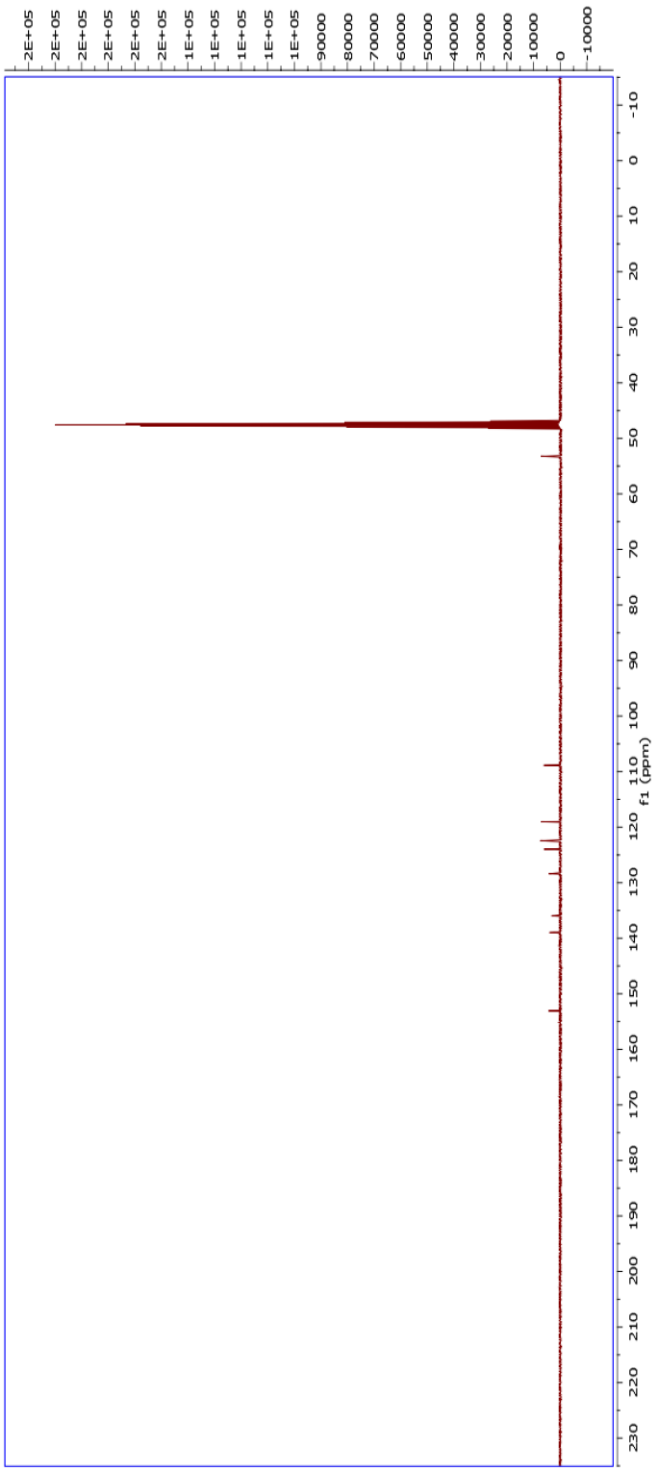

Figure 1.17: *^{13}C NMR spectrum of bis-imidazolium based FM.*

1.4.4.2 Amino-functionalized silica modification (AcNH@Si)

NH_2@Si (20 g) was suspended in DMF (100 mL) and stirred in a 250 mL round bottomed flask. Then, acetic anhydride was added (20 mL) and the suspension was stirred at room temperature overnight. Silica particles obtained after reaction were filtered off, washed with DMF (3 x 50 mL) and MeOH (3 x 50 mL), and dried in oven at 35°C overnight to yield N-acetylated silica (AcNH@Si). Ninhydrin test performed after modification resulted negative and confirmed complete functionalization of silica amino groups.

1.4.4.3 Preparation of DVB materials

Bulk resin

Bis-imidazolium based functional monomer (0.780 mmol, 358 mg), DVB (30 mmol, 4.317 mL) and ABDV (1.5% w/w of total monomers) were dissolved in 1.060 mL solution of anhydrous MeOH/Toluene (1:1 v/v %) in a 20 mL glass vial and the mixture was purged with N_2 at room temperature for 15 mins. Subsequently, the mixture was heated at 45°C to allow starting the polymerization reaction for 24 h and then the temperature was increased till 80°C for other 2-3 h. The synthesized bulk polymer was crushed, then transferred into a 50 mL centrifuge tube and washed three times with a solution of MeOH/HCl 1N (1/1 v/v%) and three times with pure MeOH. The particles were then dried in oven at 60°C overnight. The particles were crushed again and sieved, obtaining three different particle sizes: ≥ 50 μm, 50-25 μm, ≤ 25 μm. For our analysis and purpose, we used particles in the size range 50-25 μm.

Composite sorbent

A pre-polymerization mixture was first prepared as follow. In a 20 mL glass vial, bis-imidazolium functional monomer (0.210 mmol, 100 mg) and DVB (8.4 mmol, 1.173 mL) were dissolved in the porogen mixture MeOH/Toluene (1:1 v/v). Then the initiator ABDV (1.5 %

w/w % of the total monomers) was added to the solution and the pre-polymerization mixture was purged under a flow of N_2 for 15 min. In another 20 mL glass vial, AcNH@Si500 (2.2 g) were deaerated and purged with a continuous flow of N_2 and then allowed to soak the pre-polymerization mixture until particles were freely flowing. The tube was then sealed, and the polymerization started by placing the tube in an oven heated at 50 °C for 24 hours. The vial was then kept at 70 °C for 4 hours. The resulting polymer was transferred in a 50 mL polypropylene centrifugations tubes and washed with a solution of MeOH/HCl 1N (8/2 v/v) (3 × 50 mL). The solvent was then extracted in a Soxhlet apparatus with MeOH for 24 hours. The resulting composite particles were then dried under vacuum overnight.

Etched material

Part of the composite microspheres (1 g ca) were transferred into a 50 mL centrifugation tube and 40 mL of etching solution (NH_4HF_2 3M prepared in H_2O) were added. The polymer was shaken for 24 hours on a rocking plate. The resulting material was transferred in a 50 mL polypropylene centrifugation tubes and washed with a solution of MeOH/HCl 1N (8/2 v/v), for at least three times (3 x 50 mL). The solvent was then extracted in a Soxhlet apparatus with MeOH for 24 hours. The resulting etching particles were then dried under vacuum overnight.

1.4.4.4 Batch binding test

Firstly, a calibration curve of PPA in pure solvent (MeOH) was plot using the concentration range 1, 0.75, 0.5, 0.25, 0.1, 0,075, 0.05, 0.025 mM. The resulted equation of the linear regression was y=0,649x+1,9102 and R^2=0,9998. Suddenly, 10 mg of the bulk resin, composite sorbent and etched material was mixed in 1 mL of PPA at 1, 0.75, 0.5, 0.25, 0.1, 0,075, 0.05, 0.025 mM, and shaken on a rocking plate for 12 hours, at room temperature. Suddenly, all the samples were centrifuged and 500 μL of supernatant were used for reverse phase HPLC analysis

to detect the binding ability of the polymers (for HPLC-UV-Vis analysis parameters, *vide supra*).

The peak areas obtained was used to create a calibration curve and calculate the quantity of analyte caught by the different materials using the following equation:

$$B=(C_0-C_f)\cdot V/m$$

where C_0 was the initial standard concentration, C_f was the free standard concentration detected in the supernatant solution, V was the total volume of the sample, and m was the mg of polymer used for the test. For curves and results, *vide supra*.

1.5 Applications

1.5.1 Extraction of phospholipids through Solid Phase Extraction (SPE)

Standards Preparation

Stock solutions of standards were prepared in MeOH to obtain a concentration of 1 mg/mL for Sphingosine 1-phosphate (d18:1) (S1P), Fingolimod (FTY-720), Fingolimod Phosphate (FTY-720 P), 1,2-Dimyristoyl-*sn*-glycero-3-phospho-(1'-rac-glycerol) sodium salt (DMPG), 1,2-Dimyristoyl-*sn*-glicero-3-phosphatidylcoline (DMPC), 1,1',2,2'-Tetramyristoyl cardiolipin sodium salt (CL), 1,2-Dipalmitoyl-*sn*-glycero-3-phosphatidic acid sodium salt (DPPA), 1,2-dimyristoyl-sn-glycero-3-phospho-L-serine (sodium salt) (DMPS), 1,2-dimyristoyl-sn-glycero-3-phosphoethanolamine (DMPE). Then, the stock solutions were further diluted in a concentration range of 0-150 µM. Internal standard (IS) chosen for these experiments was DPPC-d62 in the concentration of 50 µM.

Human Plasma Samples Preparation

Human plasma was extracted from whole blood samples of healthy pediatric volunteers from Ospedale Pediatrico 'Giovanni XXIII' (Bari, Italy) and was treated with EDTA as anti-coagulant following the general protocol keeping it at -80°C. For lipids extractions, 100 µL of human plasma was added to 1 mL of MeOH enriched with 10 nmol/mL S1P, FTY720, FTY720-P. The mixture was vortexed for 30 seconds, sonicated for 30 minutes and centrifuged at 14.000 rpm, at 4°C, for 10 minutes to allow plasma proteins precipitation. The supernatant was transferred into fresh tubes. Loading fractions were then prepared in 1 mL volume diluting 100 µL of plasma lipids extract in 2-propanol (for extractions on bulk resin) and in ACN (for extractions using composite sorbent and etched materials).

Human Serum Samples Preparation

Commercial human serum (Human Male AB plasma, USA origin, sterile-filtered, Sigma-Aldrich) was firstly thawed. A stock solution was prepared by diluting human serum in water in the ratio 1:20. For lipids extractions, 20 mL of MeOH was added to the stock solution of human serum. The mixture was vortexed for 30 seconds, sonicated for 30 minutes and centrifuged at 14,000 rpm at 4°C for 10 minutes to allow further proteins precipitation. The final supernatant was transferred into a new fresh tube. Loading fractions were then prepared in 1 mL volume diluting 100 µL of human serum lipids extract in 2-propanol (for bulk extractions) and in ACN (for composite material).

Solid Phase Extractions (SPE) protocols

100 mg of each polymer were packed into SPE cartridges using on the top and at the bottom filters with 10 µm pore size (Mobicol Classic, MoBiTec).

For bulk material (particles size range 50-25 µm), the cartridge was equilibrated with 3 x 1 mL 2-propanol. The loading fraction was passed through the cartridge twice. The washing steps were executed with 1 mL 2-propanol and 1 mL 2-propanol/MeOH (1/1, v/v). The elution fractions were collected with 2 x 0.8 mL MeOH/$CHCl_3$ (1/1, v/v) plus 1% TFA. All fractions were then dried under vacuum and reconstituted in 100 µL MeOH, sonicated for 10 minutes and transferred into insert vial for LC-MS analysis.

For composite sorbent and the etched material, the cartridge was conditioned using 3 x 1 mL regeneration buffer MeOH/Acetic Acid/H_2O (6/3/1, v/v/v), 3 x 1 mL 2-propanol, 3 x 1 mL ACN. Next, the loading fraction was passed through the cartridge twice. The washing steps were performed with 1 mL ACN, 2 x 1 mL 2-propanol. The elution fractions were collected three times by adding 0.8 mL MeOH plus 0.1% TFA. All fractions were then dried under

vacuum and reconstituted in 100 µL MeOH sonicated for 10 minutes and transferred into insert vial for LC-MS analysis.

All the cartridges prepared have been reused after regeneration step (3 x 1 mL MeOH/Acetic Acid/H_2O (6/3/1, v/v/v)) and equilibration to obtain experiments in triplicate.

1.6 Materials characterization

All DVB cross-linked materials were characterized by optical microscopy, scanning electron microscopy (SEM), thermogravimetric analysis (TGA), Fourier Transform - Infrared spectroscopy (FT-IR), and nitrogen sorption analysis (BET).

- **Optical microscopy.** Optical micrographs were acquired using Nikon Optiphot Epi-Fluorescence microscope equipped with polarizing filters, phase contrast and a DS-U1 digital camera.

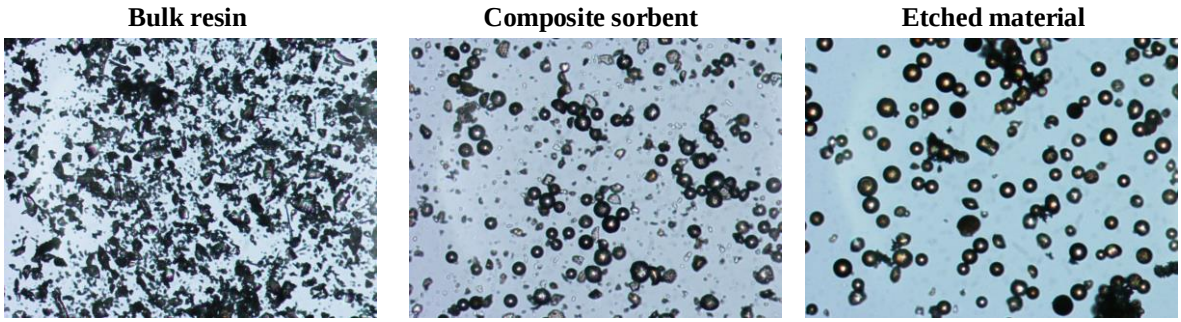

Figure 1.18: *Optical microscopy images of bulk resin, composite sorbent and etched material. Particle size= 25-50 µm.*

- **Scanning electron microscopy (SEM).** The particle morphology, size and size distribution were determined using Zeiss EVO LS 10 CANSEM (Carl Zeiss AG, Oberkochen, Germany) at T ¼ 25 °C, EHT ¼ 15 kV, WD ¼ 4.5 mm. For imaging, particles were covered by a thin layer of gold.

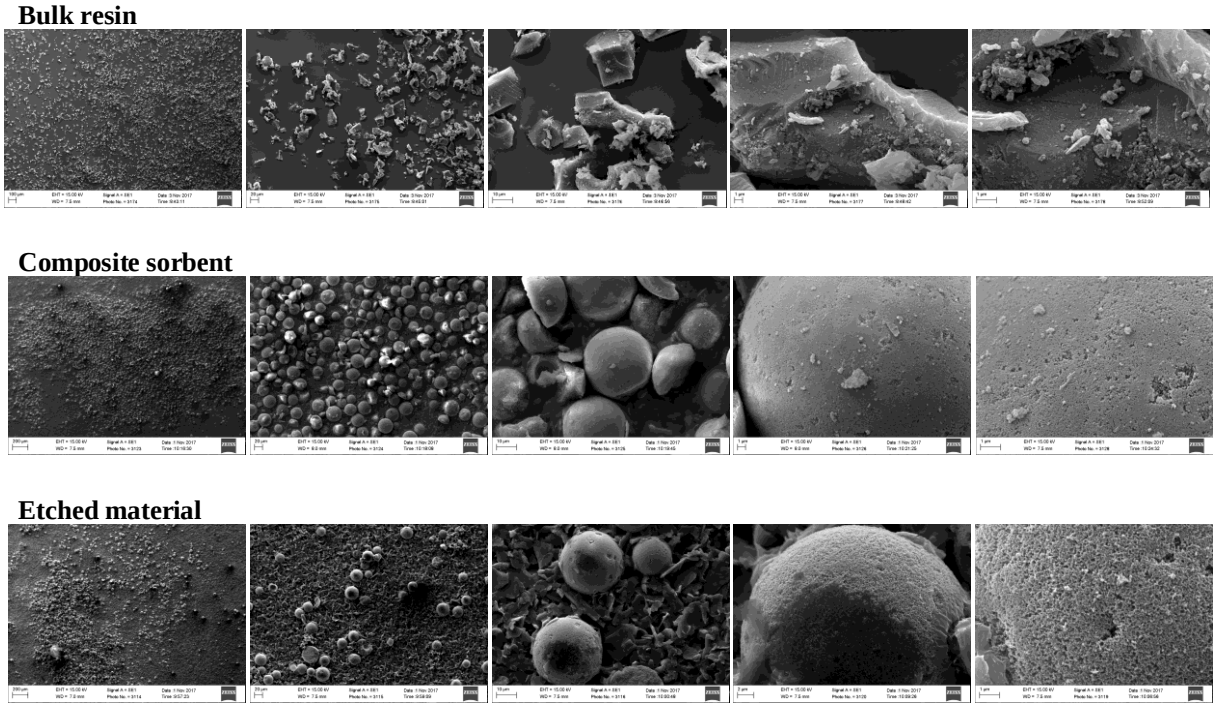

Figure 1.19: *SEM images of bulk resin, composite sorbent and etched material, taken at different magnifications 100x, 500x, 2.500x, 10.000x, 25.000x.*

- **Thermogravimetric analysis (TGA).** TGA was carried out through TGAQ500 (Ta Instruments). Ca 10 mg of each sample was placed in a platinum pan, after tare. The sample was heated at 10°C/min till 800°C, under N_2 atmosphere.

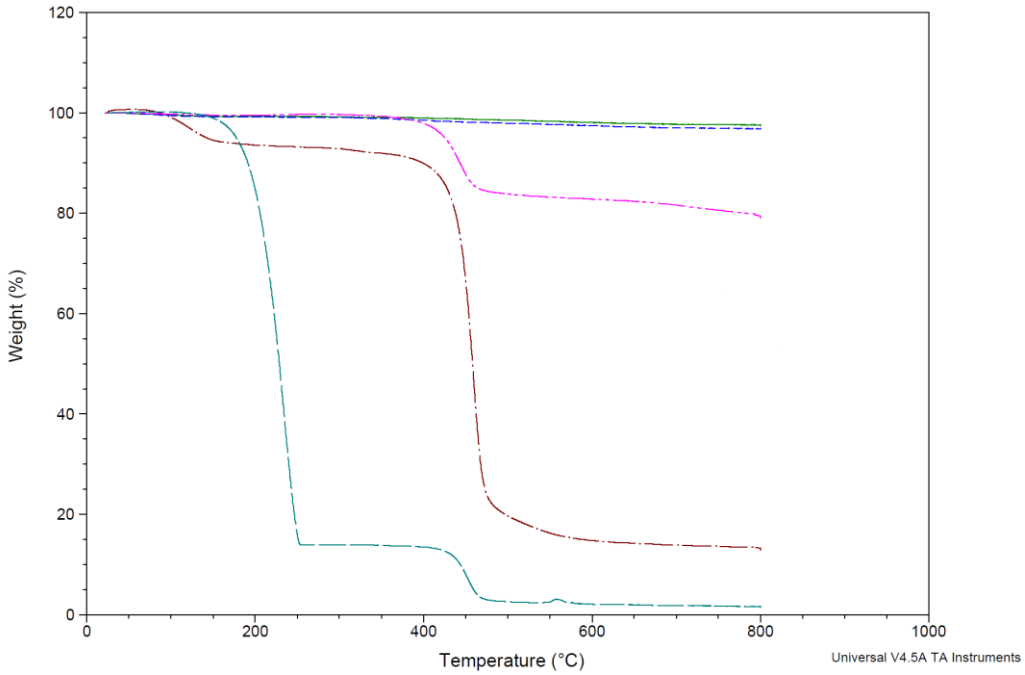

Figure 1.20: *TGA curves of NH_2@Si500MPs (green line), AcNH@Si500MPs (blue line), bulk resin (brown line), composite (pink line) and etched (dark green line) sorbents.*

Table 1.8: *Results of DVB crosslinked-MPs characterization*. For TGA, *excluding water.

	Weight (%) at 100°c	**Weight (%) at 800°c**	**Weight Loss* (%)**
Bulk resin	99,11	13,23	85,88
NH_2@Si500MPs	99,56	97,54	2,02
AcNH@Si500MPs	99,46	96,81	2,65
Composite sorbent	99,76	79,31	20,45
Etched material	100	1,66	98,33

- **Nitrogen sorption.** Nitrogen sorption measurements were performed on the Nova 4200*e* Sorption Analyzer (Quantachrome Instruments, USA). The specific surface areas *S* were evaluated by using the Brunauer–Emmett–Teller (BET) method, the specific pore volumes Vp and the average pore diameter Dp by using the Barrett–Joiner–Halenda (BJH) theory applied to the desorption branch of the isotherm.

Table 1.9: *Results of DVB crosslinked-MPs characterization*. BET data for surface area.

	Bulk resin	**Composite sorbent**	**Etched material**
S (m^2/g)	2.248	137.109	17.571

- **FT-IR spectroscopy.** Infrared spectra were recorded using a Thermo Nicolet Nexus 6700 instrument (Thermo Scientific, Waltham, MA, USA).

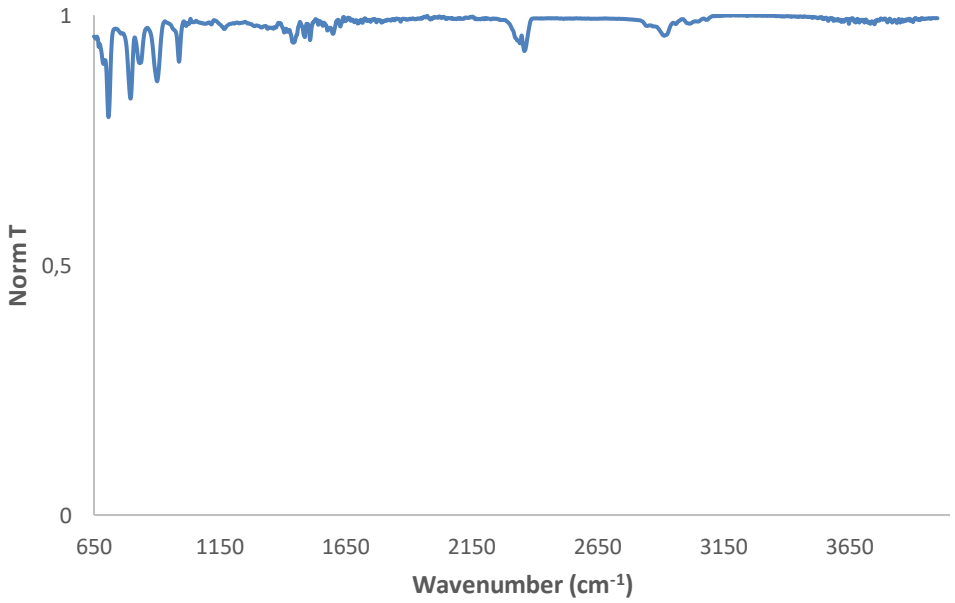

Figure 1.21: *Normalized FT-IR spectrum of DVB bulk resin.*

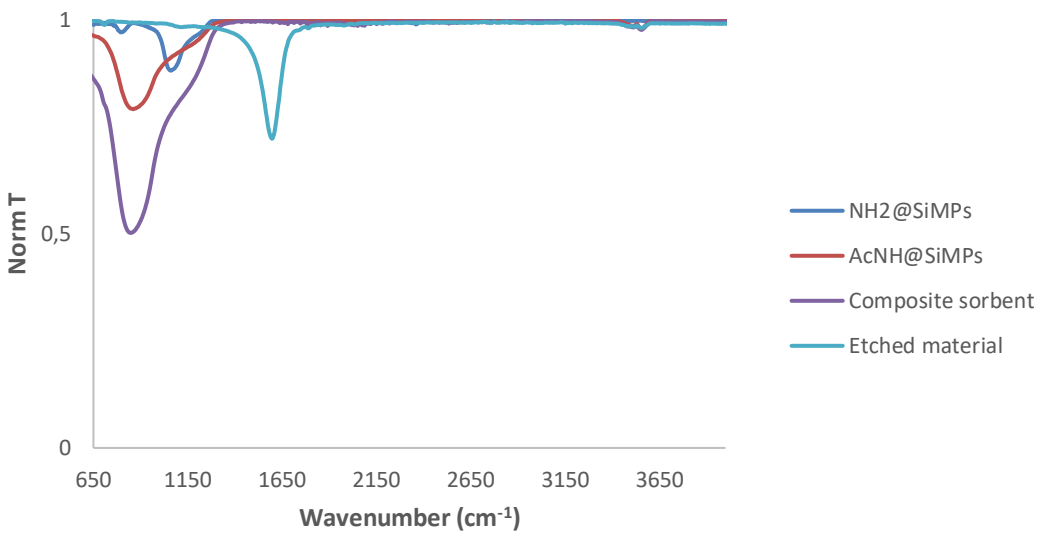

Figure 1.22: *Normalized FT-IR spectra of Silica based DVB MPs.*

Bibliography

Beach, J. V. and Shea, K. J., (1994), Designed catalysts. A synthetic network polymer that catalyzes the dehydrofluorination of 4-fluoro-4-(p-nitrophenyl)-butan-2-one, *Journal of American Chemical Society*, 116 (1), 379-80.

Bioanalytical Method Validation, Guidance for Industry, U.S. Department of Health and Human Services, Food and Drug Administration, Center for Drug Evaluation and Research (CDER), May 2018, Biopharmaceutics, available at the following website link: http://www.fda.gov/Drugs/GuidanceComplianceRegulatoryInformation/Guidances/default.htm.

Brinkmann, V., Billich, A., Baumruker, T., Heining, P., Schmouder, R., Francis, G., Aradhye, S., Burtin, P., (2010), Fingolimod (FTY720): discovery and development of an oral drug to treat multiple sclerosis, *Nature Reviews. Drug Discovery*, 9 (11), 883–97.

Cutivet, A., Schembri, C., Kovensky, J., Haupt, K., (2009), Molecularly Imprinted Microgels as Enzyme Inhibitors, *Journal of American Chemical Society*, 131 (41), 14699-14702.

Emgenbroich, M., Borrelli, C., Shinde, S., Lazraq, I., Vilela, F., Hall, A. J., Oxelbark, J., De Lorenzi, E., Courtois, J., Simanova, A., Verhage, J., Irgum, K., Karim, K., Sellergren, B., (2008), A Phosphotyrosine-Imprinted Polymer Receptor for the Recognition of Tyrosine Phosphorylated Peptides, *Chemistry: A European Journal*, 14, 9516-29.

Hall, A. J., Menosiostis, M., Emgenbroich, M., Quaglia, M., De Lorenzi, E., Sellergren, B., (2005), Urea Host Monomers for Stoichiometric Molecular Imprinting of Oxyanions, *Journal of Organic Chemistry*, 70, 1732-36.

He, X., Huang, C. L., and Schuchman, E. H., (2009), Quantitative analysis of sphingosine-1-phosphate by HPLC after napthalene-2, 3-dicarboxaldehyde (NDA) derivatization, *Journal of. Chromatography B*, 877 (10), 983-90.

Kim, S. K. (b) *et al*., (2008) A new imidazolium acridine derivative as fluorescent chemosensor for pyrophosphate and dihydrogen phosphate. *Tetrahedron*, 64, 6402–05.

Kim, S. K., (a) Singh, N. J., Kim, S. J., Kim, H. G., Kim, J. K., Lee, J. W., Kim., K. S., Yoon, J., (2003), New fluorescent photoinduced electron transfer chemosensor for the recognition of $H_2PO_4^-$, *Organic Letter*, 5 (12), 2083-86.

Kunkel, G. T., Maceyka, M., Milstien, S. and Spiegel, S., (2013), Targeting the sphingosine-1-phosphate axis in cancer, inflammation and beyond, *Nature Review. Drug Discovery*, 12 (9), 688-702.

Langton, M. J., Serpell, C. J., Beer, P. D., (2016), Anion Recognition in Water: Recent Advances from a Supramolecular and Macromolecular Perspective, *Angewandte Chemie, International Edition*, 55 (6), 1974–87.

Min, J. K., Yoo, H. S., Lee, E. Y., Lee, W. J., and Lee, Y. M., (2002), Simultaneous quantitative analysis of sphingoid base 1-phosphates in biological samples by o-phthalaldehyde precolumn derivatization after dephosphorylation with alkaline phosphatase, *Analytical Biochemistry*, 303 (2), 167-75.

Molecular Probe Handbook, Fluorophore and Their Amine Reactive Derivates. ThermoFisher Scientific.

Narayanaswamy, P., Shinde, S., Sulc, R., Kraut, R., Staples, G., Thiam, C. H., Grimm, R., Sellergren, B., Torta, F., Wenk, M. R., (2014), Lipidomic "Deep Profiling": an enhanced workflow to reveal new molecular species of signaling lipids, *Analytical Chemistry*, 86, 3043-47.

Shaner, R. L., Allegood, J. C., Park, H., Wang, E., Kelly, S., Haynes, C. A., and Merrill, A.H., (2009), Quantitative analysis of sphingolipids for lipidomics using triple quadrupole and quadrupole linear ion trap mass spectrometers, *Journal of. Lipid Research*, 50 (8), 1692-1707.

Shinde, S., Selvalatchmanan, J., Incel, A., Akhoundian, M., Bendt, A. K., Torta, F., (2018), Mesoporous polymeric microspheres with high affinity for phosphorylated biomolecules, *New Journal of Chemistry*, 42 (11), 8603-08.

Sulc, R., Szekely, G., Shinde, S., Wierzbicka, C., Vilela, F., Bauer, D., Sellergren, B., (2017), Phospholipid imprinted polymers as selective endotoxin scavengers, *Scientific Reports*, 7, 44299, DOI: 10.1038/srep44299.

Walash, M. I., Metwally, M. E., Eid, M., and El-Shaheny, R. N., (2012), Validated spectrophotometric methods for determination of Alendronate sodium in tablets through nucleophilic aromatic substitution reactions, *Chemistry Central Journal*, 6 (1), 25.

Wierzbicka, C., (a), Liu, M., Bauer, D., Irgrum, K., Sellergren, B., (2017), Cationic pTyr/pSer imprinted polymers based on a bis-imidazolium host monomer: phosphopeptide recognition in aqueous buffers demonstrated by µ-liquid chromatography and monolithic columns, *Journal of Materials Chemistry B*, 5, 953-60.

Wierzbicka, C., (b), New fractionation tools targeting elusive post-traslational modifications, Malmö University Health and Society Doctoral Dissertation, 2017:3.

Wulff, G., Gross, T., Schönfeld, (1997), Angewandte Chemie (International Ed. In English), 36, 1962-64.

Yatomi, Y., Igarashi, Y., Yang, L., Hisano, N., Qi, R., Asazuma, N., Satoh, K., Ozaki, Y. and Kume, S., (1997), Sphingosine 1-phosphate, a bioactive sphingolipid abundantly stored in

platelets, is a normal constituent of human plasma and serum. *Journal of Biochemistry*, 121 (5), 969-73.

CHAPTER II

Fluorescent Sensory Core-Shell Particles for Selective Detection of Sphingosine 1-Phosphate

2.1 Introduction

The bioactive lipid Sphingosine 1-Phosphate (S1P) has been found to be involved in multiple cellular signalling systems. The numerous biological functions of S1P include regulation of cellular proliferation, survival, migration, invasion, differentiation and cellular architecture, as well as the control of immune cell trafficking, angiogenesis and vascular integrity. Therefore, it is not surprising that S1P affects the immune system, central nervous system and cardiovascular system and has been implicated in a broad range of disease, including atherosclerosis, respiratory distress, diabetes and, most importantly, cancer, inflammatory disorders and neurodegenerative disease when its concentration in blood and lymphatic fluid increases (Kunkel *et al*., 2013). Recently, Fingolimod, a functional antagonist of S1P receptor 1 (S1PR1), known also by the registered name FTY720, has been approved by FDA for the treatment of multiple sclerosis, and we adopted its phosphorylated version, Fingolimod Phosphate (FTY720-P, FP), as structural analogue of S1P to carry out this work. Currently, S1P detection methods are based on HPLC separation of fluorophore-modified S1P (Walash *et al.*, 2012; Min *et al.*, 2002; He *et al*., 2009) and LC-MS/MS (Shaner *et al*., 2009), procedures which require time consuming steps and expensive instruments. In this context, the preparation of fluorescent molecularly imprinted polymers (MIPs) (Wan *et al*., 2013) could represent a rapid and low-cost detection method for S1P using a simplified sample preparation for the analysis of complex matrix, such as biofluids.

2.2 Results and Discussion

Addressing the robustness issue of biological receptors, lipid recognition elements in the form of macrocyclic hosts have been reported (Breslow & Zhang, 1996; Marti *et al*., 1998, Shortill *et al*., 2004; Xu *et al*, 2018; Wu *et al*., 2016) However, these typically lack the required target selectivity and are often synthetically challenging to make. In this section, we report a new strategy to detect the new biomarker S1P through the synthesis of a selective sensor material. This is based on FP-imprinted core-shell nanoparticles characterized by an NBD-urea based fluorescent functional monomer that allowed the fluorometric detection of S1P. The dummy imprinting was achieved using as template the S1P antagonist receptor FP, adding the methacrylamide (MAAm) and NBD-urea functional monomers with the role of double hydrogen bond donor catching the hydroxide (OH-) functional groups. The crosslinker ethylene glycol dimethacrylate (EGDMA) enabled the proper grafting of the monomers on the surface of 200 nm silica particles via RAFT polymerization. The synthesized materials presented selective affinity for FP and S1P when the fluorescent measurement was performed in a 1:1 (v/v) mixture of water/methanol, and other potentially interfering molecules, containing phosphate groups, did not compromise analyte access to the selective cavities on the particles. The selectivity of the polymers was further verified on spiked human serum real samples.

Considered the success obtained in a previous work in the use of NBD-urea based functional monomer for targeting glycans (Shinde *et al.*, 2015), UV/Vis absorption and fluorescent emission spectra titration of the complex FP-fluorescent NBD-urea based functional monomer were carried out in order to investigate the relevance of their interaction at different concentration levels.

Like antibodies, such receptors can be used for affinity-based separations, assays or sensors for the target analytes (Li *et al*., submitted).

In order to adapt this approach for an S1P-probe we set out the following design criteria:

1. Lacking effective template recycling rules out the use of expensive targets as templates. Most phospholipids belong to this category which explains why only few examples of MIPs targeting phospholipids have been reported (Chen *et al*., 2016; Sellergren & Hall, 2012, Whitcombe *et al*., 2014; Haupt & Ayela, 2012). We reasoned that an S1P complement can be constructed based on templating of the readily available S1P receptor antagonist FP (**Figure 2.2**). This zwitterionic drug antagonizes the receptor by a similar binding mechanism as S1P (Brinkmann *et al*., 2010; Chiba & Adachi, 2012; David *et al*, 2018).
2. The amphiphilic nature of the template/target requires an amphiphilic host capable of accommodating the polar head group and the hydrophobic chain. In our previous efforts towards a receptor for the lipid A motif of endotoxin the phosphomonoester head group could be effectively targeted based on cationic bis-imidazolium or neutral urea-based anion host monomers in a hydrophobic polymethacrylate scaffold (Sulc *et al*., 2017).
3. *Real time l*ipid quantification in live cells is complicated by the fact that lipids are largely associated with proteins or cell membranes. Probes compatible with denaturing media are therefore required. The MIP should hence report the presence of a guest with a short response time in both aqueous and non-aqueous media. Preparation of submicron-sized core/shell particles incorporating fluorescent reporter monomers such as ureas with appended (NBD) fluorophore groups has proven to be a fruitful approach for generating target specific and polymerizable fluorescent probes featuring organic

solvent compatibility combined with short response times (Wan (a) *et al*., 2013; Shinde *et al*., 2013; Wan (b) *et al*., 2017).

Based on the above design criteria, we here report on the synthesis and characterization of fluorescent particle probes for the phosphomonoester lipids S1P, DPPA and the S1P receptor antagonist FP (Li *et al*., submitted).

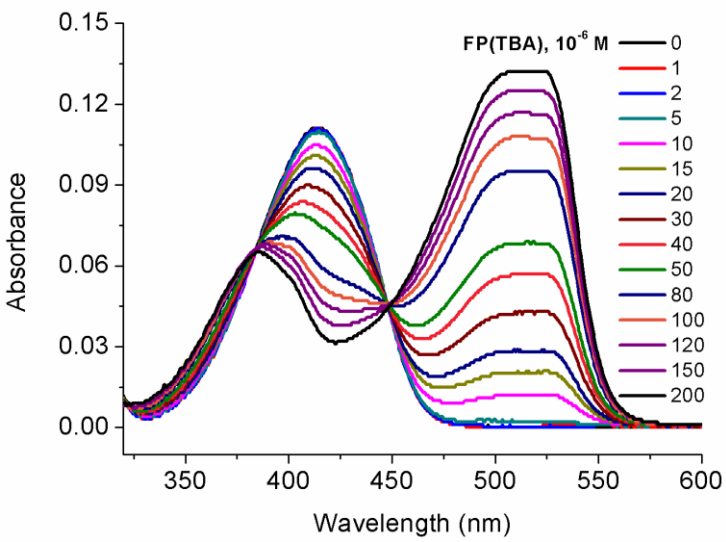

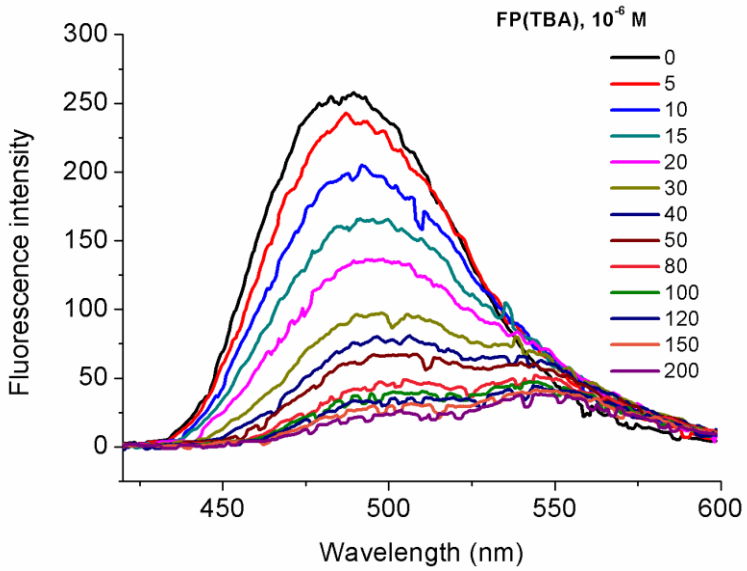

Figure 2.1: ***a)*** *UV-absorbance and* ***b)*** *fluorescence spectra of the fluorescent monomer (5 µM) and FP-TBA at different concentrations (0 up to 200 µM) in 1 mL of methanol.*

As shown in **Figure 2.1**, the shifts of the peaks in both the absorption (from 410 nm to 510 nm) and emission (from 500 nm to 570 nm) spectra of the fluorescent monomer, demonstrated the relevance of interactions of the NBD functional monomer with the FP-TBA salt template. Based on this evidence, we designed two new syntheses for core-shell molecularly imprinted polymers (MIPs) based on the use of NBD-urea functional monomer and adopting, as templates, two different molecules: FP monoTBA salt (FP(TBA), as structural analogue of S1P, used for the synthesis of a dummy polymer, and 1,2-Dipalmitoyl-*sn*-glycero-3-phosphate sodium salt (DPPA(Na)), a phospholipid without the amino-alcoholic group in its structure, used in the synthesis of a control polymer (**Figure 2.2**).

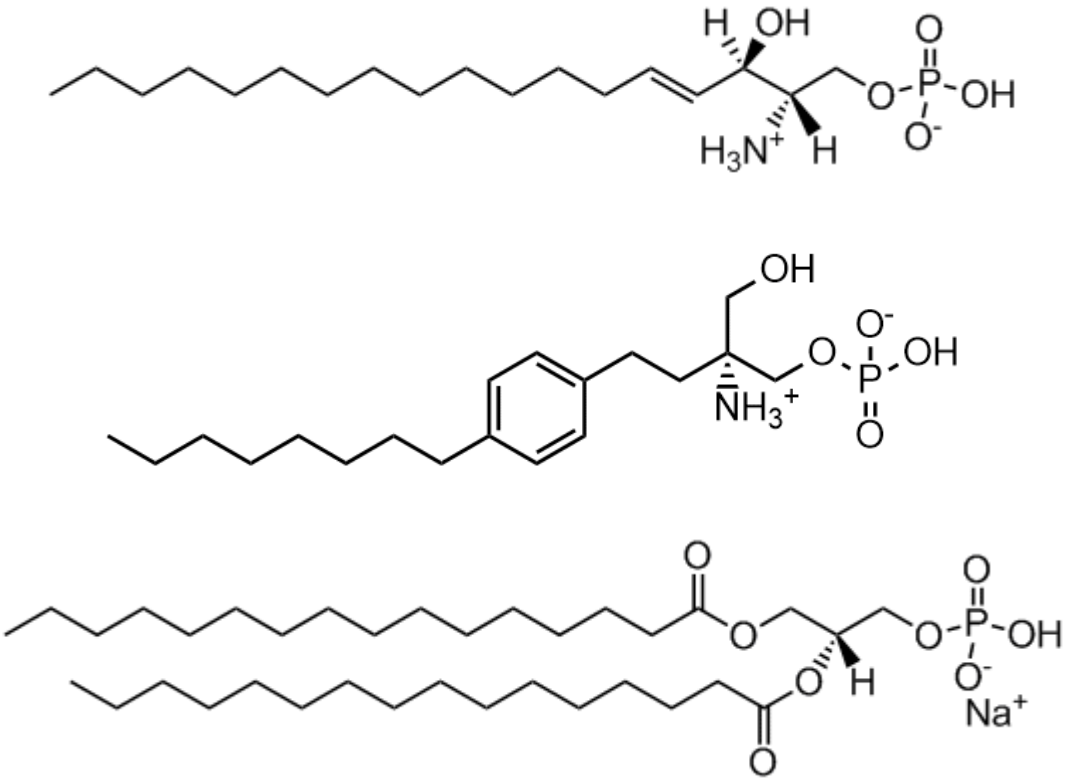

Figure 2.2: *[first] Structures of Sphingosine 1-Phosphate (S1P), [second] Fingolimod Phosphate (FP), and [third] 1,2-Dipalmitoyl-sn-glycero-3-phosphatidic acid sodium salt DPPA (Na).*

SiNPs-RAFT (150 mg) were suspended in a solution containing FP-TBA or DPPA-Na, NBD-urea functional monomer, MAAm and EGDMA (284 μL, 1.509 μmol) dissolved in 20 mL of $CHCl_3$ placed in a 20mL screw capped scintillation vial. This mixture was subjected to sonication for 30 min followed by purging with N_2 for further 10 min. ABDV (8.7 mg, 9.3 μmol) was then added and the suspension again purged for 5 min with N_2. The vials were closed with silicone insulating tape and stirred on a heated shaker (50 °C, 480 rpm) for 24 h. After polymerization, with the aim of leaving on the surface of the nanoparticles a large number of cavities able to recognize FP and S1P, the template was removed through different washing steps (3x50mL CH_3COOH:H_2O:MeOH (5%:5%:90%), 3x50 mL MeCN:$CHCl_3$ (80%:20%), 3x50 mL pure MeOH) with separation of the particles by centrifugation at 12.000 rpm, for 15 minutes, at room temperature. Finally, the particles were dried under vacuum overnight. A sketch of synthesis workflow is reported in **Figure 2.3**. The non-imprinted control particles (NIP) were synthesized under identical conditions, without addition of the template. **Table 2.1** reports a library of MIPs and NIPs synthesized.

Table 2.1: *Composition of pre-polymerization mixtures*

POLIMERs	T	T:Urea FM:MAAm	Porogen solvent
P1/M1	FP-TBA	1:2:2	$CHCl_3$
P_N1/N1	/	1:2:2	$CHCl_3$
P2/M11	DPPA-Na	1:2:2	$CHCl_3$

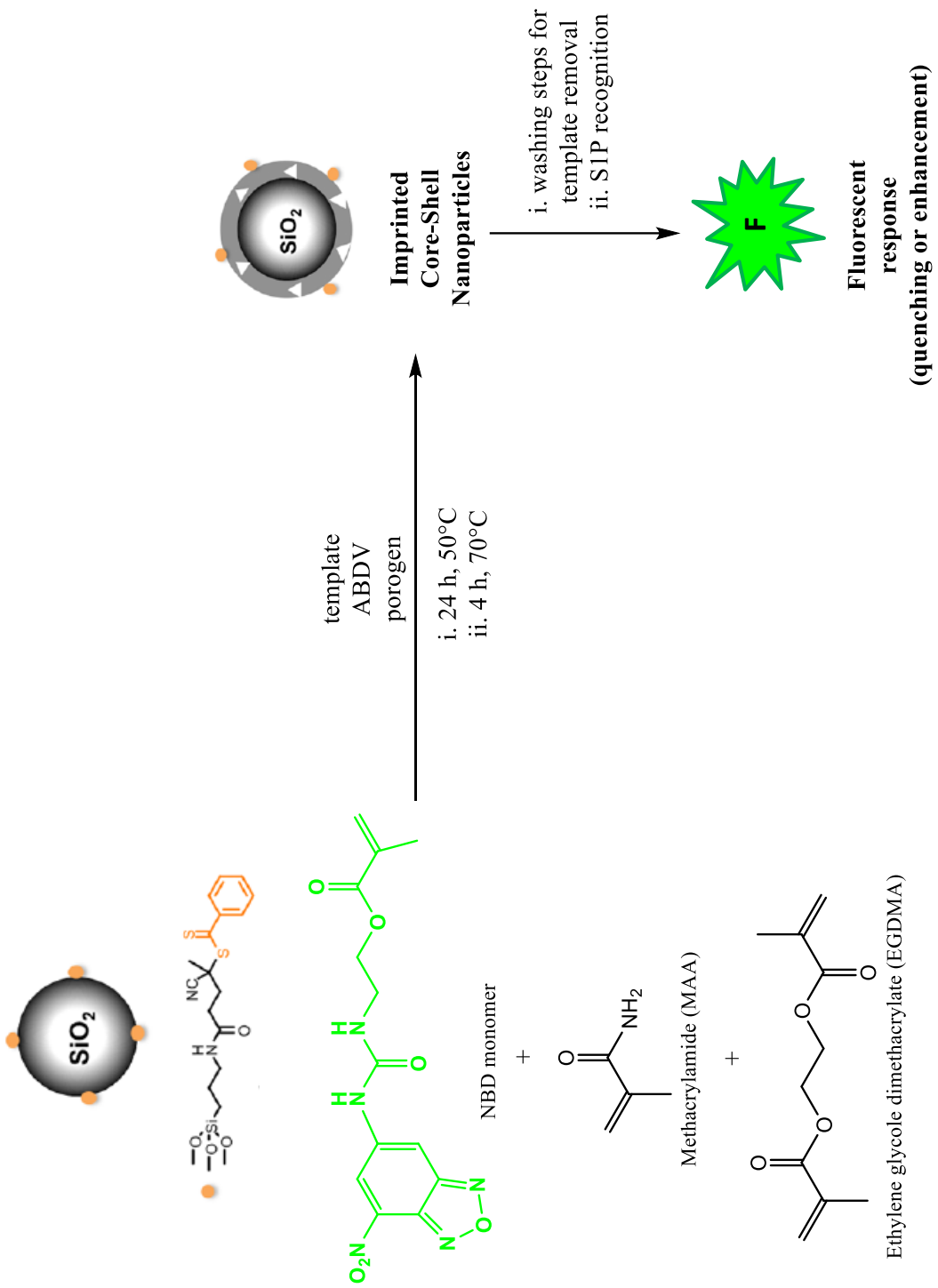

Figure 2.3: *Procedure for RAFT mediated grafting of imprinted shell on silica core particles using NBD-urea based monomer.*

The affinity of the synthesized polymers was assessed by preliminary batch extraction experiments in the following conditions: in an eppendorf vial, 5 mg of each polymer was suspended in 1 mL of 100 μM standard solutions, and after sonification for 10 minutes all the samples were left on a rocking plate overnight, at room temperature. Suddenly, 500 μL of supernatant was taken from each sample after centrifugation and precipitation of stationary phases. Among all of them, MIP 1, NIP 1 and MIP 11 were selected for further evaluations due to their higher affinity toward templates FP-Na and DPPA-Na.

The selectivity assessment for the selected polymers started with rebinding experiments using FP-Na in different H_2O:MeOH solutions (**Figure 2.4**) to find out the solvent in which the polymers could express their highest affinity. For all the polymers, the highest binding percentage was given in a solvent mixture methanol/water in the ratio of 95:5.

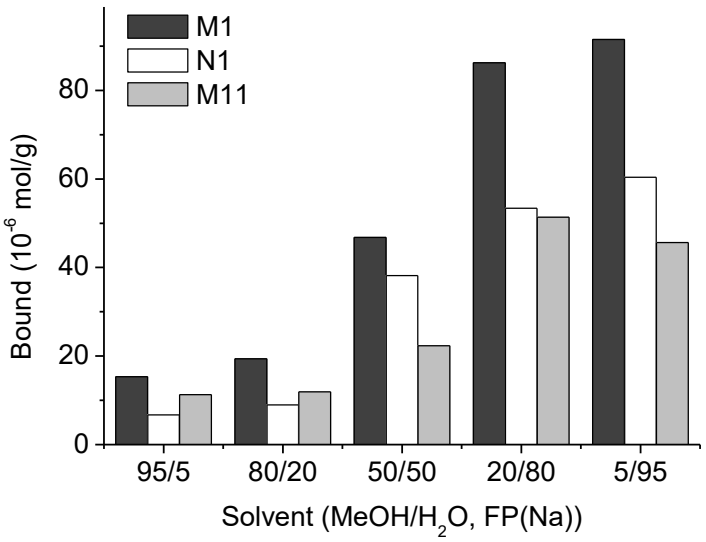

Figure 2.4: *Binding amount of polymers to FP(Na) in different ratios of methanol/water mixture; testing compound [FP(Na)]=100 μM; polymer concentration: 1 mg/mL.*

To further investigate the selectivity of MIP 1, NIP 1 and MIP 11, a screening fluorescence test was set up with the same solvent ratios. Fluorescence measurement was performed by a Perkin Elmer Luminescence Spectrometer LS 50 B as following: a suspension of nanoparticles (1 mg mL^{-1}) was prepared in 2 mL solution. The fluorescence intensity (F_0) of the suspension was measured at 512 nm using an excitation wavelength of 440 nm. After addition of testing molecules, the mixture was stirred for 30 seconds before the fluorescence intensity (F) was measured at different time intervals. The results, reported in **Figure 2.5**, highlight a significant difference between systems containing mainly methanol or water. Quenching was observed when FP was dissolved in methanol/water 95/5, on the other hand, when water was the main solvent the system showed enhancement (**Figure 2.5 a**). For DPPA (**Figure 2.5 b**), it was possible to notice only a fluorescent enhancement in every solvent mixture. Comparing these experiments, a switching point to differentiate FP(Na) and DPPA(Na) was the mixture methanol/water in the ratio 50:50, chosen as the optimized solvent. The explanation to the two opposite fluorescent response mechanisms could be found in the structure of lipids and the interactions between the target and the polymers in the different solvent ratio. Probably, the phosphate hydrophilic group could interact with the urea portion of the NBD-monomer resulting in quenching fluorescent response. On the other side of the molecule, the hydrophobic lipid tails did not switch off the monomer fluorescence because no interactions were possible between them, so they stayed on the surface of the nanoparticles giving the enhancement in the fluorescence test.

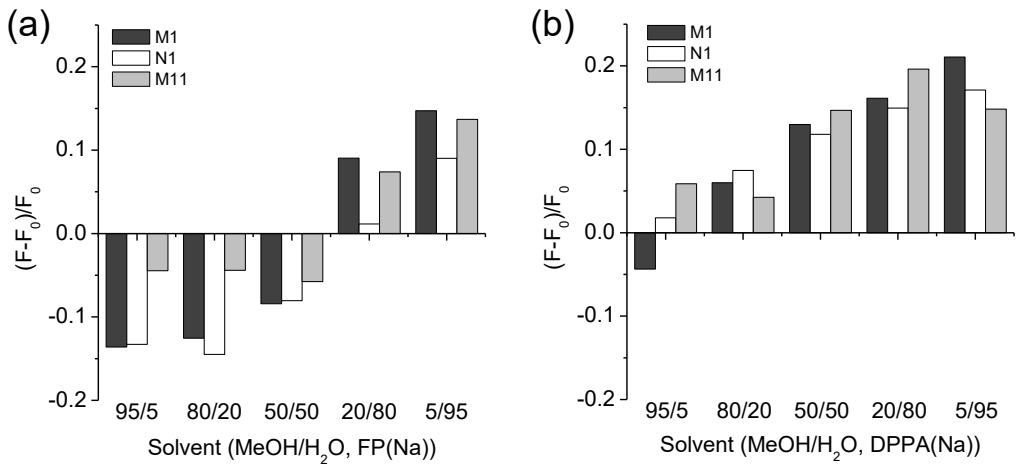

Figure 2.5: *Fluorescence response of polymers to the testing compounds (FP(Na) and DPPA(Na)) in co-solvent of methanol/water with different ratios; testing compound concentrations=100 μM; polymer concentration: 1 mg/mL.*

Suddenly we set up an "interferences experiment" and real sample experiments using the procedure as following: a suspension of nanoparticles (1 mg mL^{-1}) was prepared in 2 mL solution. The fluorescent emission spectrum of the suspension was measured using an excitation wavelength of 440 nm. After adding a concentrate solution of testing molecules or real sample (human serum), the mixture was stirred for 10 min before the new fluorescent emission spectrum was measured. The "interferences experiment", performed with molecules having phosphate moiety, namely AMP (adenosine monophosphate) and DPPA, allowed to confirm the selectivity of MIP 1 towards S1P and FP (**Figure 2.6 b**). This test (**Figure 2.6**) was set up using as solvent methanol/water (1:1).

A further confirmation of the strong interaction with such molecules appeared in a competitive test when S1P(Na) was added to a mix solution of AMP, DPPA and FP(Na). The polymers showed no response for S1P because FP(Na) occupied quite all the selective cavities. This evidence confirmed the existence of cavities on the surface of the nanoparticles able to recognize molecules having both, sphingosine and phosphate moiety.

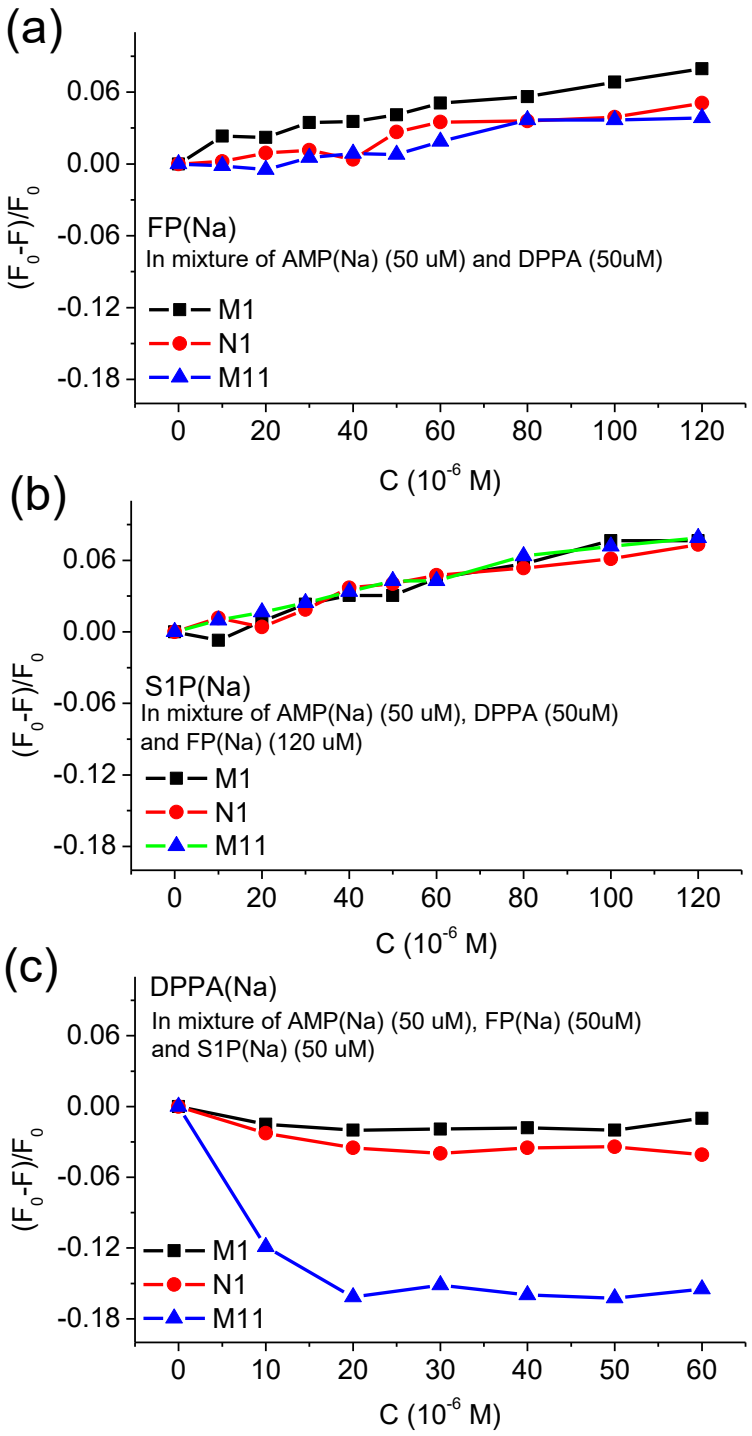

Figure 2.6: *Effect of interferences on fluorescence response of polymers towards FP(Na), S1P(Na) and DPPA(Na); polymer concentration: 1 mg/mL. Solvent: MeOH/H_2O=1/1 (v/v).*

Since the fluorescent response could be influenced by the acidity or basicity of the functional groups in solution, we checked also the pH effect (**Figure 2.7**). Usually in the pH range from 6 to 8, the fluorescent intensity should decrease, so the pH points choose for the tests were 6.0, 7.4 and 8.0. At pH=6, MIP 1 showed higher fluorescent response for S1P compared with FP and DPPA, but at pH=7.4 it showed fluorescent quenching for FP and S1P and high enhancement for DPPA. In the basic solution at pH=8, the polymers did not show any response to S1P and FP. Therefore, because of the different fluorescent behaviours at pH=7.4 towards FP(Na),S1P(Na) and DPPA(Na), it was possible to confirm that MIP 1 showed a better selectivity in neutral solutions, result that could be applied in the human serum samples.

For real sample experiments, two tests were performed on human serum (Sigma-Aldrich human male AB plasma, sterile-filtered). In the first test, human serum was diluted 25 times to reproduce physiological concentration. As shown in **Figure 2.8 a)** and **b)**, MIP 1 gave the highest fluorescent response intensity for FP(Na) and S1P(Na), compared with NIP1 and MIP11, in absence of standards spike. The opposite result was registered when S1P(Na) and FP(Na) were spiked in the polymers systems created to detect FP(Na) and S1P(Na), respectively (**Figure 2.8c)** and **d)**).

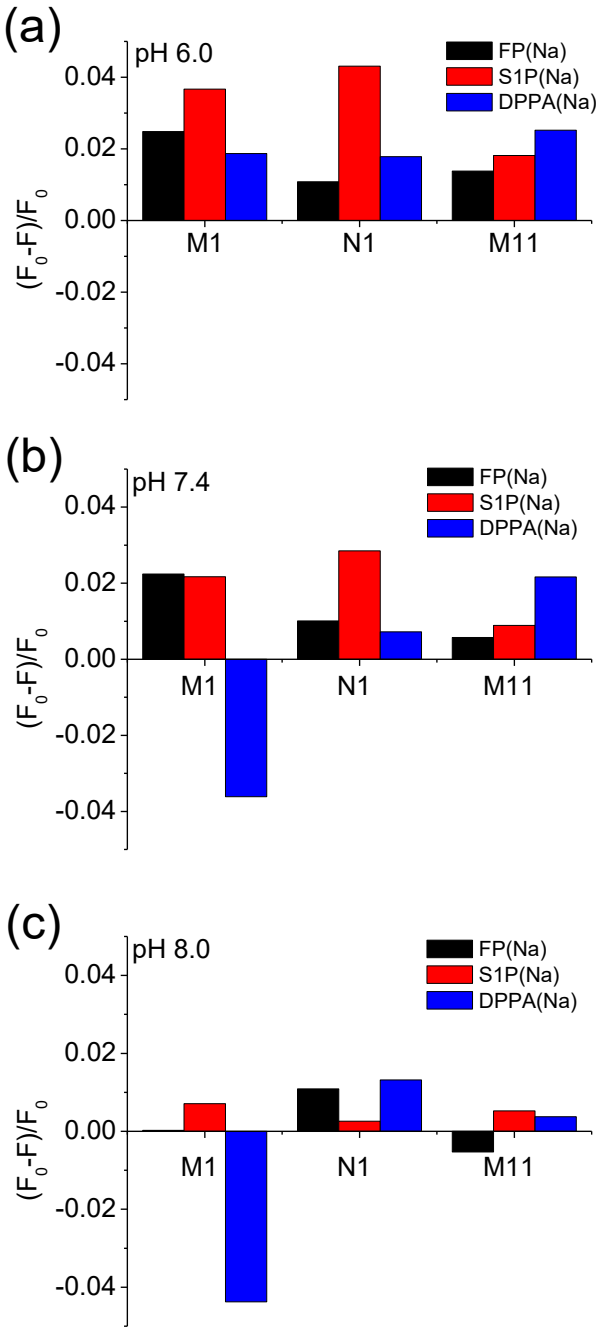

Figure 2.7: a), b) and **c)** *pH effect on the fluorescence response of polymers (M1, N1 and M11) towards FP(Na), S1P(Na) and DPPA(Na) in MeOH/PB (2.5 mM phosphate + 30 mM NaCl) = 1/1 (v/v)*; polymer concentration: 1mg/mL; targets concentration: 20 μM.

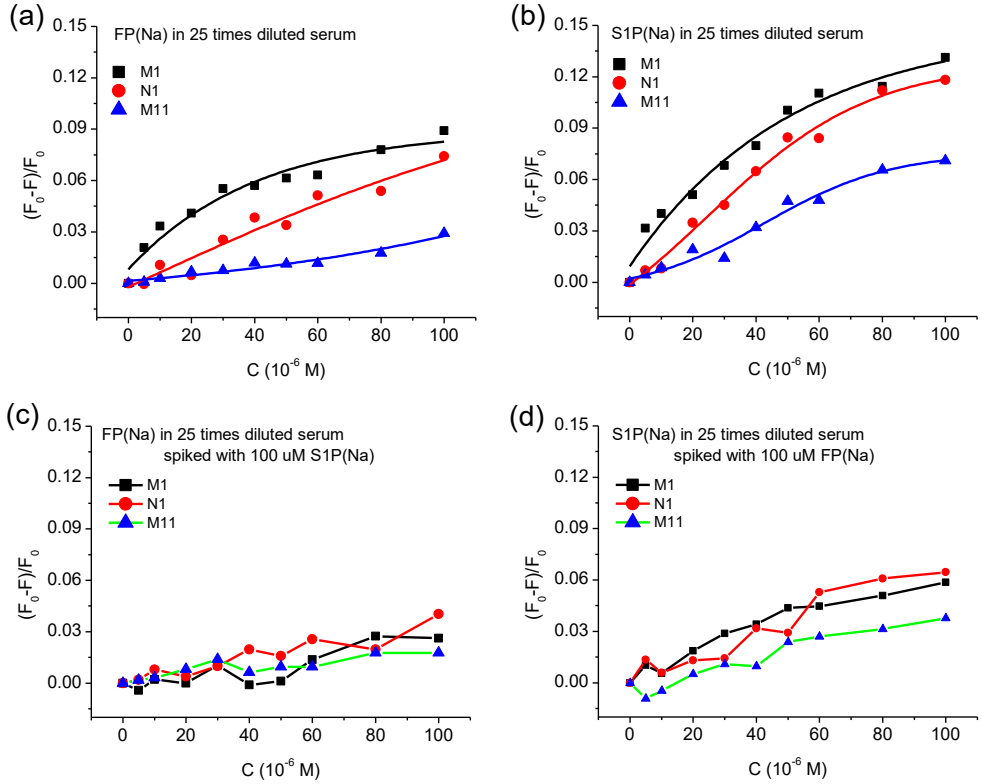

Figure 2.8: **a)** and **b)** *Fluorescence response of polymers* (MIP 1, NIP 1 and MIP 11) towards FP(Na) and S1P(Na) in 25 times diluted human serum without S1P and FP spikes; **c)** and **d)** Fluorescence response of polymers (MIP 1, NIP 1 and MIP 11) towards FP(Na) and S1P(Na) in 25 times diluted human serum with S1P and FP spikes as interferences. Polymer: 1mg/mL.

Because S1P concentration is higher in pathological conditions, the dilution was 4 times and DPPA(Na) and S1P(Na) standards were prepared in the concentration of 20 µM. Once more, MIP1 gave the highest fluorescent intensity response to S1P (**Figure 2.9**).

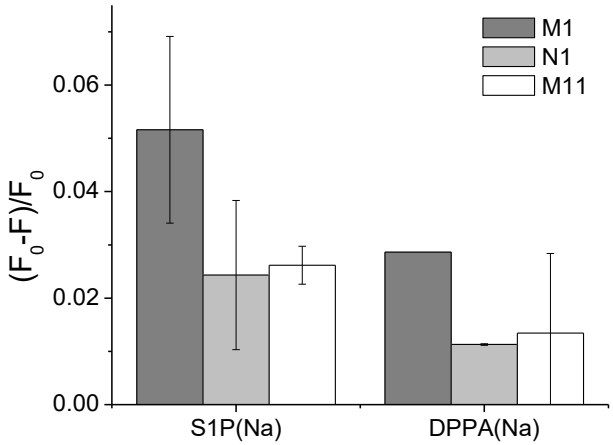

Figure 2.9: *Fluorescence response of polymers (M1, N1 and M11) towards S1P(Na) and DPPA(Na)* at a concentration of 20 µM in 4 times diluted human serum in MeOH/H_2O=1/1; polymer concentration: 1 mg/mL.

A calibration curve was performed in the range 2-20 µM for FP and 2-15 µM for S1P, respectively. The limit of detection (LoD) was found at 2 µM, a concentration one thousand time higher than the physiological one (200 nM). With the addiction of more target to the polymer, the curve reached a plateau, indicating the saturation of the material (**Figure 2.10**).

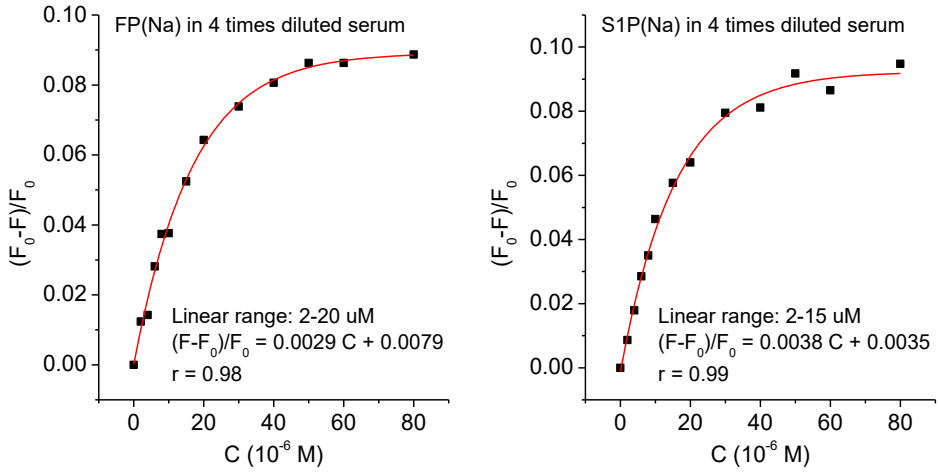

Figure 2.10: *Fluorescence response of FP imprinted nanoparticle (M1) to the targets of FP(Na) and S1P(Na) in diluted human serum (4 times dilution).* Polymer: 1 mg/mL.

2.3 Conclusions

In summary, we have used a rational selection of template, fluorogenic host monomer, polymer scaffold and particle architechture to prepare ***fluorogenic phospholipid sensors*** for the signaling lipid S1P and the S1P-receptor antagonist FP. The sensors display short response times and pronounced lipid recognition for measurements in dilute human serum. In view of the LoD exceeding ca 5x the physiologically relevant concentration (ca 1 μM) further work is required to translate this sensor concept to a practically useful sensor.

2.4 Experimental

2.4.1. Chemicals and Materials

Tetraethyl orthosilicate (TEOS), 3-aminopropyltriethoxysilane (APTES), 4-cyano-4-(thiobenzoylthio)pentanoic acid) (CPDB), triethylamine (TEA), tetrabutylammonium hydroxide solution, 1.0 M in methanol (TBA-OH), ethyl chloroformate, chloroform (anhydrous), methacrylamide (MAAm) were purchased from Sigma Aldrich (Steinheim, Germany). Ethylene glycol dimethacrylate (EGDMA) was purchased from Sigma Aldrich (Steinheim, Germany), and was passed through a column of activated basic alumina to remove inhibitor. It was stored at -20 °C before use. Methanol was purchased from Acros Organics (Geel, Belgium). Acetonitrile was obtained from Merck (Darmstadt, Germany). Milli-Q water was obtained with a Milli-Q® ultrapure water purification system (Millipore Synthesis A10).

2.4.2 Lipids standards and real samples

Lipids used during the experiments were: Sphingosine 1-phosphate (d18:1) (S1P), 1-Palmitoyl-2-oleoyl-*sn*-glycero-3-phosphoethanolamine (POPE, 16:0-18:1), 1,2-Dipalmitoyl-*sn*-glycero-3-phosphocholine (DPPC, 16:0-16:0), and 1-Palmitoyl-2-oleoyl-*sn*-glycero-3-phosphocholine (POPC, 16:0-18:1) were purchased from Avanti Polar Lipid Inc. (Alabaster, Alabama, USA). 1,2-Dipalmitoyl-*sn*-glycero-3-phosphatidic acid sodium salt (DPPA) was purchased from Codenpharma (Switzerland). Fingolimod Phosphate (FTY-720 P, FP) was purchased from Novartis Institutes for BioMedical Research (Switzerland). FP-TBA salt was prepared in equimolar ratio (1:1) of lipid and TBA-OH in methanol, stirring the solution overnight at room temperature, then the salt was dried under vacuum. Adenosine 5'-monophosphate (AMP) was purchased from Sigma Aldrich (Steinheim, Germany).

Commercial human serum from human male AB plasma, USA origin, sterile-filtered, was purchased from Sigma-Aldrich (Steinheim, Germany).

2.4.3 Apparatus

- **High performance liquid chromatography (HPLC) coupled to UV detector.** HPLC analysis were performed on Agilent 1100 instrument equipped with a UV-DAD detector and autosampler.
- **UV spectroscopy.** UV absorbance measurements were performed on a Shimadzu UV Spectrophotometer UV-1800. Samples were places into Quartz cuvettes equipped with a cap to avoid evaporation of the solvent.
- **Fluorescence spectroscopy.** Fluorescence spectra were recorded by LS-50B Spectrofluorometer (Perkin Elmer, UK). Samples were places into Quartz cuvettes equipped with a small magnetic bar stirrer and a cap to avoid evaporation of the solvent.

2.4.4 Methods

2.4.4.1 Synthesis of fluorescent NBD-urea based functional monomer

The fluorescent functional monomer 2-(3-(4-nitrobenzo[c][1,2,5]oxadiazo-7-yl)ureido)ethylmethacrylate (NBD-urea) was synthesized according to our previously published protocol (Wan *et al.*, 2013).

2.4.4.2 Preparation of silica nanoparticles (SiNPs)

Silica nanoparticles (SiNP) were prepared following a modified (Shinde *et al.*, 2015) Stöber method. 25% ammonia solution (7.6 mL), 99.9% pure ethanol (50 mL), and milli-Q water (76.5 mL) were mixed in a round bottom flask and stirred at 600 rpm. Subsequently, a mixture of TEOS (11.4 mL) and ethanol (114 mL) was added. The reaction mixture turned turbid white as

soon as SiO_2 nanoparticles were formed after circa 10 minutes. The reaction was stirred for 8 hours, at room temperature. Thereafter, the particles were collected by centrifugation (10.000 rpm, 10 min, at room temperature), and washed by redispersion in ethanol at least three times. Finally, the product was dried under vacuum, at room temperature, overnight.

2.4.4.3 Amino-modified silica nanoparticles (NH_2@SiNPs)

RAFT-SiNPs were synthesized according to our previously reported method (Shinde *et al.*, 2015). A suspension of SiO_2 nanoparticles (SiNPs) (14 g) in anhydrous toluene (200 mL) was added to a three-necked round-bottom flask and stirred under nitrogen. Based on the theoretical number of silanol groups (8 μmol/m^2), an excess of 3-aminopropyltriethoxysilane (APTES) (2.37 g, 10.7 mmol) was then added and the mixture refluxed for 12 hours, at 130 °C, under nitrogen. The mixture was then cooled down till room temperature. The particles were collected by centrifugation (10 000 rpm, 10 min, at room temperature), and washed by methanol at least three times. Finally, the amino functionalized silica nanoparticles (NH_2@SiNPs) were dried under vacuum, at room temperature for two days.

2.4.4.4 Preparation of RAFT modified silica nanoparticles (RAFT@SiNPs)

RAFT-SiNPs were synthesized according to our previously reported method (Shinde *et al.*, 2015). A solution of CPDB (0.385 g, 1.38 mmol), ethylchloroformate (132 µL, 1.38 mmol) and triethylamine (TEA, 192 µL, 1.38 mmol) in THF (50 mL) was added to a three-necked round bottom flask (250 mL). The solution was purged with nitrogen and cooled in an ethanol-liquid nitrogen bath for 40 minutes at -70 °C. At the same time, a stock solution of NH_2@SiNPs (7.0 g in 70 mL THF) was prepared and added to the RAFT solution at -10 °C. The reaction allowed to proceed overnight at room temperature. The RAFT reagent modified silica nanoparticles

(RAFT@SiNPs) were collected by centrifugation (10 000 rpm, 10 min, at room temperature), washed with ethanol at least five times and dried under vacuum, at room temperature, overnight.

2.4.4.5 Preparation of molecularly imprinted core shell nanoparticles

In a 20 mL glass vial (vial 1), 150 mg of RAFT@SiNPs were purged for 5 minutes under N_2 flow, suspended in 15 mL $CHCl_3$ (dry), and sonicated for 15 minutes. In another 20 mL glass vial (vial 2), NBD-urea based functional monomer (15.2 µmol, 5.1 mg) and the template, FP (TBA) (**P1**) (4.8 mg, 7.6 µmol) or DPPA (Na) (**P2**) (5.1 mg, 7.6 µmol), were solubilized in 4 mL of $CHCl_3$ (dry), and left shaking on the rocking plate for 15 minutes, at room temperature to allow formation of the functional monomer-template complex (FM-T). Then, the co-functional monomer MAAm (306 µmol, 26 mg) was added, and the mixture shacked for other 5 minutes. At this point, the content of vial 2 (FMs-T) was slowly added to the vial 1 (RAFT@SiNPs). In an ice bath, the crosslinker EGDMA (1.5 mmol, 297.3 mg, 282 µL) and the initiator ABDV (35 µmol, 8.7 mg) were mixed in an eppendorf with the help of 1 mL $CHCl_3$ (dry). Vial 1, containing RAFT@SiNPs and the mix FMs-TEMPLATE, was placed in the ice bath and solution CL-I was added. The pre-polymerization mixture obtained was purged under a flow of N_2 for 10 minutess. The sealed system was left reacting on a thermo-shacking block at 60°C for 18 hours, then 3 hours at 70 °C.

A NIP (non-imprinted polymer) was prepared using the same protocol, without addiction of the template. At the end of the reactions, vials containing polymers were cooled down till room temperature. The synthesized materials were transferred into 50 mL centrifuge tubes, washed with ACN:$CHCl_3$ (70:30) for three times, and successively with MeOH (100%) to allow sedimentation of the particles by centrifugation at 10.000 rpm, for 15 minutes, at room temperature. The polymers were then dried overnight, in a vacuum pump, at room temperature.

2.4.4.6 Binding test for FP

10 mg of core-shell nanoparticles (P1) were suspended in 1 mL solution containing the template molecule FP-TBA in the concentration of 100 µM . After 4 hours incubation on a rocking plate at room temperature, all samples were centrifuged, and the supernatant was used for reverse phase HPLC-UV/Vis analysis to detect the binding ability of the polymers. The HPLC-UV/Vis analysis was performed following our previous developed method (Narayanaswamy *et al.*, 2014). The peak areas obtained were used to create a calibration curve and calculate the quantity of analyte caught by the different materials using the following equation:

$$B=(C_0-C_f)\cdot V/m$$

where C_0 was the initial standard concentration, C_f was the free standard concentration detected in the supernatant solution, V was the total volume of the sample, and m was the mg of polymer used for the test.

2.4.4.7 Fluorescent binding solvent study

To obtain the best binding ability of the synthesized materials, different solvent mixtures composed of organic and aqueous phase were tested. The organic solvent chosen was MeOH, since it represents the best solvent in which lipids are commonly solubilized. 2 mg of each polymer were suspended in 2 mL phase prepared in the percentage (%) as reported: 100% aqueous, 25% organic, 50% organic, 70% organic, 80% organic, 90% organic, 100% organic. A spike of 20 µM of the template was added in each suspension. The tubes were then sonicated for 30 minutes, covered with aluminium foil to protect materials from light degradation, and incubated overnight at room temperature on a shaking plate. All the experiments were performed in Quartz cuvettes equipped with caps to avoid solvent evaporation. Fluorescence spectra were recorded exciting at λ_{ex} 440 nm, and the emission spectra were collected between 450-600 nm.

2.4.4.8 Fluorescent kinetic study

To study the response time of the synthesized materials, fluorescence spectra were collected at different times. 2 mg of each polymer were suspended in 2 mL phase H_2O:MeOH of different volume ratio, and the tubes were sonicated for 30 minutes. All the experiments were performed in Quartz cuvettes equipped with a small magnetic bar stirrer and a cap to avoid evaporation of the solvent. Fluorescence spectra were recorded exciting at λ_{ex} 440 nm, and the emission spectra were collected between λ_{em} 450-600 nm. Before measuring spectra of spiked materials, a blank was collected. Then a spike of 100 µM of the target molecules FP-Na and DPPA-Na was added in each suspension and fluorescence spectra were recorded at different times, as report: 0 mins (after spike), 5, 10, 15, 30, 45, and 60 minutes.

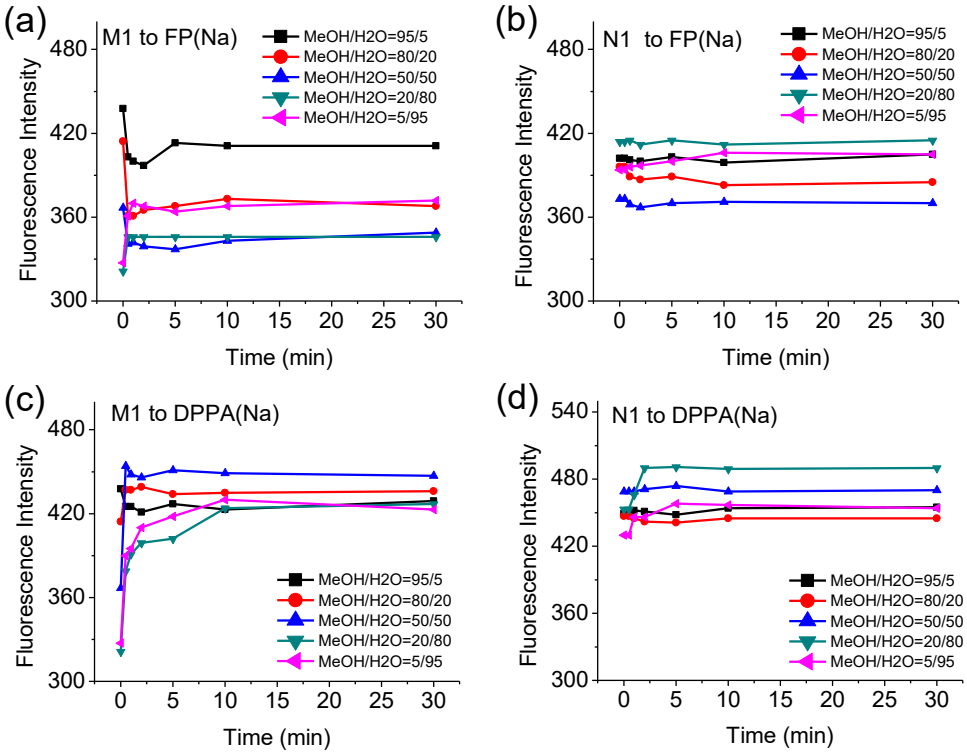

Figure 2.11: *Fluorescence emission intensity versus time for the indicated core/shell polymers after addition of lipids in methanol/water of different volume ratios. Polymer concentration: 1 mg/mL; test molecule concentration: 100 µM.*

2.5 Application

2.5.1 Sensing titration protocol

Target molecules used for the sensing titrations protocol were S1P-Na, FP-Na and DPPA-Na. Lipids stock solutions were prepared in the concentration of 1 mM in MeOH. 2 mg of each material was suspended in 2 mL H_2O:MeOH (1:1) solution, and, after 30 minutes sonication, the tubes were covered to protect polymers from light degradation and incubated overnight at room temperature on a shaking plate. All the experiments were performed in Quartz cuvettes equipped with a small magnetic bar stirrer and a cap to avoid evaporation of the solvent. Fluorescence spectra were recorded exciting at λ_{ex} 440 nm, and the emission spectra were collected between λ_{em} 450-600 nm. Before measuring spectra of template spiked materials, a blank was collected. Then the particles suspensions were titrated with the lipids at increasing concentrations in the range 0.5-1-5-10-20-50-100 µM, and fluorescence spectra were collected every 10 minutes after addiction to allow suspension equilibration under a continuous gentle stirring.

2.5.2 Fluorescence detection in real sample matrix

The matrix chosen for spiked real sample detection of the lipids was human serum. Frozen human serum was thawed for 45 minutes, till room temperature. Then 1 mL of concentrated human serum was collected and diluted 1:20 in milliQ H_2O. An equivalent volume of MeOH was added to the diluted serum, then the mixture was vortexed for 1 minute, sonicated for 30 minutes and centrifuged at 10.000 rpm, at 4°C, for 20 minutes to allow protein precipitation. The supernatant obtained was transferred in a fresh 50 mL falcon tube and stored at -20°C before use.

For the titration in human serum matrix, 2 mg of each material was suspended in 2 mL human serum matrix solution, and, after 30 minutes sonication, the tubes were covered with aluminium foil to protect polymers from light degradation, and incubated overnight at room temperature on a shaking plate. All the experiments were performed in Quartz cuvettes equipped with a small magnetic bar stirrer and a cap to avoid evaporation of the solvent. Fluorescence spectra were recorded exciting at λ_{ex} 440 nm, and the emission spectra were collected between λ_{em} 450-600 nm. Before measuring spectra of materials in spiked human serum matrix, a blank was collected. Then, to create the calibration curves, the particles suspensions were titrated with the lipids S1P-Na and FP-Na at increasing concentrations in the range 0.5-1-5-10-20-50-100 µM, and fluorescence spectra were collected every 10 minutes after addiction to allow suspension equilibration under a continuous gentle stirring.

2.5.3 Study of the accuracy of the sensor

To study the accuracy of the sensor, human serum spiked with targets, FP(Na) or S1P(Na), was mixed with 1 mL methanol for 30 min. After centrifugation, 1 mL supernatant was mixed with 1 mL of a suspension (2 mg/mL) of the core-shell particles in H_2O:MeOH (1:1) solution. The suspension was gently stirred for 10 min before measurements. All the experiments were performed in Quartz cuvettes equipped with a small magnetic bar stirrer and a cap to avoid evaporation of the solvent. Fluorescence spectra were recorded exciting at λ_{ex} 440 nm, and the emission spectra were collected between λ_{em} 450-600 nm. Before measuring spectra of materials in spiked human serum matrix, a blank was collected. The results corresponded to averages of three independent experiments. Assuming a linear correlation between fluorescence signal and adsorbed amount of analytes, we used equilibrium binding analysis to estimate the dissociation constant, Kd for the analyte-particle interaction. The response curves in **Figure 2.9** (*vide supra*) were fitted to the Langmuir single site model using Graphpad Prism v7.0. The limit

of detection (LoD) was estimated as the concentration producing a signal corresponding to a minimum of three times the standard deviation (SD) of the blank signal.

2.6 Materials Characterization

Sensors object of interest in this chapter were characterized by scanning electron microscopy (SEM), transmission electron microscopy (TEM), dynamic light scattering (DLS), thermogravimetric analysis (TGA) and Fourier Transform - Infrared spectroscopy (FT-IR).

- **Scanning electron microscopy (SEM).** The particle morphology, size and size distribution were determined using Zeiss EVO LS 10 CANSEM (Carl Zeiss AG, Oberkochen, Germany) at T ¼ 25 °C, EHT ¼ 15 kV, WD ¼ 4.5 mm.

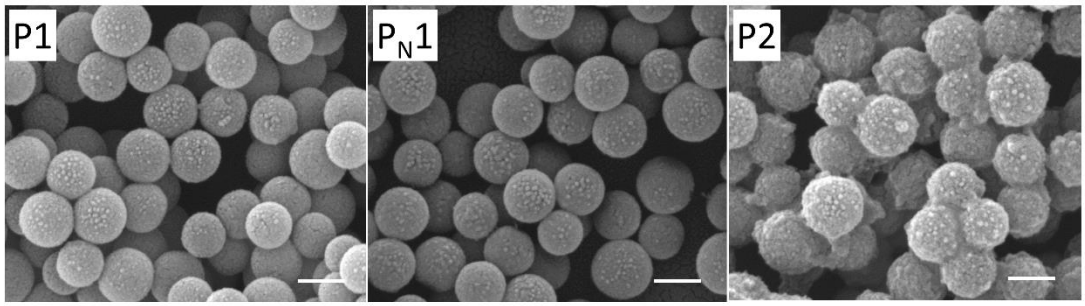

Figure 2.12: *SEM images of P1, P_N1 and P2. Scale bar=200 nm.*

- **Transmission electron microscopy (TEM).** The particle core was observed and studied by a Tecnai G2 transmission electron microscope (FEI, USA).

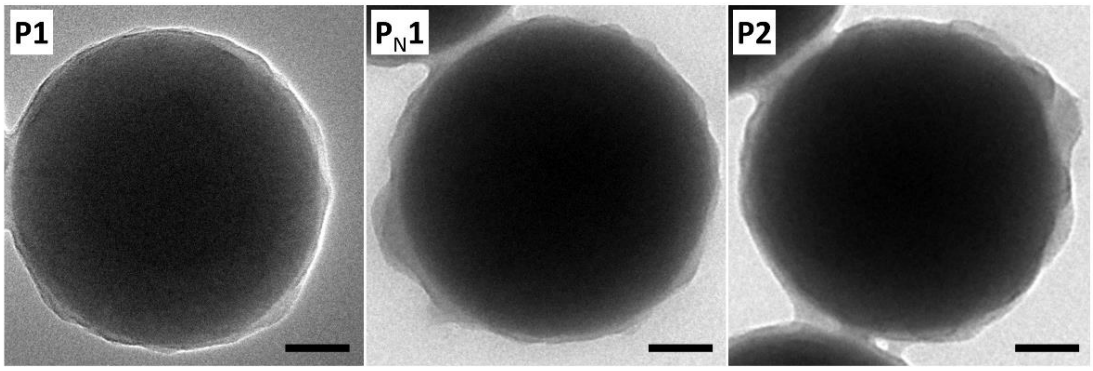

Figure 2.13: *TEM characterization results corresponding to the core-shell particles of P1, P_N1 and P2. Scale bar = 50 nm.*

- **Dynamic Light Scattering (DLS).** Particle sizes were measured by a Zeta Potential/Particle Sizer NICOMP™ 380 ZLS instrument with ZPW388 software from Particle Sizing Systems (USA). Ca 1mg of obtained particles were dispersed in methanol to a concentration ~0.1 mg mL^{-1} and sonicated for 10 min, then analysed by DLS at 25°C.

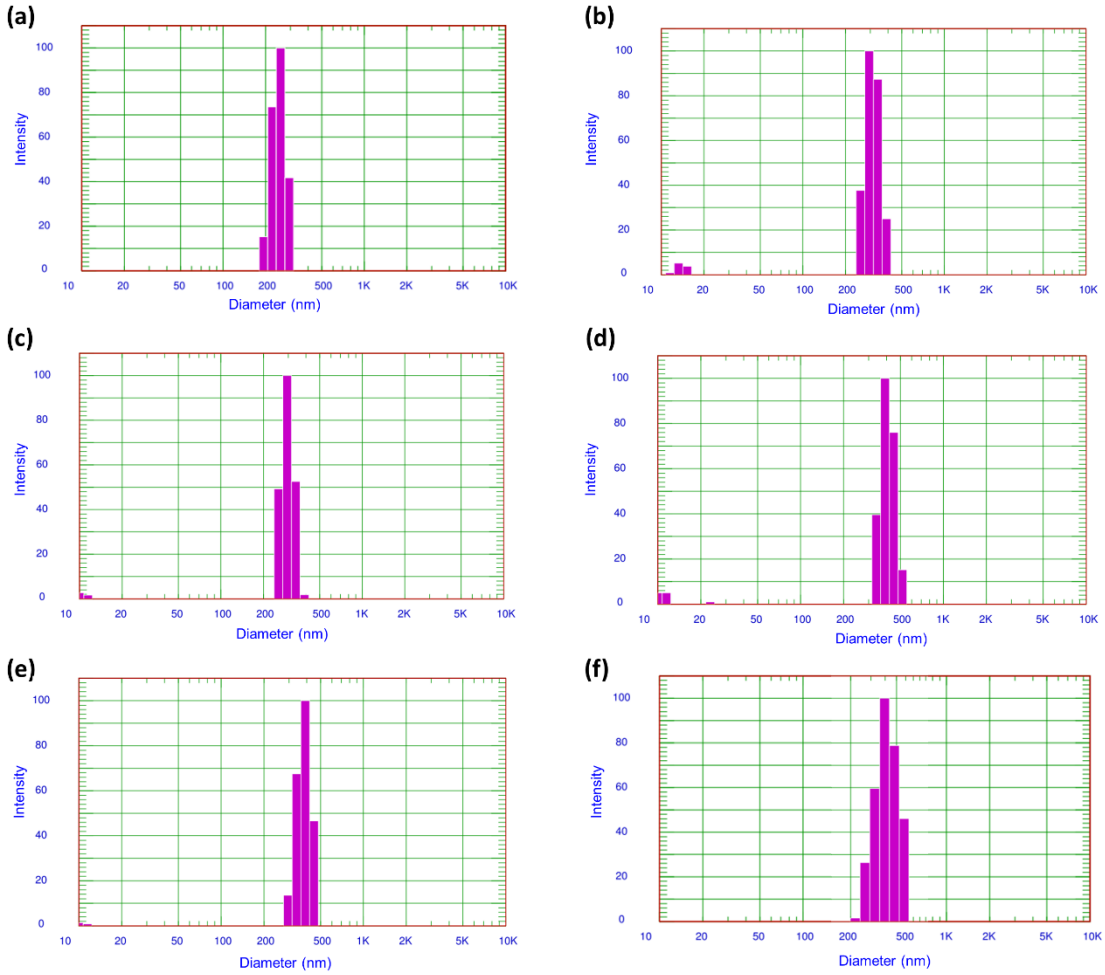

Figure 2.14: *Particle size distribution of SiNP (a), SiNP-NH_2 (b), SiNP-RAFT (c), FP-imprinted nanoparticle (P1, d), non-imprinted nanoparticle (P_N1, e) and DPPA-imprinted nanoparticle (P2, f), measured by dynamic light scattering (DLS) in methanol.*

- **Thermogravimetric analysis (TGA).** TGA was carried out through TGAQ500 (Ta Instruments). Ca 10 mg of each sample was placed on a platinum pan, after tare. The sample was heated at 10°C/min till 800°C, under N_2 atmosphere.

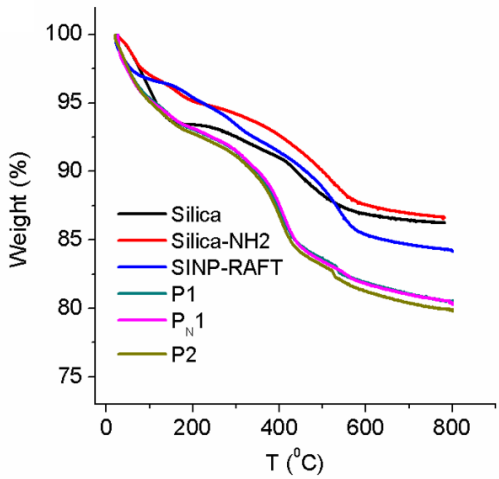

Figure 2.15: *TGA curves of Silica nanoparticle, Amino-functionalized Silica nanoparticles, RAFT-silica nanoparticles, and polymers P1, P_N1 and P2.*

- **FT-IR spectroscopy.** Infrared spectra were recorded using a Thermo Nicolet Nexus 6700 instrument (Thermo Scientific, Waltham, MA, USA).

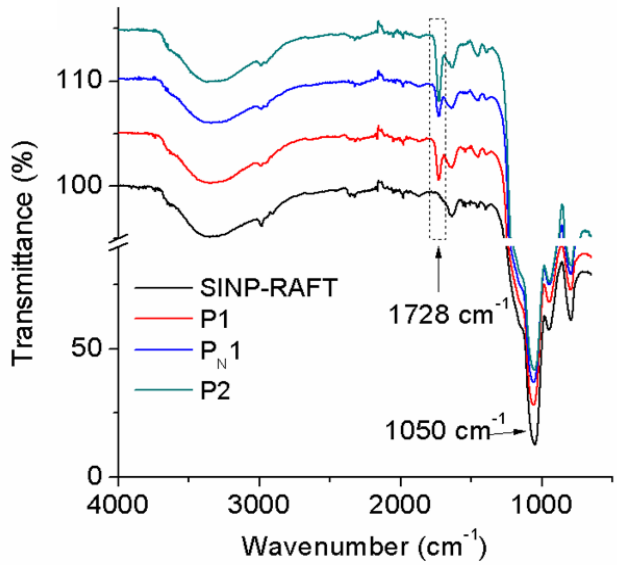

Figure 2.16: *IR characterization of RAFT functionalized Silica nanoparticles, and polymers P1, P_N1 and P2.*

Comments		SiNP	SiNP@NH_2	SiNP@RAFT	P1	P_N1	P2
DLS	Average size, nm	266±15	322±7	295±3	407±4	410±25	443±65
TGA	Weight loss*, %	9.7	10.4	12.6	14.9	14.9	15.3
FT-IR	I_{1728}/I_{1050}**	/	/	0	0.043	0.048	0.063

Table 2.1: *Results from core-shell particles characterization*. For TGA, *excluding water; for FT-IR, **ratio of C=O (1728 cm^{-1}) to Si-O (1050 cm^{-1}) vibrations.

Bibliography

Breslow, R.; Zhang, B. (1996), Cholesterol recognition and binding by cyclodextrin dimers, *Journal of the American Chemical Society*, 118, 8495-8496.

Brinkmann, V., Billich, A., Baumruker, T., Heining, P.,Schmouder, R., Francis, G., Aradhye, S, Burtin, P., (2010), Fingolimod (FTY720): discovery and development of an oral drug to treat multiple sclerosis, *Nature. Reviews. Drug Discovery*, 9, 883-97.

Chen, L.; Wang, X.; Lu, W.; Wu, X.; Li, J., (2016), Molecular imprinting: perspectives and applications. *Chemical Society Reviews*, 45, 2137-2211.

Chiba, K., and Adachi, K., (2012), Sphingosine 1-Phosphate Receptor 1 as a Useful Target for Treatment of Multiple Sclerosis, *Pharmaceuticals*, 5 (5), 514-28.

David, O. J., Berwick, A., Pezous, N., Lang, M., Tiel-Wilck, K., Ziemssen, T., Li, P., Hara, H.; Schmouder, R, (2018), Determination of Seminal Concentration of Fingolimod and Fingolimod-Phosphate in Multiple Sclerosis Patients Receiving Chronic Treatment With Fingolimod, *Clinical Pharmacology in Drug Development*, 7 (2), 217-21.

Haupt, K., and Ayela, C., (2012), Molecular Imprinting; Springer.

He, X., Huang, C. L., and Schuchman, E. H., (2009), Quantitative analysis of sphingosine-1-phosphate by HPLC after napthalene-2, 3-dicarboxaldehyde (NDA) derivatization, *Journal of Chromatography B*, 877 (10), 983-990.

Kunkel, G. T., Maceyka, M., Milstien, S. and Spiegel, S., (2013), Targeting the sphingosine-1-phosphate axis in cancer, inflammation and beyond, *Nature Review. Drug Discovery*, 12, 688-702.

Li, Q.; Shinde, S., Grasso, G., Caroli, A., Abouhany, R., Lanzillotta, M., Pan, G., Wan, W., Rurack, K., Sellergren, B., Fluorescent Sensory Core-shell Particles for Selective Detection of Sphingosine1-Phosphate. *Submitted*.

Marti, T.; Peterson, B. R.; Fürer, A.; Mordasini-Denti, T.; Zarske, J.; Jaun, B.; Diederich, F.; Gramlich, V., (1998), Macrotricyclic steroid receptors by Pd-0-catalyzed cross- coupling reactions: Dissolution of cholesterol in aqueous solution and investigations of the principles governing selective molecular recognition of steroidal substrates, *Helvetica Chimica Acta*, 81, 109-144.

Min, J. K., Yoo, H. S., Lee, E. Y., Lee, W. J., and Lee, Y. M., (2002), Simultaneous quantitative analysis of sphingoid base 1-phosphates in biological samples by o-phthalaldehyde precolumn

derivatization after dephosphorylation with alkaline phosphatase, *Analytical Biochemistry*, *303*(2), 167-175.

Narayanaswamy, P., Shinde, S., Sulc, R., Kraut, R., Staples, G., Thiam, C. H., Grimm, R., Sellergren, B., Torta, F., Wenk, M. R.,(2014), *Analytical Chemistry*,86, 3043-3047.

Sellergren, B., and Hall, A. J., *Molecularly Imprinted Polymers. In Supramolecular Chemistry: from Molecules to Nanomaterials*, Steed, J. W., Gale, P. A., Eds.; John Wiley & Sons Ltd: Chichester, UK, 2012; pp 3255-3282.

Shaner, R. L., Allegood, J. C., Park, H., Wang, E., Kelly, S., Haynes, C. A., Merrill A. H., (2009), Quantitative analysis of sphingolipids for lipidomics using triple quadrupole and quadrupole linear ion trap mass spectrometers. *Journal of Lipid Research*, 50 (8), 1692-1707.

Shinde, S., El-Schich, Z. Malakpour, A., Wan, W., Dizeyi, N., Mohammadi, R., Rurack, K., Gjörloff Wingren, A., Sellergren, B., (2015), Sialic Acid-Imprinted Fluorescent Core–Shell Particles for Selective Labeling of Cell Surface Glycans; *Journal of American Chemical Society*, *137* (43), 13908–13912.

Shorthill, B. J.; Avetta, C. T.; Glass, T. E., (2004), Shape-Selective Sensing of Lipids in Aqueous Solution by a Designed Fluorescent Molecular Tube, *Journal of the American Chemical Society*, 126, 12732-12733.

Sulc, R., Szekely, G., Shinde, S., Wierzbicka, C., Vilela, F., Bauer, D., Sellergren, B., (2017), Phospholipid imprinted polymers as selective endotoxin scavengers, *Scientific Reports*, 7, 44299, DOI: 10.1038/srep44299.

Walash, M. I., Metwally, M. E., Eid, M., El-Shaheny, R. N., (2012), Validated spectrophotometric methods for determination of Alendronate sodium in tablets through nucleophilic aromatic substitution reactions, *Chemistry Central Journal*, 6 (1), 25.

Wan, W., (a) Biyikal, M., Wagner, R., Sellergren, B., Rurack, K., (2013), Fluorescent sensory microparticles that "light-up" consisting of a silica core and a molecularly imprinted polymer (MIP) shell, *Angewandte Chemie. (International Ed. In English)*, 52, 1-6, 7023-7027.

Wan, W., (b) Descalzo, A. B., Shinde, S., Weisshoff, H., Orellana, G., Sellergren, B., Rurack, K., (2017), Ratiometric fluorescence detection of phosphorylated amino acids through excited-state proton transfer by using molecularly imprinted polymer (MIP) recognition nanolayers, *Chemistry: an. European Journal*, 23, 15974-15983;

Whitcombe, M. J., Kirsch, N., Nicholls, I. A., (2014), Molecular imprinting science and technology: a survey of the literature for the years 2004-2011, *Journal of Molecular Recognition*, 27, 297-401.

Wu, N. W., and Rebek,J. J., (2016), Cavitands as chaperones for monofunctional and ring-forming reactions in water, *Journal of the American Chemical Society*, 138, 7512-7515.

Xu, M.; Kelley, S. P.; Glass, T. E., (2018), A multi-component sensor system for detection of amphiphilic compounds, *Angewandte Chemie International Edition* 2018, 57, 12741-12744.

Yatomi, Y., Igarashi, Y., Yang, L., Hisano, N., Qi, R., Asazuma, N., Satoh, K., Ozaki, Y., Kume, S., (1997), Sphingosine 1-phosphate, a bioactive sphingolipid abundantly stored in platelets, is a normal constituent of human plasma and serum, *Journal of Biochemistry*, *121* (5), 969-973.

PART 3

FUTURE PROSPECTIVES

CHAPTER III

PC-MIP: Targeting Phosphatidylcholine by Molecularly Imprinted Polymers

3.1 Introduction

Lipids are a large group of naturally occurring molecules that play fundamental biological roles: they are involved in energy storing, signalling and are structural components of cell membranes (Dowhan *et al.*, 2016). Among phospholipids class, phosphatidylcholine (PC) is the major component of eukaryotic cell membranes and one of the most commonly used phospholipids for reconstitution of membrane proteins into carrier systems such as lipid vesicles, micelles and nano-discs. Selectively deuterated versions of this lipid have many applications, especially in structural studies using techniques such as NMR, neutron reflectivity and small-angle neutron scattering. However, the selective deuteration of phosphatidylcholine (PC), through biosynthesis in a genetically modified strain of Escherichia Coli (Maric *et al.*, 2015), represents a complex matrix that needs several steps of treatment. A practical way of improving recovery experiments regarding lipids could be the use of more selective stationary phases, in both sample pre-treatment and chromatographic separation. With this purpose, the synthesis of Molecularly Imprinted Polymers (MIPs) (Sellergren, 2001) and their application as Solid Phase Extraction (SPE) could represent a promising option for the development of selective capture materials aiming to the separation of the specific target molecule, phosphatidylcholine (PC). We here report preliminary results from our attempts to explore this possibility. A library of imprinted and non-imprinted phospholipid capture materials was tested for their ability to enrich PC with minimal cross-reactivity of non-zwitterionic lipids. The specific enrichment factor and binding capacity will be reported for tests of PC enrichment from engineered E. Coli lysates.

3.2 Results and Discussion

Lipid extraction and fractionation is still largely based on partitioning procedures developed in the 1950s. Unfortunately, within the same class of lipids, tiny differences can exist thus making challenging the separation and analysis of single lipids. In the past, the Lipidomic analysis relied on the use of thin layer chromatography (TLC) or gas chromatography (GC) after the derivation of polar functionalities, but nowadays electrospray ionization mass spectrometry (ESI-MS) is by the far the most frequently used analytical technique due to several significant advantages over other techniques, such as excellent sensitivity, easy coupling with liquid-phase separation techniques, structural details based on the use of tandem mass spectrometers with high mass accuracy, applicable for a wide range of lipids analysable either in positive- or negative-ion modes, and very low sample consumption (Holčapek *et al.*, 2018).

The aim of this project is the development of advanced MIP materials using the combination of imprinting approach and supramolecular recognition properties of the solid substrate. Molecularly imprinted polymer (MIP) is a very attractive technique to obtain a smart material having the selective recognition ability for targeting compounds by simple preparation procedures.

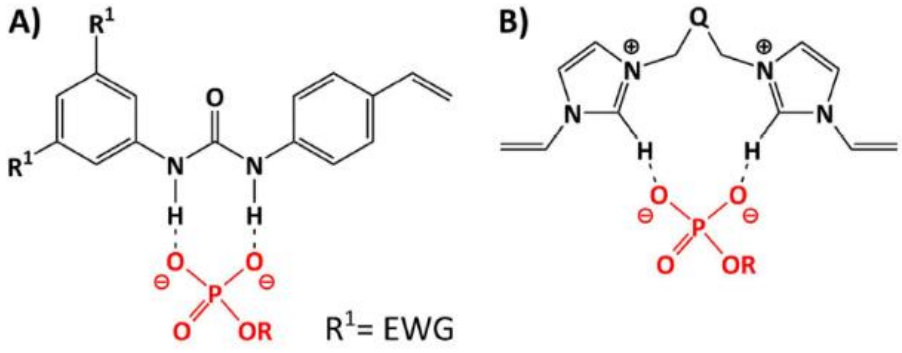

Figure 3.1: *Monomers and binding ability*. Theoretical hydrogen bonding interactions with the target phosphate group and (**A**) 1,3-diarylurea host monomer and (**B**) bis-imidazolium host monomers (Sulc *et al.*, 2017).

As mentioned before, imidazolium cycles (host) have been recognized as chemical moieties able to coordinate phosphate ions (guest) through strong hydrogen bonds between the carbon atoms (-C-H) of imidazolium and the oxygen atoms (O=P- and OH-P-) of $H_2PO_4^-$. An additional hydrogen bond has been derived from the pyridinium heterocycle used as spacer (Q), between the imidazolium moieties, and gave a further stabilization in the binding between guest and host (**Figure 3.1 B**). Another work of our group reported on a range of imprinted anion receptors for carboxylates, phosphates and sulphates featuring 1,3-disubstituted ureas (Wierzbicka (a) *et al*.,2017) have been defined as neutral receptors for anions. Thys type of hosts are potent hydrogen bond donors capable of forming two-fold cyclic hydrogen bonds with anions guest (**Figure 3.1 A** and **Figure 3.2**).

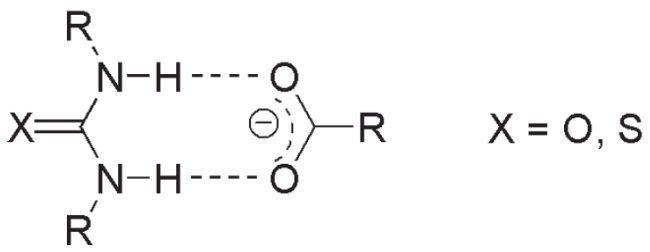

Figure 3.2: *Schematic representation of the interaction between urea (X=O) or thiourea (X=S) receptors and carboxylate anions* (Wierzbicka (b), 2017).

The strength of interaction increases with the acidity of urea protons and basicity of complexed anions. Another factor influencing the strength of interaction is the type of solvent in which the recognition occurs. Neutral receptors, such as urea, are highly susceptible to competition with polar protic solvents for anion binding. Thus, this type of receptors is most effective in aprotic organic solvents. The 1,3-diarylurea based functional monomer of this study was evaluated by NMR titration experiments with TBA salt of PPA guest in DMSO-d6 (**Figure 3.3**) (Wierzbicka (b), 2017). The data points obtained were fitted in to 1:1 interaction model to determine values of association contant (K_a) and maximum complexation induced shift (CIS) (**Table 3.1**).

Table 3.1: *Association constant, stoichiometry and complexation induced shifts for complexes formed between 1,3-diarylurea based host monomer and PPA-TBA guest in DMSO-d_6.*

[a] Complexation induced shifts (CIS) and Hill slope based on the shift value of the resonance signals indicated (Wierzbicka (a) *et al*., 2017).

Host monomer	Guest	Proton	K_a (M^{-1})	Cplx (H:G)	CIS[a] (ppm)	h[a]
1,3-diarylurea	PPA-TBA	NH (7, 8)	7350±320	1:1	2.90	1.0

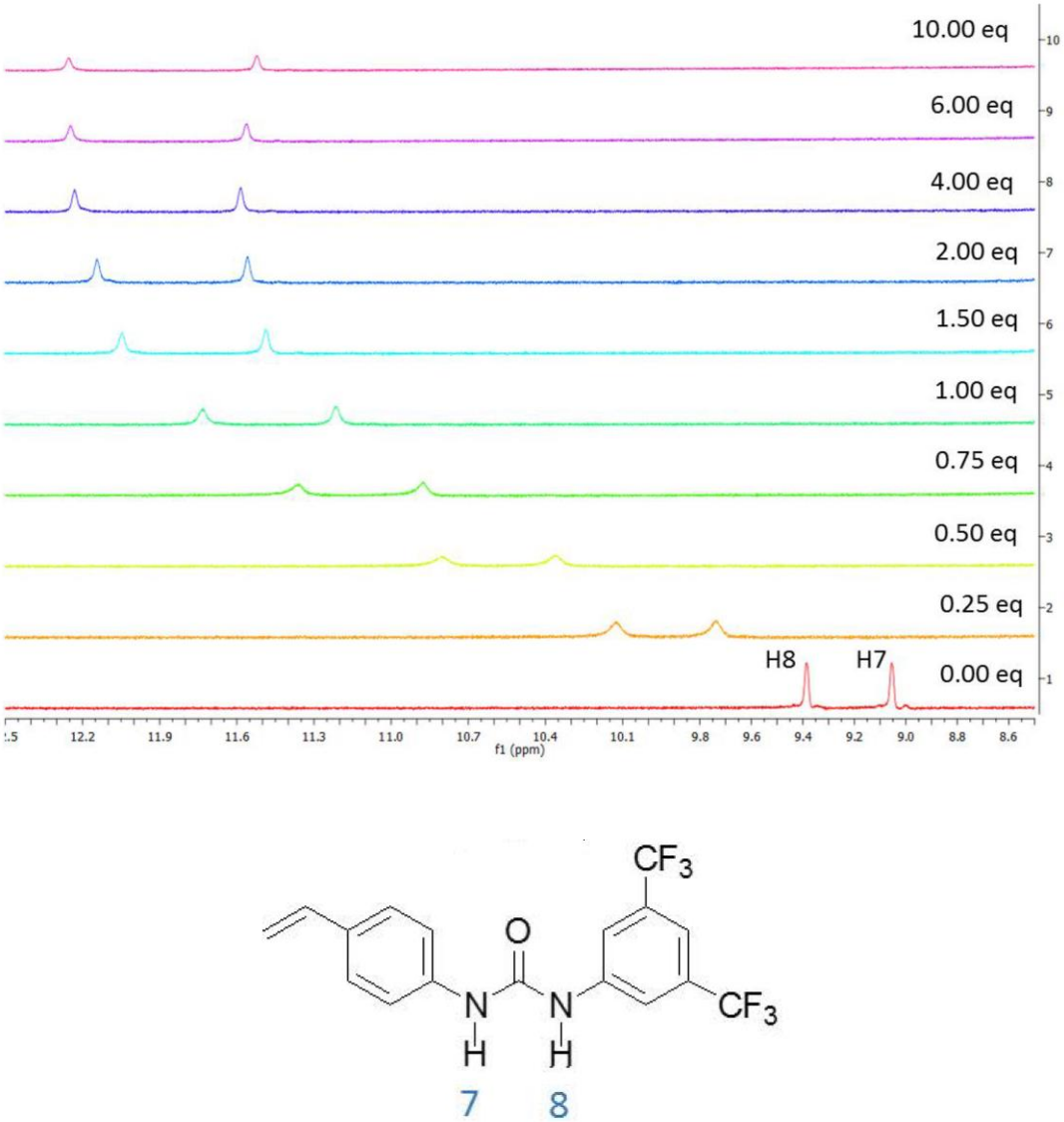

Figure 3.3: *Zoomed portion (8.5-12.5 ppm) of the ^{1}H-NMR spectra of 1,3-diarylurea based funcitional monomer (host) titrated with an increasing amount of PPA-TBA (guest) up to 10 equivalent, recorded in DMSO-d_6 at 25°C* (Wierzbicka (b), 2017).

In order to extend the capacity and ability of stationary phases to retain phosphorous-containing molecules, such as phospholipids, target molecules of our studies, the project focused on the synthesis of materials created by the combination of the two monomers. A library of MIPs and NIPs (**Table 3.2**) has been synthesized by using two different templates, PPA and DPPA-Na (**Figure 3.4**), both mimicking the common phosphorus-moiety of phospholipids and probe the affinity towards the phosphate group.

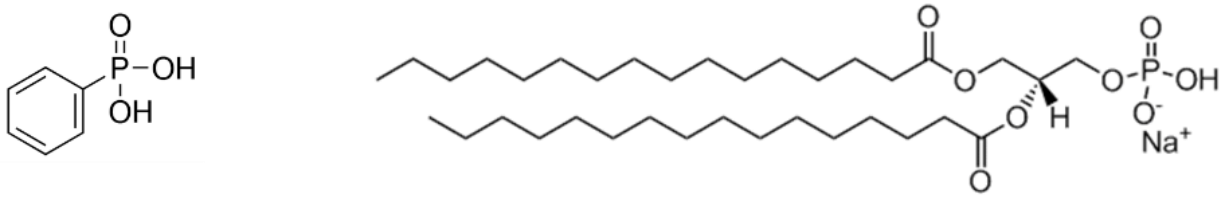

Figure 3.4: *template molecule structure of phenyl phosphonic acid (PPA) on the left, and structure of 1,2-dipalmitoyl-sn-glycero-3-phosphate sodium salt (DPPA) on the right.*

The polymers were synthesized with functionalities (FM) either bis-imidazolium, diarylurea based monomers or the combination of both. The crosslinker employed was EGDMA used in the ratio a 1 to 40 to the template. The components were solubilized in an appropriate porogen solvent and the final pre-polymerization mixture was activated adding ABDV as initiator and the reaction was carried out at 50°C for 24 h and finally at 70°C for 2 h. The solid polymer product was slightly crushed and Soxhlet extracted with MeOH:HCl 0.1M (1:1) for 48 h. The washed materials were then crushed and sieved to obtain three different particle sizes: <25 µm, 25-36 µm, and 36-50 µm. Another set of polymers were prepared without the use of templates, using the same protocol. These non-imprinted polymers (NIPs) were used as a control polymer for the comparison with the corresponding MIPs.

Table 3.2: *Molecularly imprinted polymers synthesized*.

Materials		Template	FMs	Ratio T/FM
Neutral Polymers	CPM1	PPA	1,3-diarylurea	1/2
	CPN1	/		0/2
	PRSSM3	DPPA		1/1
	PRSSN3	/		0/1
Cationic Polymers	PRSSM1	DPPA	Bis-imidazolium	1/2
	PRSSM2	DPPA	Bis-imidazolium + 1,3-diarylurea	1/2/1
	PRSSN2	/		0/2/1

For testing MIPs/NIPs, two techniques have been adopted: the molecular imprinting solid phase extractions (MISPE) for materials of 25-36 µm particle size, and the batch extraction technique employed for those materials who showed a strong backpressure during SPE protocol (**Figure 3.5**). Since the materials were made by two different monomers, the neutral 1,3-diarylurea and the cationic bis-imidazolium, also two different protocols were engaged for the extraction elution procedures. To study the cross-selectivity of the polymers, different phospholipids (**Table 3.3**) were chosen to be then charged in the MISPE cartridges or in the Eppendorf.

Table 3.3: *List of phospholipids used in SPE experiments*.

Lipids	Abbr.	M. W. (g/mol)
1,2-Dimyristoyl-*sn*-glycero-3-phosphorylglycerol (sodium salt)	DMPG	688.843
1,2-Dimyristoyl-*sn*-glycero-3-phosphocholine (sodium salt)	DMPC	677.933
1,2-Dimyristoyl-*sn*-glycero-3-phosphoethanolamine (sodium salt)	DMPE	635.853
1,2-Dipalmitoyl-*sn*-glycero-3-phosphate (sodium salt)	DPPA	670.410
1,1’,2,2’-Tetramyristoyl cardiolipin (sodium salt)	CL	1285.597

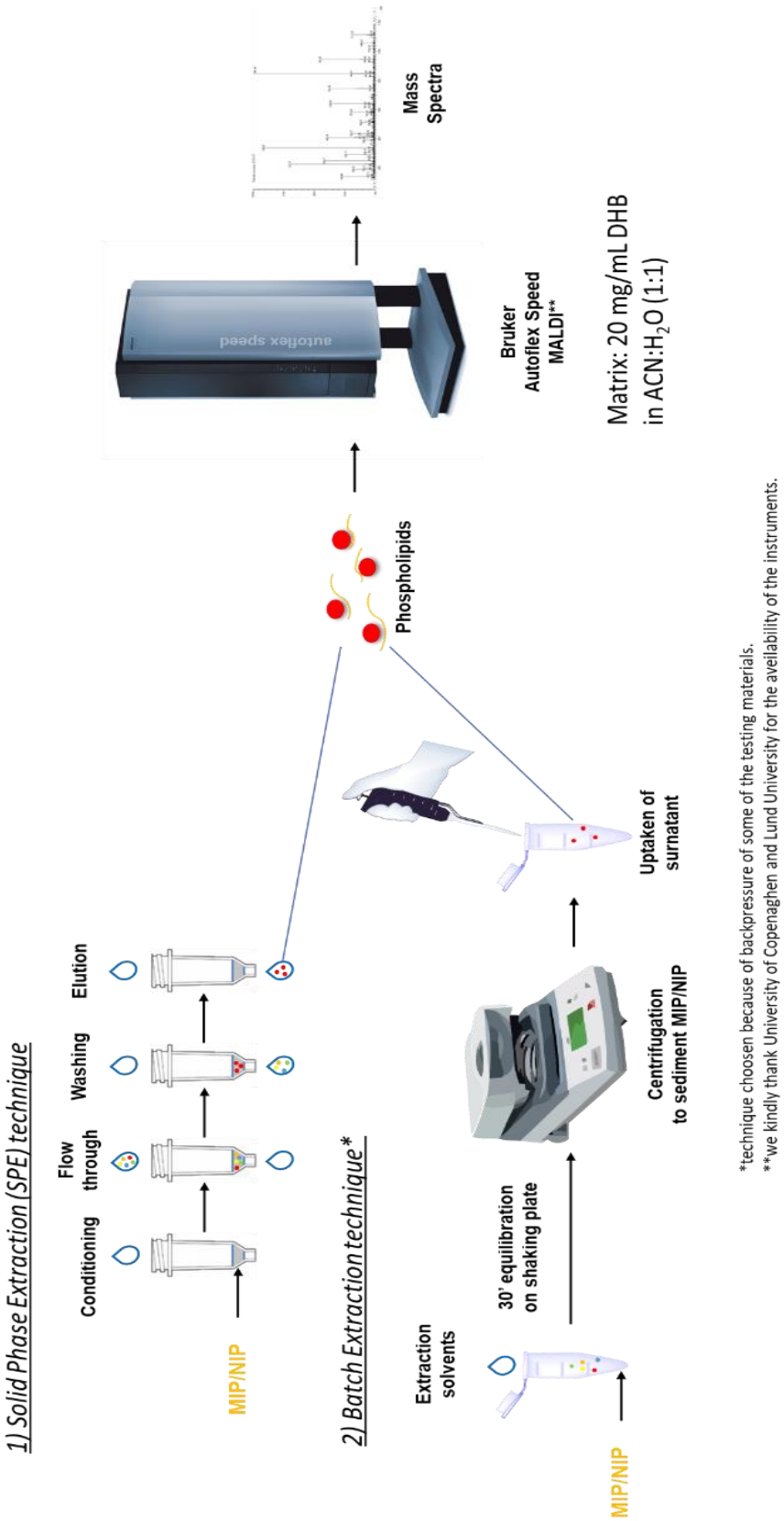

Figure 3.3: *Methods and workflow for phospholipids extractions.*

After dryness and reconstitution of the fractions in 100 µL MeOH, a first MALDI-TOF screening analysis was performed to demonstrate affinity and selectivity of the synthesized stationary phases towards lipids. Thanks to this MS technique, it was possible to establish, through the study of relative lipids peak intensities, the promising materials in the selectivity towards DMPC (**Figure 3.5**), target molecule of this project.

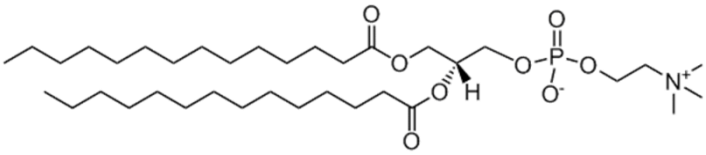

Figure 3.5: *Structure of the target molecule 1,2-dimyristoyl-sn-glycero-3-phosphocholine (DMPC).*

As reported in the **Table 3.4**, all polymers showed affinity towards different categories of lipids, instead CPN1 was not selective at all for any lipid.

Table 3.4: *Selectivity study of the polymers using MALDI-TOF spectra peaks intensities.*

Materials		Selectivity*				
		DMPC	DMPG	DMPE	DPPA	TMCL
Neutral Polymers	CPM1	✓	✓			
	CPN1					
	PRSSM3	✓				
	PRSSN3	✓			✓	✓
Cationic polymers	PRSSM1	✓	✓			✓
	PRSSM2		✓			
	PRSSN2		✓			✓

For the purpose of this project, the most promising stationary phase resulted CPM1 and PRSSM3, polymers obtained using the urea-based functional monomer with recovery % being in the range between 45% and 55% (**Figure 3.6**).

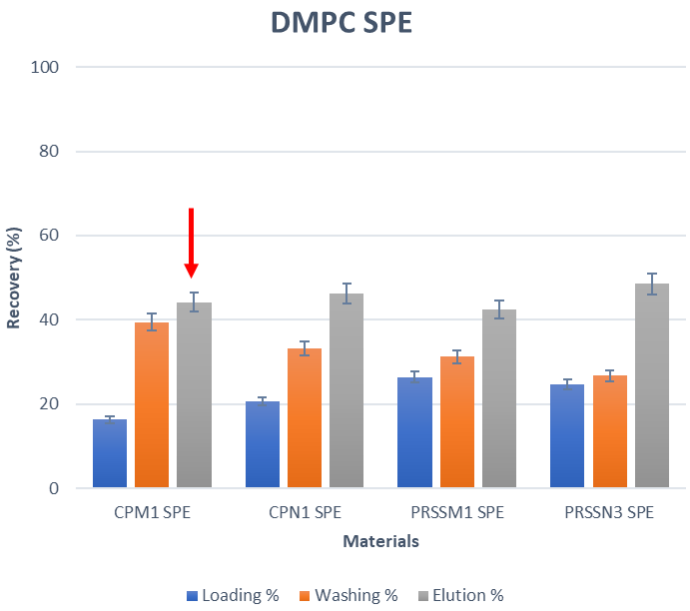

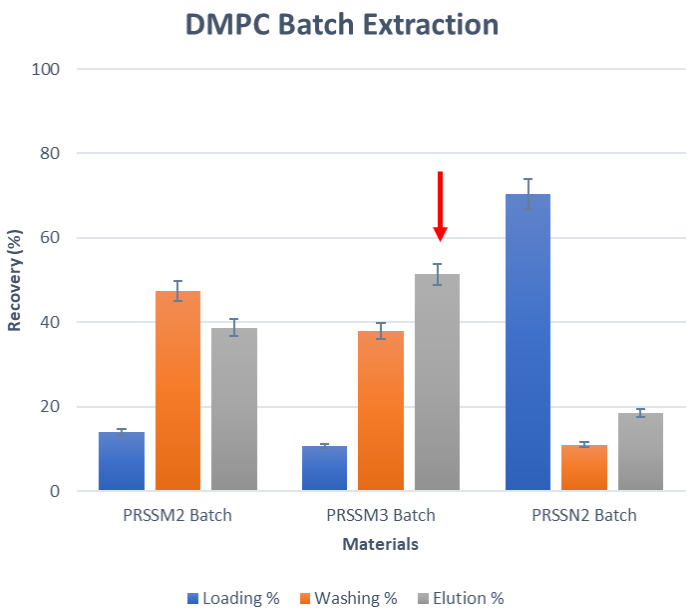

Figure 3.6: *Recovery (%) preliminary evaluation have showed that materials CPM1, PRSSM1, PRSSM3 and PRSSN3 had selectivity towards DMPC.* Only CPM1 and PRSSM3 showed a significant selectivity for the target molecule.

3.3 Conclusions

Concluding, a set of ***new batches of sorbents***, prepared using 1,3-diarylurea and/or bis-imidazolium functional monomers, have been synthesized to target phosphorous-containing molecules. They have been designed as ***neutral and cationic capture receptors*** prepared using EGDMA as crosslinker. All the stationary phases displayed enhanced affinity and selectivity for the phospholipids in MISPE and batch extraction experiments carried out in pure solvent. Two of them have showed a relevant selectivity towards DMPC. For the validation of the method, a new batch of experiments, using the promising materials, will be set up and quantification analysis will be performed by LC-MS/MS detection to evaluate accuracy and precision. The obtained materials will be evaluated as media for selective pre-concentration and/or sample clean-up and will find application in the extraction of phosphatidylcholine (PC) and its deuterated form from *E. Coli* strain.

Bibliography

Dowhan, W., Bogdanov, M., Mileykovskaya, E., (2016), *Biochemistry of Lipids. Lipoproteins and Membranes*, Elsevier, (UK).

Hall, A. J., Manesiotis, P., Emgenbroich, M., Quaglia, M., De Lorenzi, E., Sellergren, B., (2005), *Journal of Organic Chemistry*, 70 (5), 1732-36.

Holčapek, M., Liebisch, G., Ekroos, K., (2018), Lipidomic Analysis, *Analytical Chemistry*, 90, 4249−57.

Kim, S. K., Singh, N. J., Kim, S. J., Kim, H. G., Kim, J. K., Lee, J. W., Kim., K. S., Yoon, J., (2003), New fluorescent photoinduced electron transfer chemosensor for the recognition of $H_2PO_4^-$. *Organic Letter*, 5 (12), 2083-2086.

Maric, S., Thygesen, M. B., Schiller, J., Marek, M., Moulin, M., Haertlein, M., Trevor Forsyth, V., Bogdanov, M., Dowhan, W., Arleth, L., Günther Pomorski, T., (2015), Biosynthetic preparation of selectively deuterated phosphatidylcholine in genetically modified Escherichia coli, *Applied Microbiology and Biotechnology*, 99 (1), 241–254.

Sellergren, B., (2001), *Molecularly Imprinted Polymers: Man-Made Mimics of Antibodies and their Applications in Analytical Chemistry*, Elsevier (Amsterdam).

Sulc, R., Szekely, G., Shinde, S., Wierzbicka, C., Vilela, F., Bauer, D., Sellergren, B., (2017), Phospholipid imprinted polymers as selective endotoxin scavengers, *Scientific Reports*, 7, 44299, DOI: 10.1038/srep44299.

Wierzbicka, C., (a) Liu, M., Bauer, D., Irgrum, K., Sellergren, B., (2017), Cationic pTyr/pSer imprinted polymers based on a bis-imidazolium host monomer: phosphopeptide recognition in aqueous buffers demonstrated by µ-liquid chromatography and monolithic columns, *Journal of Materials Chemistry B*, 5, 953-60.

Wierzbicka, C., (b) New fractionation tools targeting elusive post-traslational modifications, Malmö University Health and Society Doctoral Dissertation, 2017:3.

ABBREVIATIONS

ABC	ATP binding cassette
ABCA1	ATP binding cassette A1
ABCC1	ATP binding cassette C1
ABCG1	ATP binding cassette G1
ABDV	*N,N'*-azobis-(2,4-dimethyl)-valeronitrile
ACN	Acetonitrile
CL	Cross-linker
CNS	Central nervous system
COX	Cytochrome *c* oxidase
DMPC	1,2-dimyristoyl-*sn*-glycero-3-phosphocholine
DMPE	1,2-dimyristoyl-*sn*-glycero-3-phosphoethanolamine
DMPG	1,2-dimyristoyl-*sn*-glycero-3-phospho-(1'-rac-glycerol) (sodium salt)
DMPS	1,2-dimyristoyl-*sn*-glycero-3-phospho-L-serine (sodium salt)
DMSO	Dimethyl sulfoxide
DPPA (Na)	1,2-dipalmitoyl-*sn*-glycero-3-phosphate (sodium salt)
DVB	divinylbenzene
E	Elution
ER	Endoplasmic reticulum
ESI LC-MS	Electrospray ionization coupled to liquid chromatography with mass spectrometry
EtOH	Ethanol

F	Fingolimod
FDA	Food and Drug Administration
FM	Functional monomer
FMs	Functional monomers
FP	Fingolimod Phosphate
FT	Flow-through
FTY720	Fingolimod
FTY720-P	Fingolimod Phosphate
GC	Gas-chromatography
HDACs	Hystone deacetylases
HPLC	High performance liquid chromatography
IAE	Immuno-affinity extraction
IL-17	Interleukin-17
ILCNC	International Lipid Classification and Nomenclature Committee
IPA	2-propanol
LC	Liquid chromatography
LCB	Long chain base
LPP	Lipid phosphate phosphohydrolase
LPP3	Lipid phosphate phosphohydrolase 3
MeOH	Methanol
MIP	Molecularly Imprinted Polymer
MIPs	Molecularly Imprinted Polymers
MISPE	Molecular imprinting solid phase extraction
MIT	Molecularly imprinting technology

MRM	Multiple reaction monitoring
MS/MS	Tandem mass
NBD	Nitrobenzoxadiazole
NBD-Cl	4-chloro-7-nitrobenzofurazan
PA	Phosphoric acid
PC	Phosphatidyl choline
PHB2	Prohibin 2
PPA	Phenyl phosphonic acid
S1P	Sphinsine 1-Phosphate
S1PR1	Sphingosine 1-Phosphate receptor 1
S1PR5	Sphingosine 1-Phosphate receptor 5
S1PRs	Sphingosine 1-Phosphate receptors
SD	Standard deviation
SPE	Solid phase extraction
SPEs	Solid phase extractions
SPHK1	Sphingosine kinase 1
SPHK2	Sphingosine kinase 2
SPHKs	Sphingosine kinases
SPNS2	Spinster homolog 2 protein
Spns2	Spinster homolog 2 gene
T	Template
TBA	Tetrabuthyl ammonium
T_{CM}	Central memory T cell
T_E	T effector cell

Abbreviations

T_{EM}	T effector memory cell
TFA	Trifluoroacetic acid
T_H1	T helper 1
T_H17	T helper 17
TM-CL	1',3'-bis[1,2-dimyristoyl-*sn*-glycero-3-phospho]-glycerol (sodium salt)
UHPLC	Ultra high performance liquid chromatography
US-FDA	United States – Food and Drug Administration
W	Washing

ACKNOWLEDGEMENTS

This work would not have been possible without the support of all people I have met during my three years PhD study course.

First of all, I would like to thank the Head of the Doctoral School of the department of Pharmacy Prof. Gianluca Sbardella (Università degli Studi di Salerno, Italy), Prof. Chiara Monti (Università degli Studi di Salerno, Italy) and Prof. Antonello Petrella (Università degli Studi di Salerno, Italy), to have trusted and given me the possibility to start this adventure in the PhD course in September 2016.

I would kindly thank my Italian supervisor Prof. Carlo Crescenzi (Università degli Studi di Salerno, Italy) and my Swedish supervisor Prof. Börje Sellergren (Malmö University, Sweden) for the opportunity to work in their research groups, for the possibility to develop my research and scientific skills and knowledge during the three years PhD project, facing difficulties and overcoming them always by smiling and keeping enthusiastic and optimistic mood. I would like also to thank my co-supervisor Prof. Nunziatina De Tommasi for advices and constant support. My sincere gratitude goes to Prof. Claudio Baggiani (Università degli Studi di Torino, Italy) and Prof. Börje Sellergren (Malmö University, Sweden) for having found time in reviewing and evaluation of this PhD thesis.

A warm thank goes also to all collaborators I have met and with whom I was pleased to work with: Dr. Sudhirkumar Shinde (Queen's University of Belfast, United Kingdom), Dr. Qianjin Li (Nanjing Normal University, China), Dr. Antonio Caroli (Università degli Studi del Salento, Italy), Prof. Guoqing Pan (Jiangsu University, China), Prof. Knut Rurack and Dr. Wan Wei (Bundesanstalt für Materialforschung und -prüfung - BAM, Germany) for their collaboration project; Dr. Rahma Abouhany (Malmö University, Sweden) for her patience,

knowledge transfer and our relationship beyond lab and work; Prof. Pietro Campiglia, Dr. Eduardo Maria Sommella and Fabrizio Merciai (Università degli Studi di Salerno, Italy) for providing LC-MS/MS analysis; Dr. Wanda Navarra and Prof. Vincenzo Venditto (Università degli Studi di Salerno, Italy) for their availability in running BET analyses; Prof. Maritè Càrdenas (Malmö University, Sweden) and Dr. Selma Màric (MAX IV Lund, Sweden).

I am grateful to all my colleagues in LAB 18 in Università degli Studi di Salerno: Prof. Luca Campone, Dr. Rita Celano, Dr. Imma Pagano and Serena Rizzo. Thanks for supporting and put up with my constant anxious status, especially in the last months of PhD, and to have shared lunches, dinners, Christmas play time and life, even if for short and intense periods. A special thank also to Dr. Massimiliano D'Ambola and Dr. Ginevra Petitto for our trekking days in forests and mountains around Campania region, funny evenings and laughs that made my stay in Salerno lighter, and our friendship that crosses Italy and Europe.

I am grateful also to all my colleagues, present and past, in Malmö University: Michele Lanzillotta, Dr. Mona Rouhi, Dr. Razieh Sahraei, Dr. Aura Rosio Hernandez Camargo and Dr. Natcha Laplan for having had fun together during and after work, and for our travels around Sweden in 2017; Dr. Celina Wierzbicka for her kind company and example during my first period in Malmö; Dr. Sing Yee Yeung for enjoying our weekends in lab, performing experiments singing and dancing, and for days at Lomma beach during the incredibly warm Swedish summer 2017; Radvilė Zubrytė, my Lab wife with whom I shared most of my crazy research time in the last two years; Skaidre Jankovskaja for the time spent close to our "Princess" (LC-MS/MS); Dr. Yulia Sergeeva, Dr. Adam Tillo, Anil Īncel, Liliia Mavliutova and Thomas Janssens.

A kind thought is for collaborators in Stockholm University: Prof. Jan Holmbäck and Prof. Leopold Ilang for the possibility to work in their labs, Dr. Francesco Iadaresta and Dr. Alessandro Quaranta for our intense-till night time in lab waiting for good results.

Many thanks to my Italian student Rosanna Lanzieri (Università degli Studi di Salerno, Italy), and to Erasmus + Program Exchange students: Alessia Viola and Davide Soricelli (Università degli Studi di Salerno, Italy) for our crazy travel to catch the Northern Lights in 2017; Charles Colin (Sigma Clermont, France), Chiara de Soricellis and Angela Riccio (Università degli Studi di Salerno, Italy) for assistance in the projects on-going and to have challenged my supervising skills.

The financial supports from Swedish Vetenskapsradet (VR) under grant number 2014-3794, the Marie Skłodowska-Curie Actions BioCapture (H2020-MSCA-ITN-2016, 722171), the Sweden Knowledge Foundation (KK-stiftelsen) for research under grant numbers 20150086 and 20120014, and the National Natural Science Foundation of China (grant no. 21705073) is gratefully acknowledged. Finally, thanks to the Novartis Company (Basel, Switzerland) for supplementing FTY720.

PARTNERS & FINANCIAL SUPPORTS

UNIVERSITÀ DEGLI STUDI DI SALERNO

DIFARMA

dsf

MALMÖ UNIVERSITY
BIOFILMS RESEARCH CENTER FOR BIOINTERFACES

Vetenskapsrådet
Swedish Research Council

KK-stiftelsen

Smart Capture Materials
BIOCAPTURE
Targeting Tumor Specific Markers

Marie Skłodowska-Curie Actions

BAM
Bundesanstalt für Materialforschung und -prüfung

国家自然科学基金委员会
NSFC
National Natural Science Foundation of China

NOVARTIS

EBRIS
European Biomedical Research Institute of Salerno